12-9-2022

Examining the Relationship between Stomiiform Fish Morphology and their Ecological Traits

Mikayla L. Twiss

Thesis of
Mikayla L. Twiss

Submitted in Partial Fulfillment of the Requirements for the Degree of

Master of Science
Marine Science

Nova Southeastern University
Halmos College of Arts and Sciences

December 2022

Approved:
Thesis Committee

Committee Chair: Rosanna J. Milligan, Ph.D.

Committee Member: Tracey T. Sutton, Ph.D.

Committee Member: Jon A. Moore, Ph.D.

NOVA SOUTHEATERN UNIVERSITY

HALMOS COLLEGE OF ARTS AND SCIENCES

EXAMINING THE RELATIONSHIP BETWEEN STOMIIFORM FISH MORPHOLOGY AND THEIR ECOLOGICAL TRAITS

By

Mikayla L. Twiss

Submitted to the Faculty of
Halmos College of Arts and Sciences
in partial fulfillment of the requirements for
the degree of Master of Science with a specialty in:

Marine Biology

Nova Southeastern University

December 2022

Abstract

Trait-based ecology characterizes individuals' functional attributes to better understand and predict their interactions with other species and their environments. Utilizing morphological traits to describe functional groups has helped group species with similar ecological niches that are not necessarily taxonomically related. Within the deep-pelagic fishes, the Order Stomiiformes exhibits high morphological and species diversity, and many species undertake diel vertical migration (DVM). While the morphology and behavior of stomiiform fishes have been extensively studied and described through taxonomic assessments, the connection between their form and function regarding their DVM types, morphotypes, and daytime depth distributions is not well known. Here, three computer-aided morphometric techniques were used to analyze stomiiform fishes body shapes to examine the relationship between their morphology and established functional traits. Additionally, the feasibility of the three techniques to quantify preserved specimens' shapes was assessed by measuring their ability to predict an individual's taxonomic identity. In the present study, computer-aided morphometric techniques were relatively successful in distinguishing between some taxa. Still, the extent of its success varied according to the taxa and the technique used. Functional traits associated with DVM and vertical distributions were generally significant but showed similar variability across techniques and taxa. The results of this study showed that combining computer-aided morphometric techniques with taxonomic and traditional assessments can open a wide range of new potential applications to further understand deep-sea fish morphologies and how they relate to their functioning within the deep sea. Computer-aided morphometric techniques are considered suitable methods for exploring deep-sea fish morphology variability and for a rough assessment of ecological traits within and between individuals.

Keywords: Trait-based ecology, Diel vertical migration, Momocs, Shape indicator measurements, Landmark configuration analysis, Outline analysis

Acknowledgements

This research was made possible in part by a grant from The Gulf of Mexico Research Initiative, and in part by the National Oceanic and Atmospheric Administration's RESTORE Science Program under award NA19NOS4510193 to Nova Southeastern University. Data are publicly available through the Gulf of Mexico Research Initiative Information and Data Cooperative (GRIIDC) at https://data.gulfresearchinitiative.org.

First and foremost, I would like to thank my major advisor, Dr. Rosanna Milligan for her constant guidance, support, and encouragement throughout this project and my time at NSU. I would also like to thank my committee members, Dr. Tracey Sutton, and Dr. Jon Moore, for their input, ideas, and advice throughout my research.

I would also like to thank Nina Pruzinsky and Ashley Marranzino for all their guidance with proper specimen handling techniques and providing feedback on my writing submissions. Thank you to all my Seascape Ecology lab members, past and present, for their support, feedback, and collaboration. Finally, a very big thank you to my family and friends who kept me going along the way by providing me with the encouragement and support to complete my graduate studies and thesis research.

List of Figures

Figure 1. Unified typology depicting functional traits 2
Figure 2. Depiction of how benthic and pelagic fish body shapes vary with depth 4
Figure 3. Body plan of the four families with Order Stomiiformes..... 6
Figure 4. Progression of morphometric measurement techniques..... 9
Figure 5. Sample grid and station identifications used during the ONSAP 12
Figure 6. Vertical distribution plots for 23 stomiiform fishes captured..... 15
Figure 7. Set-up for photographing the specimens 16
Figure 8. Standard orientation and imaging set-up of specimens 17
Figure 9. Five landmark points used during landmark configuration analysis..... 21
Figure 10. Left image represents the original photograph..... 22
Figure 11. Correlation matrix of ANOSIM R statistics from species assessment of shape indicator measurements using a Bray Curtis matrix..... 29
Figure 12. Correlation matrix of ANOSIM p-values from species assessment of shape indicator measurements using a Bray Curtis matrix 30
Figure 13. Correlation matrix of ANOSIM R statistics from genus assessment of shape indicator measurements using a Bray Curtis matrix 31
Figure 14. Correlation matrix of ANOSIM p-values from genus assessment of shape indicator measurements using a Bray Curtis matrix 32
Figure 15. Correlation matrix of ANOSIM results from family assessment of shape indicator measurements using a Bray Curtis matrix 33
Figure 16. Normalized principal component analysis through shape indicator measurements 34
Figure 17. Principal component analysis on the Procrustes superimposition..... 36
Figure 18. Correlation matrix of ANOSIM R statistics from species assessment of landmark configuration analysis using a Bray Curtis matrix..... 38
Figure 19. Correlation matrix of ANOSIM p-values from species assessment of landmark configuration analysis using a Bray Curtis matrix 39
Figure 20. Correlation matrix of ANOSIM R statistics from genus assessment of landmark configuration analysis using a Bray Curtis matrix 40
Figure 21. Correlation matrix of ANOSIM p-values from genus assessment of landmark configuration analysis using a Bray Curtis matrix 41
Figure 22. Correlation matrix of ANOSIM results from family assessment of landmark configuration analysis using a Bray Curtis matrix 42
Figure 23. Normalized principal component analysis through landmark configuration analysis 43
Figure 24. Box and whisker plot of calibrated harmonic power..... 44
Figure 25. Ptolemy figures of the species..... 45
Figure 26. Example showing the shape each harmonic represented 45

Figure 27. Correlation matrix of ANOSIM R statistics from species assessment of outline analysis using a Bray Curtis matrix 47
Figure 28. Correlation matrix of ANOSIM p-values from species assessment of outline analysis using a Bray Curtis matrix 48
Figure 29. Correlation matrix of ANOSIM R statistics from genus assessment of outline analysis using a Bray Curtis matrix 49
Figure 30. Correlation matrix of ANOSIM p-values from genus assessment of outline analysis using a Bray Curtis matrix 50
Figure 31. Correlation matrix of ANOSIM results from family assessment of outline analysis using a Bray Curtis matrix 51
Figure 32. Normalized PCA-ordinations of body shape among the 23 stomiiform 52
Figure 33. Normalized PCA-ordinations of body shape among stomiiform fish genera...53
Figure 34. Normalized PCA-ordinations of body shape among stomiiform fish families..... 54
Figure 35. Normalized metric CAP of all individuals grouped by species 58
Figure 36. Normalized metric CAP of all individuals grouped by genus..... 61
Figure 37. Normalized metric CAP of all individuals grouped by family..... 63
Figure 38. Correlation matrix of ANOSIM results from DVM types assessment of shape indicator measurements using a Bray Curtis matrix 65
Figure 39. Correlation matrix of ANOSIM results from morphotypes assessment of shape indicator measurements using a Bray Curtis matrix 65
Figure 40. Correlation matrix of ANOSIM results from daytime depths assessment of shape indicator measurements using a Bray Curtis matrix..... 66
Figure 41. Normalized principal component analysis of traits through shape indicator measurements..... 67
Figure 42. Correlation matrix of ANOSIM results from DVM types assessment of landmark configuration analysis using a Bray Curtis matrix..... 70
Figure 43. Correlation matrix of ANOSIM results from morphotypes assessment of landmark configuration analysis using a Bray Curtis matrix..... 70
Figure 44. Correlation matrix of ANOSIM results from daytime depths assessment of landmark configuration analysis using a Bray Curtus matrix..... 71
Figure 45. Normalized principal component analysis of traits through landmark configuration analysis 72
Figure 46. Normalized PCA-ordinations of body shape among DVM types..... 74
Figure 47. Normalized PCA-ordinations of body shape among morphotypes..... 75
Figure 48. Normalized PCA-ordinations of body shape among daytime depth..... 76
Figure 49. Correlation matrix of ANOSIM results from DVM types assessment of outline analysis using a Bray Curtis matrix 77
Figure 50. Correlation matrix of ANOSIM results from morphotypes assessment of outline

analysis using a Bray Curtis matrix 77
Figure 51. Correlation matrix of ANOSIM results from daytime depths assessment of outline analysis using a Bray Curtis matrix 78
Figure 52. Normalized metric CAP of all individuals grouped by morphotypes 80
Figure 53. Normalized metric CAP of all individuals grouped by DVM types 83
Figure 54. Normalized metric CAP of all individuals grouped by daytime depth 84

List of Tables

Table 1. List of the dominant stomiiform fishes that were assessed during this study 14
Table 2. The shape indicator measurements, equations, definitions, purposes, and the references used within this study 19
Table 3. Global ANOSIM results from taxonomic rank assessment of shape indicator measurements using a Bray Curtis matrix 28
Table 4. Global ANOSIM results from taxonomic rank assessment of landmark configuration analysis using a Bray Curtis matrix 37
Table 5. Procrustes ANOVA of Centroid Size for taxonomic rank 42
Table 6. Procrustes ANOVA of Body Shape for taxonomic rank 42
Table 7. Global ANOSIM results from taxonomic rank assessment of outline analysis using a Bray Curtis matrix 46
Table 8. Confusion matrix of normalized CAP predictions at species level for landmark configuration analysis 55
Table 9. Confusion matrix of normalized CAP predictions at species level for shape indicator measurements 56
Table 10. Confusion matrix of normalized CAP predictions at species level for outline analysis 57
Table 11. Confusion matrix of normalized CAP predictions at genus level 59
Table 12. Confusion matrix of normalized CAP predictions at family level 62
Table 13. Global ANOSIM results from the ecological traits assessment of shape indicator measurements using a Bray Curtis matrix 65
Table 14. Global ANOSIM results from the ecological traits assessment of landmark configuration analysis using a Bray Curtis matrix 69
Table 15. Procrustes ANOVA of Centroid Size for ecological traits 69
Table 16. Procrustes ANOVA of Body Shape for ecological traits 69
Table 17. Global ANOSIM results from the ecological traits assessment of outline analysis using a Bray Curtis matrix 76
Table 18. Confusion matrix of normalized CAP morphotype predictions 79
Table 19. Confusion matrix of normalized CAP DVM type predictions 81
Table 20. Confusion matrix of normalized CAP for daytime depth predictions 82

Table of Contents

Abstract i
Acknowledgements ii
List of Figures iii
List of Tables vi
Introduction 1
The Role of Computer-Aided Vision in Morphometric Analyses 8
Study Aims 10
Methods 11
Data Collection 11
Species Selection and Traits 13
Imaging Process and Preparation 16
Shape Indicator Measurements 18
Landmark Configuration Analysis 20
Outline Analysis 22
Multivariate Analyses 24
Predictive Power 25
Results 26
Testing vs. Taxonomy 26
Shape Indicator Measurements 26
Landmark Configuration Analysis 35
Outline Analysis 44
Predicting Taxonomic Identity 54
Predicting Species 54
Predicting Genus 54
Predicting Family 62
Testing vs. Traits 64
Shape Indicator Measurements 64
Landmark Configuration Analysis 68
Outline Analysis 73
Predicting Traits 79
Predicting Morphotypes 79
Predicting DVM types 81
Predicting Daytime Depths 81
Discussion 85
Part 1: Body Shape vs. Taxonomy 85
Part 2: Body Shape vs. Traits 86
Part 3: Evaluation of Computer-Aided Moprhometric Techniques 88

Part 4: Considerations for Future Work 91
Conclusion 95
References 96

Introduction

Trait-based ecology is an approach that characterizes important characteristics and functional features of individuals to better understand and predict their interactions with other species and their environments (Kremer et al., 2016). McGill et al. (2006) defined traits as heritable features that can be measured at the individual level and may include measures of organismal morphology, physiology, behavior, and/or phenology linked to ecological functions (e.g., resource acquisition, growth, reproduction, and survival; Violle et al., 2007; Kremer et al., 2016; Caillon et al., 2018; *Figure 1*). The rationale behind trait-based ecology is that the functional roles played by individual organisms within their ecosystems are better represented by their traits rather than their taxonomic classification (Kiørboe et al., 2018). For example, many marine taxa change their functional roles throughout their lives as they grow (i.e., swordfish larvae feed on zooplankton, and as they grow, their position within the food web switches to an apex predator feeding on larger fishes and cephalopods; Rooker et al., 2012). Functional changes (e.g., ontogenic dietary shifts) over an individual's life would not be captured by its species identity. An individual's identity represents all the traits they express as defined by their niche space and does not necessarily focus on particular traits of interest. Rather than solely focusing on the identity of the individual, the use of their functional traits aids in classifying individuals in an ecological context and identifying what ecosystem services those individuals provide (Petchy et al., 2004; Mouillot et al., 2013; Violle et al., 2014).

In the marine realm, fishes have been the focus of many trait-based studies due to their commercial and ecological importance (e.g., Blanchard et al., 2005; Collins et al., 2005; Piet & Jennings, 2005). Common trait-based approaches include the use of size- and shape-based morphometrics (i.e., the practice of quantitatively analyzing the shape, size, and overall structure of an individual or object; Mindel, 2016) and meristics (i.e., counts of important features; gill rakers, fins, spines; Turan et al., 2006; Mojekwu & Anumudu, 2015; Figure 2(a); Figure 3(b)). The morphology of a fish provides insights into its behavior and life history (Wainwright, 1991). For example, fish body shape directly impacts locomotion (Webb, 1984; Tytell et al., 2010), defensive strategies (Tytell et al., 2010), niche determination (Farré et al., 2016b), trophic positions (Farré et al., 2016b), and the ability to acquire food (Wainwright & Richard, 1995; Langerhans & Resnick, 2010). Shape- and size-based approaches like these have the potential to

allow the structure and function of poorly studied ecosystems and their assemblages to be assessed (Degen et al., 2018).

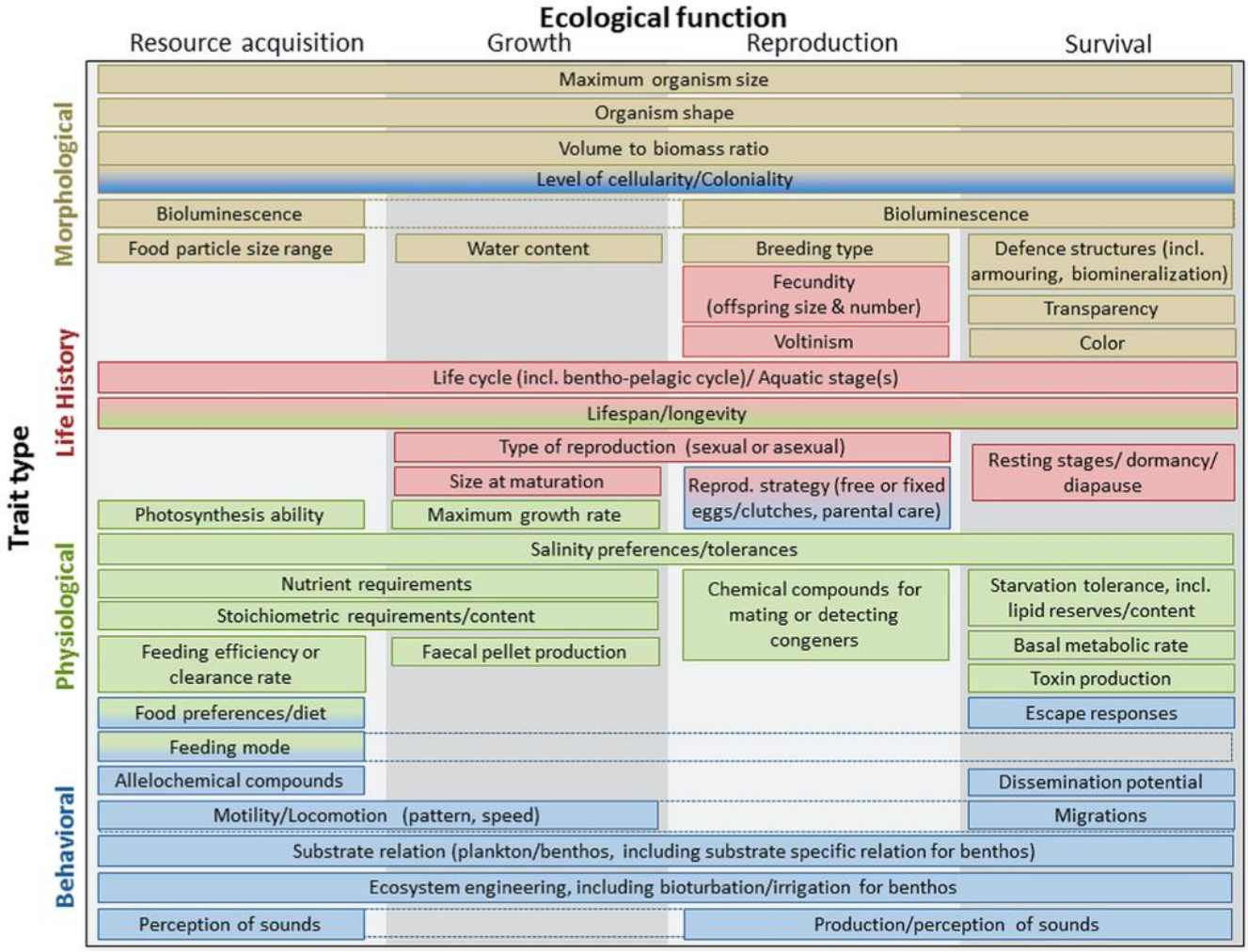

Figure 1 – Unified typology depicting functional traits. Traits are classified by type and ecological function (Adapted from Martini et al., 2021).

One such environment where trait-based approaches could be usefully applied is the deep sea (>200m water depth; Robison, 2009). The deep sea is the largest habitat on Earth, comprising the seafloor and water column, and houses the most abundant fishes on the planet (Ingels et al., 2016; Sutton & Milligan, 2018). In the pelagic realm, deep-sea fishes play important roles in open-ocean food webs, and create connectivity between surface waters and the deep sea. For example, commercially important apex predators and marine mammals (e.g., swordfishes and northern elephant seals) rely on these deep-sea fishes migrating from depth to the surface layers

as a food source (Drazen & Sutton, 2017; Sutton et al., 2020b). Additionally, deep-sea fishes aid in global biological processes such as sequestering carbon and recycling nutrients (Thurber, 2014; Levin et al., 2019; Marks et al., 2020).

In deep-living pelagic fishes, body shape has been linked to locomotor ability, feeding guilds, and hunting strategies (Videler, 1993). *Etmopterus* spp., *Isistius* spp., *Tetragonurus* spp., and *Squaliolus* spp. are some predators that typically show fusiform or torpedo-like body shapes, while *Idiacanthus* spp., *Eustomias* spp., and *Monognathus* spp., are some species that show elongated, eel-like body shapes. High-speed endurance swimming (associated with e.g., a fusiform body shape; *Figure 2(a)*) is not as beneficial regarding hunting and escaping predators at depth as it is closer to the surface due to limited energy flux in the deep sea (Childress, 1995; Seibel et al., 2000; Neat & Campbell, 2013). The energy flux to the deep sea is generated in the euphotic zone and is transported to depths as small particles, which decreases exponentially with depth (Buesseler et al., 2007; Smith et al., 2008). Priede and Tytler (2006) demonstrated with metabolic rate calculations that as the speed of the fish increases, the metabolic rate increases. The increased metabolic rates become much harder to maintain when prey is scarce. As a result, deep-sea fishes have evolved several adaptations to reduce energy expenditure and focus on growth and reproduction. Elongated, eel-like fishes have been estimated to be four to six times more efficient at swimming regarding energy consumption than non-eel-like fishes (van Ginneken et al., 2005). Borazjani and Sotiropoulous (2009) investigated the hydrodynamics of anguilliform swimmers and predicted that this form of swimming with elongated bodies would become increasingly efficient as the water viscosity increases. As water viscosity increases with increasing depth (increasing pressure and decreasing temperature), the efficiency of anguilliform swimmers increases (Borazjani & Sotiropoulous, 2009). Additionally, body size and shape are basic-level traits that may contribute to higher-level traits such as differing DVM patterns and daytime depth distributions (Riddell & Leggett, 1981; Kipanyula & Maina, 2016). For example, certain pelagic species that remain at depth exhibit more watery tissues, weak muscles, and reduced fins (e.g., *Cyclothone* spp.; Martinez et al., 2021). However, nearly all understanding of fish locomotor diversity, body shapes, migration patterns, and habitat utilization comes from observations of shallower-water inhabitants, but many factors that affect locomotion change with depth (Martinez et al., 2021). Further investigation is needed to identify how deep-sea fish's body

shape varies with the structural complexity of their habitats (Claverie & Wainwright, 2014; Friedman et al., 2020; Larouche et al., 2020).

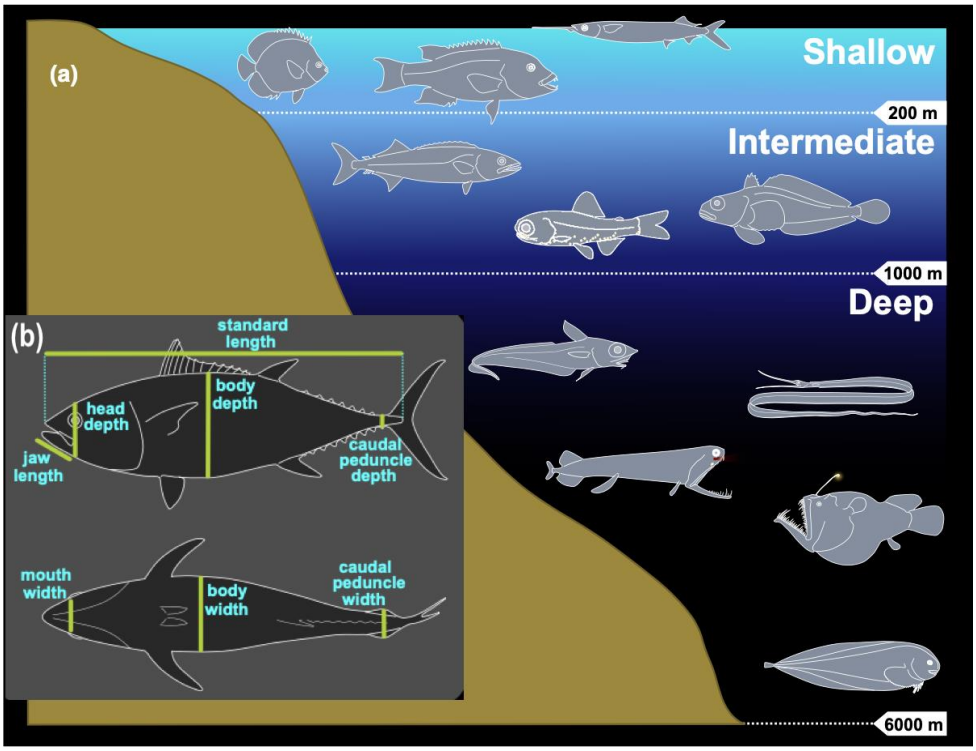

Figure 2 – (a) Depiction of how benthic and pelagic fish body shapes vary with depth. Shallow waters encompass 0-200 m, intermediate waters encompass 200-1000 m, and deep waters encompass 1000-6000 m. (b) Morphometrics measurements are typically measured when describing a species (Adapted from Martinez et al., 2021).

Within the deep-pelagic realm, the stomiiform fishes exhibit exceptionally high morphological and species diversity (Gjøsæter, 1980; Fink, 1985; Sutton, 2003; Sutton et al., 2020b). The Order Stomiiformes comprises four families ((Gonostomatidae (bristlemouths), Phosichthyidae (lightfishes), Sternoptychidae (hatchetfishes), and Stomiidae (dragonfishes and their relatives)), and a total of 51 genera and 321 known species (Fricke et al., 2022). Stomiiformes contains some of the most abundant predators of the mesopelagic zone (i.e., waters extending from 200 to 1,000 m; *Eustomias schmidti*, *Photostomais guernei*; Sutton, 2003; Marks et al., 2020). Due to their migratory behavior and consumption of migratory taxa, piscivorous stomiiform fishes play important roles as trophic mediators and assist in carbon sequestration in deep-sea ecosystems (Marks et al., 2020). Sutton (2003) described three main body plans that

encompass all known species within order Stomiiformes. Body plan A includes fishes from the family Stomiidae, which are usually elongated, black, or dark brown, and the dorsal and anal fins are placed farther back on the body. Stomiids have several defining characteristics, including fang-like dentition and the presence of barbels (*Figure 3(a)*; Sutton, 2003). Body plan B is usually observed in species that are a part of the families Gonostomatidae (*Figure 3(d)*), Phosichthyidae (*Figure 3(c)*), and some species of Sternoptychidae (i.e., Maurolicinae spp.). Species included in plan B tend to exhibit a relatively compressed and elongated, "minnow-like" body (*Figure 3(c)*). Within body plan B, the dorsal and anal fins tend to occur mid-body, with studded bristle-like teeth. Body plan C is exhibited by most species in the family Sternoptychidae (*Figure 3(b)*). The typical body shape observed is laterally compressed, short, and has an abdominal keel to give the taxa a "hatchet-like" look. While the morphology of stomiiform fishes has been extensively studied and described, little is known about inter- and intra-specific variability of body shapes and functional traits (e.g., DVM "types").

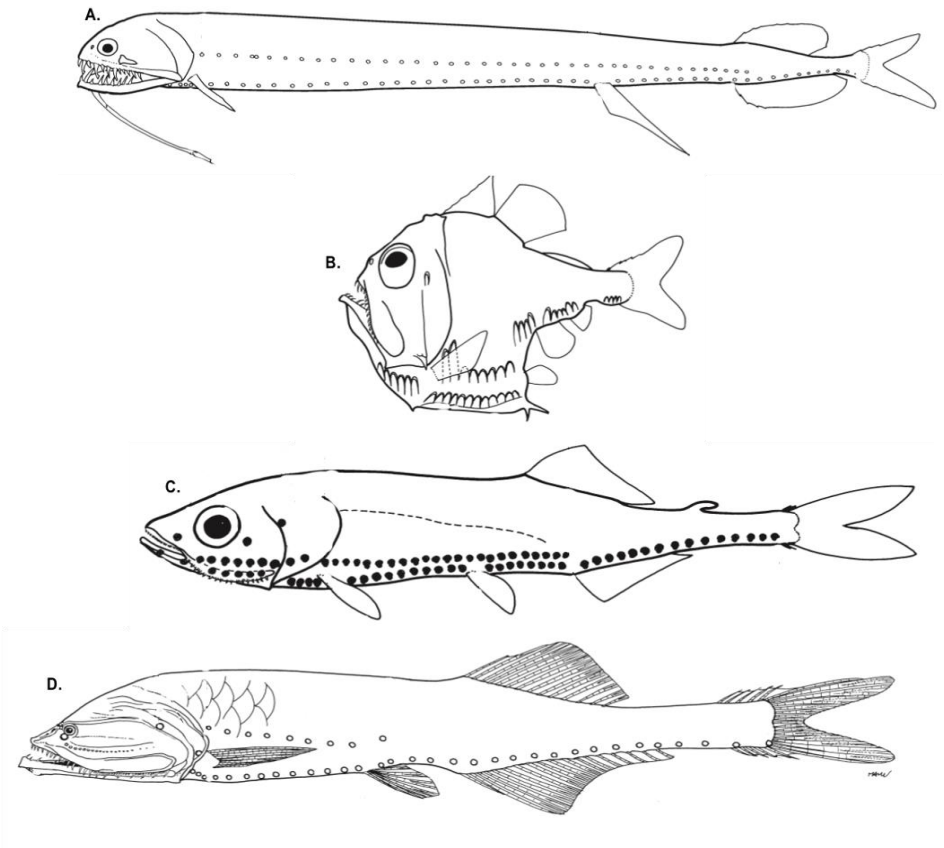

Figure 3 - Body plans of the four families within Order Stomiiformes: Stomiidae (A), Sternoptychidae (B), Phosichthyidae (C), and Gonostomatidae (D) (Adapted from Sutton et al., 2020b). Images are not drawn to scale.

A key behavioral trait exhibited by many mesopelagic species, including many stomiiform fishes, is diel vertical migration (DVM). DVM is the largest migration (by biomass) on the planet and is exhibited every day by trillions of organisms in the World Ocean (Hays, 2003). A recent global survey estimated that approximately 50% of sound-scattering mesopelagic biomass undergoes some form of DVM (Klevjer et al., 2016). While several patterns of DVM have been identified, the general form involves fauna remaining at depth (typically in the mesopelagic zone) during the day, and migrating to surface waters (typically the epipelagic zone; i.e., waters extending from 0 to 200 m), at night (Badcock & Merrett et al., 1976). Several migration behavioral "types" have been described for species participating in DVM. In the present study, I followed the definitions provided by Staby and Salvanes (2018). They identified seven types of migration patterns, including: 1) complete migrators that migrate to mesopelagic depths (below 200 m) during the day and back to the epipelagic zone at dusk, 2)

seasonal migrators, 3) non-migrating fishes that always remain at depth, 4) partial migrators that follow a similar pattern, but only a portion of the population migrates each day, and 5) reverse migrators that follow the opposite patterns of complete and partial migrators by migrating to the epipelagic zone during the day and back to the mesopelagic zone at dusk (Staby & Salvanes, 2018). The migration type, timing, and extent of DVM may vary between species, stocks, regions, age, life stage, and environmental conditions (e.g., changes in photoperiod with regards to diel, seasonal, and lunar variability; Gjøsæter & Kawaguchi, 1980; Staby et al., 2011; Dypvik et al., 2012). Stomiiform fishes, for example are reported to exhibit a variety of DVM "types" (Sutton, 2003), including complete migration, non-migration, and partial migrations, and differ in the frequency of migration and lengths of time spent at different depths (e.g., Miya & Nemoto, 1986; Miya & Nemoto, 1987; Sutton, 2003).

For smaller migratory fishes DVM is especially energetically costly due to long vertical ascents and descents within the water column; therefore, the benefits from DVM must be worth the energetic cost compared to non-migration (Afonso et al., 2014; Brierley, 2014). The deeper the fish goes, the more energetically expensive it becomes to fill the swim bladder, as the swim bladder is filled with oxygen from the bloodstream. Predator avoidance and hunger-driven strategies are the most accepted hypotheses selected for DVM. These have been well explained by previous studies showing that as the abundance of prey (e.g., zooplankton and micronekton) decreases, DVM occurs less often (i.e., partial migration patterns; Zaret & Suffern, 1976; Stich & Lampert, 1981; Pearre, 2003). DVM fishes inhabit deeper depths (e.g., 200-1000 m) during the day to avoid epipelagic visual predators (Romero-Romero et al., 2019) while migrating to surface layers (0-200 m) at night allows fishes to feed upon zooplankton and other fishes that are most abundant in the epipelagic zone (Wang et al., 2019) compared to the relatively energy-poor mesopelagic environment. Specific migration cues are not yet fully understood (Freer & Hobbs, 2020) but likely include changes in light intensity linked to depth, weather conditions (e.g., clouds), turbidity, time of day, satiation, and season (Angel & Pugh, 2000).

Fishes participating in DVM can swim hundreds of meters in 24 hours and need to have specific adaptations to endure the energy expenditure and risks associated with migrating large distances. Deep-sea fishes that participate in DVM have a variety of body forms including; anguilliform or elongation (e.g., *Idiacanthus* spp. and *Stomias affinis*), compressiform (e.g.,

Argyropelecus spp.), elongated compressiform (e.g., *Chauliodus* spp.; *Stomias boa*; *Stomiidae* spp.), depressed (e.g., *Lophiodes* spp.), and fusiform or perch-like body forms (e.g., Gadiformes and lanternfishes; Sutton, 2003; Sutton, 2020b; Staby & Salvanes, 2018). In vertically migrating deep-sea fishes, the advantages and disadvantages of different body shapes and their influence on migration patterns are not widely known. However, there are some advantages to certain body forms that may play a role in DVM. Elongation or anguilliform body shapes have been known to conserve energy better than other body forms concerning sustained swimming periods (Sébert et al., 2009). Non-migrating species of deep-sea fishes tend to exhibit a reduction in the number and size of fins and an elongation of the body (Sutton, 2003; Neat & Campbell, 2013) and a reduction in skeletal density and degradation of muscle in the body. While these latter adaptations may benefit fishes focusing on growth and reproduction, they are not sustainable for long ascents and descents for food acquisition (Neat & Campbell, 2013). While the morphology, locomotor abilities, and behavior of stomiiform fishes have been extensively studied and described through taxonomic assessments (Fink, 1985; Eduardo et al., 2020; Sutton et al., 2020b), the connections between their intraspecific traits, form, and function regarding diel vertical migration (DVM) types, and daytime depth distributions are not well known.

The Role of Computer-Aided Vision in Morphometric Analyses

By studying subtle changes in the morphology of important structures on and within fishes (e.g., fins or swim bladders), accurate descriptions of individuals' shapes can be obtained and used to describe the species' overall form (Bonhomme et al., 2014). Traditional morphometric analyses rely upon numerous shape indicator measurements (e.g., lengths, areas, and angles; *Figure 2(b)*; Hubbs & Lagler, 1964) to recreate selected aspects of the shape of the individual (Bookstein et al., 1985; Caillon et al., 2018). The purpose of computer-aided morphometric techniques is to quantify and compare the entire shape of an organism in a uniform network to increase the likelihood of describing morphometric differences within and between species (Bonhomme et al., 2014; Rohlf, 1990).

Three general styles of computer-aided morphometric techniques are often recognized, distinguished by the nature of the data being analyzed (*Figure 4*). Shape indicator measurements (SIM) can be described as size metrics (i.e., continuous traits) that are favored for explaining size

changes and are calculated by computer (Rosin, 2005). For example, the SIM of circularity uses the size metrics of perimeter and area to describe how circular an individual is. Landmark configuration analysis (LCA) uses discrete anatomical Cartesian geometric coordinates within a 2- or 3-dimensional plot to describe the shape of an organism (Webster & Sheets, 2010). The landmark coordinates are homologous for each specimen between or within populations and represent biologically significant points on all specimens in the study (Bookstein, 1991). Finally, outline analysis quantifies the outline (i.e., perimeters) of organisms without fixed landmarks through Elliptical Fourier analysis (EFA; MacLeod, 2002; Webster & Sheets, 2010). When computer-aided morphometric techniques are used in conjunction with multivariate statistics, they offer a valuable tool to graphically display differences in shape (Rohlf et al., 1996).

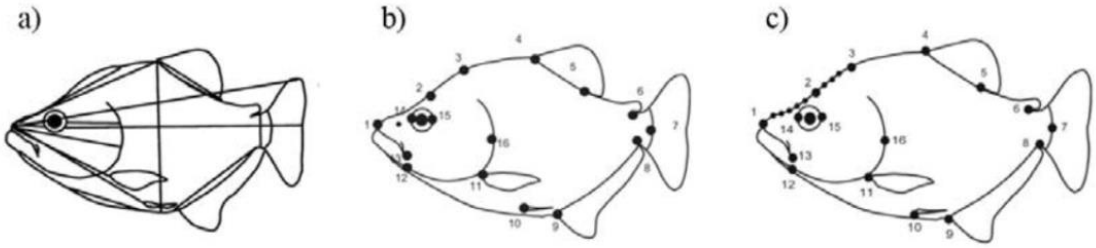

Figure 4 - Progression of morphometric measurement techniques: (a) linear measurements, (b) landmark-based computer-aided measurements, and (c) both landmark and outline-based computer-aided morphometric measurements (Adapted from Zeldtich et al., 2012).

Previous studies within deep-sea fish ecology have described computer-aided morphometric analyses as a novel, and potentially powerful tool for quantifying and comparing an individual's body shape (Mindel et al., 2016; Caillon et al., 2018; Radinović & Kajtez, 2021). A study conducted by Caillon et al. (2018) used elongation of the body and development of the dorsal, caudal, and pelvic fins to test if outline analysis (i.e., EFA; Kuhl & Giardina, 1982) was effective in describing the morphological diversity of shape for 85 fish species found in the North Sea. Caillon et al. (2018) found that EFA effectively described morphological and functional diversity. In a community, functional diversity (i.e., the value and variety of functional traits that organisms can exhibit within a community; Tilman, 2001) is an important index to understand because it demonstrates how a community can affect the surrounding ecosystem. In another example of a trait-based approach study, Mindel et al. (2016) examined the morphological traits of head size, gape size, mouth angle, eye position, and caudal fin aspect

ratio. These morphological traits were used to assess the functional diversity of a demersal fish assemblage along a depth gradient down the continental slope in the Northeast Atlantic. Functional richness (i.e., the amount of occupied niche space by different species within a community; Mason et al., 2005) and size diversity (i.e., the range of sizes found within a community; Quintana et al., 2015) were both highest at around the 800-1000 m depth range. Caillon et al. (2018) and Mindel et al. (2016) used computer-aided techniques to describe and better understand their communities. Using these quantitative tools rather than solely using taxonomic descriptions revealed morphometric differences between species.

While computer-aided morphometric analyses are becoming an increasingly common tool for examining shape variation of fixed fish specimens, the effects of preservation as a potential source of error are not well known (Sotola et al., 2019). Previous studies have suggested that the preservation of biological specimens may result in some change of body shape (Roper & Sweeney, 1981; Vervust et al., 2009; Sotola et al., 2019). For example, standard body lengths tend to decrease after ethanol preservation, and some species of fish increased in weight when treated with a 10% formalin solution (Shields & Carlson, 1996; Greszkiewicz & Fey, 2018). Roper and Sweeney (1981) suggested that freezing specimens could result in an abnormal shape and configuration. The present study will consider the effects of fixation on body shape.

Study Aims

In this study, I used preserved stomiiform species of the most abundant species collected from the northern Gulf of Mexico by two intensive survey programs to:

1. Assess the feasibility of using computer-aided morphometric tools to quantify body shapes using three common morphometric methods of increasing complexity (SIMs, LCA, and outline analysis). The success of the techniques was assessed by measuring their ability to predict taxonomic identity at species, genus, and family levels.
2. Correlate measured body shapes with ecological traits primarily related to DVM behavior, daytime depth distributions, and morphotypes within each species across a range of body sizes.

Methods

Data Collection

This project used fishes previously collected during the Offshore Nekton Sampling and Analysis Program (ONSAP) between November 2010 and September 2011 and the Deep Pelagic Nekton Dynamics of the Gulf of Mexico (DEEPEND) research program (2015-2018; *Figure 5*; Cook et al., 2020). The ONSAP data were collected during two cruise series that used different research vessels main gear types (Sutton et al., 2020a) to collect samples. The M/V *Meg* Skansi cruise series utilized a 10-m^2 Multiple Opening/Closing Net and Environmental Sensing System (MOCNESS) midwater trawl, and the FRV *Pisces* cruise series used a large, high-speed rope trawl (HSRT; Sutton et al., 2020a). The HSRT used during the FRV *Pisces* cruise series had a large, slanted opening (mouth area of ~165 m^2) that tapered towards the back of the net (to ~19 mm^2), allowing for larger and more mobile fauna to be collected (Judkins et al., 2016; Marks et al., 2020; Sutton et al., 2020a); the HSRT was fished as one oblique tow to depth.

During the *Meg Skansi* and DEEPEND sampling, micronekton were obtained using a 10-m^2 MOCNESS that was deployed at five discrete-depth intervals (0-200 m, 200-600 m, 600-1000 m, 1000-1200 m, and 1200-1500 m; Cook et al., 2020). Sampling occurred during the day (centered around solar noon) and at night (centered around solar midnight) to examine faunal depth distributions and vertical migration behaviors (Cook et al., 2020).

Micronekton obtained from the three sampling regimes was processed similarly (Cook et al., 2020). Specimens were fixed in a 10% formalin:seawater solution and dispersed to predetermined laboratories depending on taxon, where experts identified the organisms to the lowest taxonomic level possible (Cook et al., 2020) before being transferred to ethanol for long-term storage. Most specimens (e.g., fishes, crustaceans, and gelatinous zooplankton) collected from both programs were brought back to the Oceanic Ecology Laboratory and the Deep-Sea Ecology Laboratory, located at the Oceanographic Center at Nova Southeastern University (NSU) in Dania Beach, FL, where they are currently stored (Cook et al., 2020).

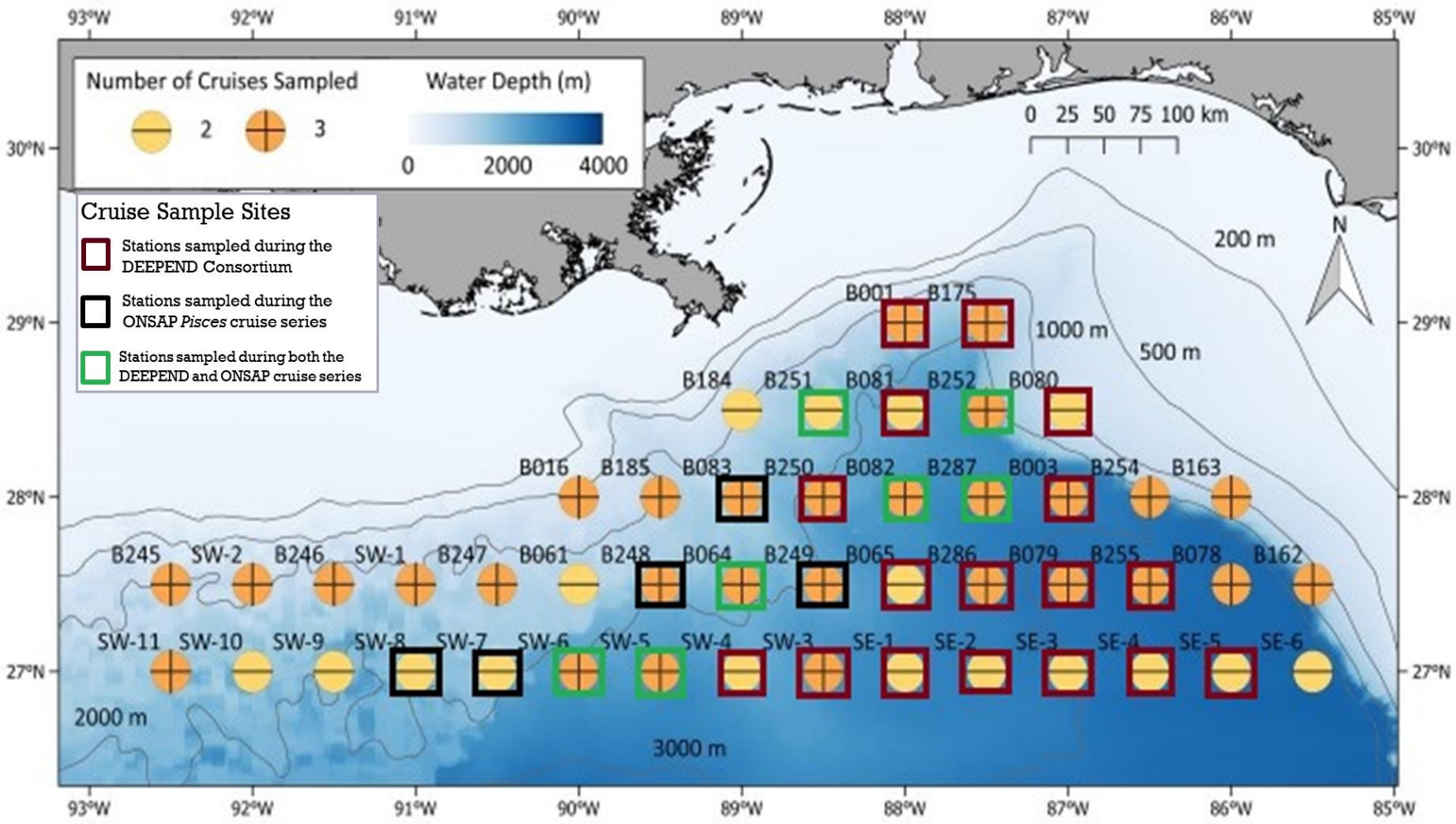

Figure 5 - Sample grid and station identifications used during the ONSAP and DEEPEND programs in the northern Gulf of Mexico: colored squares represent sites sampled during each cruise series (all stations were sampled during the ONSAP M/V Meg Skansi cruise series). Stations are colored to represent the number of times they were sampled (adapted from Cook et al., 2020).

Species Selection and Traits

For the present study, 23 species of stomiiform fishes were selected, spanning all four families (*Table 1*), representing the most abundant taxa in the collection, a range of different DVM "types" and including specimens from the three morphotypes previously identified by Sutton (2003). For each species, 9-10 specimens were selected for analysis, covering a range of body lengths for each species (*Table 1*).

The following DVM "types" were applied to the stomiiform fishes analyzed during this study, based on patterns described previously in the literature: 1) Non-migrators, 2) Complete migrators or migrators that move to mesopelagic depths during the day, and 3) Partial migrators where only a portion of individuals migrate each day (Staby & Salvanes, 2018).

The DVM patterns and the daytime depth distributions of the selected stomiiform fishes were identified and assigned from qualitative patterns observed in species T-plots (*Figure 6*), which were created using the standardized counts (total counts per 100000 m^3) per depth interval for 23 stomiiform species caught during the DEEPEND and ONSAP programs. Previous literature was used to confirm the DVM "types" for each species analyzed during this study. (Priede, 2006; Staby & Salvanes, 2018; R. Milligan, unpublished data). The morphotypes previously identified by Sutton (2003) were also assigned to each species.

Table 1: List of the dominant stomiiform fishes that were assessed during this study. Morphotypes followed the body plans described by Sutton (2003). Size ranges represented the median standard-length measurement of specimens analyzed within this study. Daytime depth distributions were based on individuals captured within the northern Gulf of Mexico. The species and genus identifiers represented the code used to identify individuals. The number of individuals was representative of how many specimens per species were used (Data collected from Sutton, 2003; Sutton et al., 2020b. DVM type and daytime depths were assessed by R. Milligan, unpublished data).

Species	Daytime Depth	DVM Type	Morphotype (following Sutton, 2003)	Species and Genus Identifier	Number of Individuals	Standard length measurements
Cyclothone braueri	200-600 m	Non-migrator	B	CB	10	21-40 mm
Argyropelecus gigas	200-600 m	Non-migrator	C	AG	10	9-34 mm
Cyclothone obscura	1000-1500 m	Non-migrator	B	CO	10	27-49 mm
Argyropelecus hemigymnus	200-600 m	Non-migrator	C	AH	10	10-28 mm
Cyclothone alba	200-600 m	Non-migrator	B	CA	10	17-27 mm
Cyclothone pseudopallida	200-1000 m	Non-migrator	B	CP	10	26-44 mm
Cyclothone pallida	200-1200 m	Non-migrator	B	CPA	10	25-46 mm
Cyclothone acclinidens	600-1000 m	Non-migrator	B	CAC	10	26-34 mm
Polyipnus clarus	200-600 m	Non-migrator	C	PC	9	15-29 mm
Sternoptyx pseudobscura	600-1200 m	Non-migrator	C	SP	9	14-22 mm
Sigmops elongatus	200-1000 m	Complete migrator	B	SE	9	23-126 mm
Vinciguerria nimbaria	200-600 m	Complete migrator	B	VN	9	17-33 mm
Argyropelecus aculeatus	200-1000 m	Complete migrator	C	AA	9	18-33 mm
Pollichthys mauli	200-600 m	Complete migrator	B	PM	9	22-49 mm
Stomias affinis	200-600 m	Complete migrator	A	SA	9	20-113 mm
Sternoptyx diaphana	200-1000 m	Complete migrator	C	SD	9	18-28 mm
Maurolicus weitzmani	0-600 m	Partial migrator	B	MW	9	21-50 mm
Margrethia obtusirostra	200-600 m	Partial migrator	B	MO	9	17-33 mm
Gonostoma atlanticum	200-600 m	Partial migrator	B	GA	9	15-20 mm
Vinciguerria poweriae	200-600 m	Partial migrator	B	VP	9	18-35 mm
Valenciennellus tripunctatus	200-600 m	Partial migrator	B	VT	9	23-33 mm
Photostomias guernei	200-600 m	Partial migrator	A	PG	9	30-113 mm
Chauliodus sloani	200-1000 m	Partial migrator	A	CS	10	38-171 mm

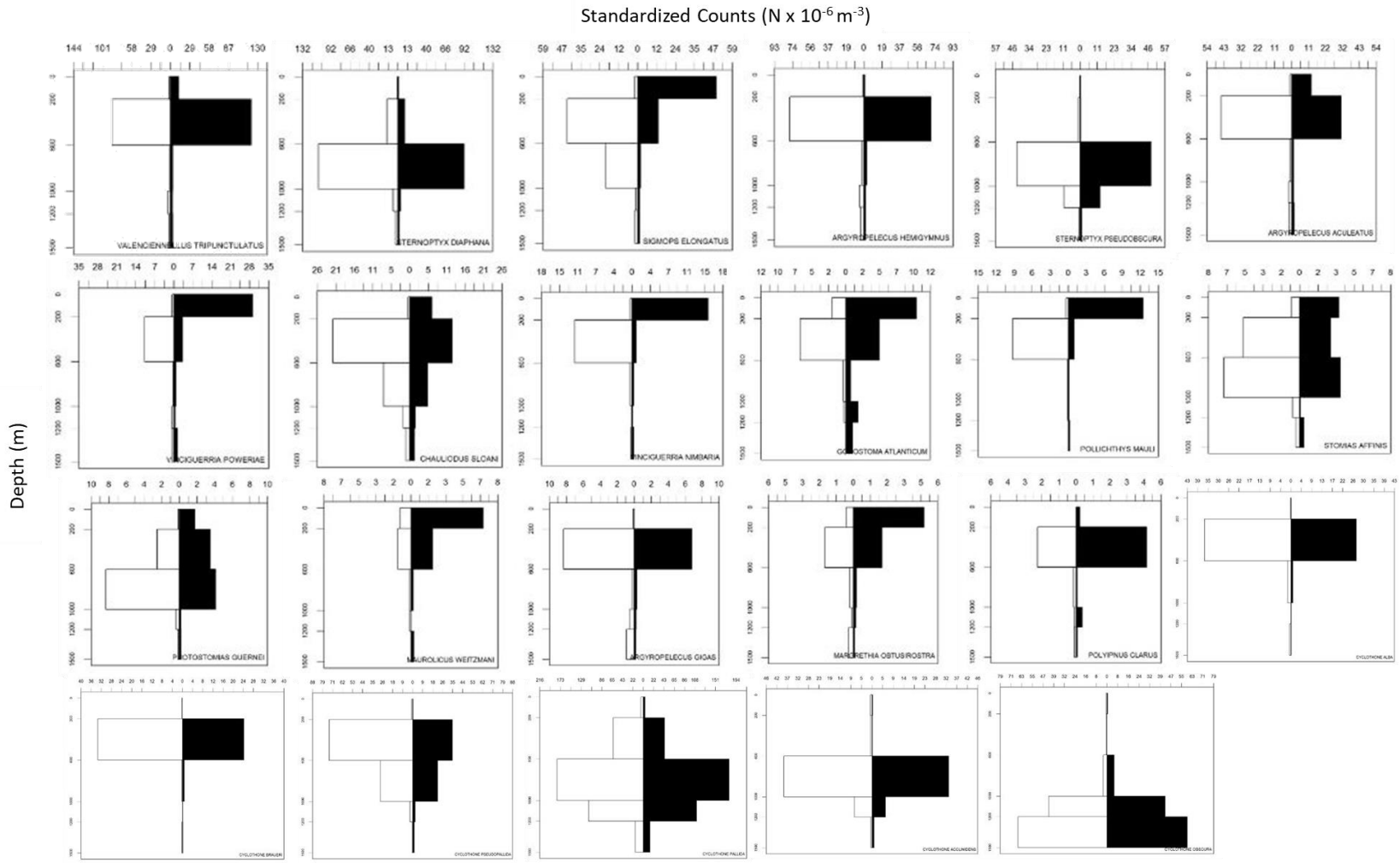

Figure 6 - Vertical distribution plots for 23 stomiiform fishes captured with a MOCNESS net between 2011 - 2017. The white boxes represent captures during the day (centered around solar noon), and the black boxes represent the captures at night (centered around solar midnight). Each bar represents the total number of species captured and was standardized by trawl volume and the depth range sampled (R. Milligan, unpublished data).

Imaging Process and Preparation

The photographs for analysis were taken using a Canon DSLR EOS 77D camera with a Tokina ATX-I 100 mm, F2.8 FF macro lens. The camera was mounted on a custom imaging stand that allowed the camera to be mounted at a fixed height above the specimen (*Figure 7*). The specimens were illuminated using a combination of two Neewer dimmable 5600K USB LED video lights, battery-powered LED push-lights and the on-camera flash. For computer-aided analyses, the best illumination of the specimen provided a sharp contrast between the background of the image and the specimens to capture a clear outline.

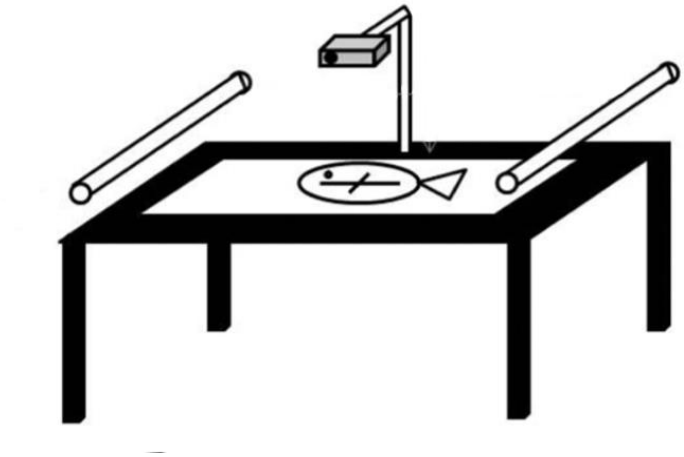

Figure 7 - Set-up for photographing the specimens. Lights were placed on either side of the specimen, and the camera was suspended above the transparent tray and ruler (adapted from Navarro et al., 2016).

For consistency of images, specimens were always oriented towards the left (*Figure 8*). Specimens were then placed in a glass petri dish filled with ethanol, a plastic ruler underneath to provide a scale, and were photographed over a matte black or white background (*Figure 8*). Depending on the specimens used, achieving a neutral body posture for each individual was not straightforward. The body of a fish is a flexible structure, and the specimen shape will be influenced by both the specimen and its mode of preservation. Due to the preservation techniques utilized, image analysis techniques, and specimen conditions, it was not possible to accurately and repeatably capture the shape of the fins and therefore, only the body shape of each individual was analyzed.

Each image went through a series of quality control checks before being accepted for analysis, including: 1) no bubbles or debris within the ethanol the specimens were submerged in, 2) no warped specimens, and 3) sharp focus of the specimen's outline. If any image did not meet the quality control criteria, they were retaken. In addition, each specimen was given a unique identifier that remained consistent throughout the study. Each identifier consisted of two letters and three numbers where the letters represented the genus and species (i.e., AG = *Argyropelecus gigas*; *Table 2*), and the numbers were unique to the individual of that species (i.e., AG001= the first specimen of the species *Argyropelecus gigas*).

Figure 8 - Standard orientation and imaging set-up of specimens to photograph the left side of the body. This example is specimen AG008. Note the damage to the fins.

Shape Indicator Measurements

SIMs were calculated in R ver. 4.0.2 (R Core Team, 2020) via the Momocs package (Modern Morphometrics; Bonhomme et al., 2014; Claude, 2008; R Development Core Team, 2013). SIMs are equations that use size metrics to describe the shape of an object being studied. For example, the caliper size, also known as "Feret's diameter," describes the longest distance between two points of the shape. SIMs are helpful for general descriptions of the object's shape (e.g., how circular or elongated a specimen is), and the measurements included in this method can be found in *Table 2* with the equation and a brief definition. The Momocs package is coded to generate 15 SIMs for each specimen analyzed. Once the SIMs were calculated in Momocs, they were analyzed in PRIMER ver. 7 (Clarke & Gorley, 2015; see the *Multivariate Analyses* section below).

Table 2 - The shape indicator measurements, equations, definitions, purposes, and the references used within this study.

Shape Indicator Measurements	Equation	Definition	Purpose of measurement	References
Caliper	$\ll F \gg = \frac{P}{\pi}$	$\ll F \gg$ is equal to the ratio of the object perimeter (P) and pi.	Calculates the longest distance between two points the shape provided. Also known as Feret's diameter	Rosin, 2005
Centroid Size	$CS = \sqrt{\sum_{i=1}^{n} \left\| \left\| p_i - t \right\| \right\|^2}$	Centroid size is the square root of the sum of squared distances of all landmarks from their centroid or central point	Centroid size is the center of a plane figure is the arithmetic mean position of all points in the figure	Rosin, 2005
Haralick Circularity	$\frac{\mu R}{\sigma R}$	R is the distance between the center and any point on the perimeter, μ is the expectation and σ is the standard deviation	Circularity calculates the compactness (e.g., how close together the outline is) of the individual. High circularity values correspond to circular shapes. Normal circularity measurements are biased to digitization noise of an image	Haralick, 1974
Convexity	$\frac{area(X)}{area(CH(X))}$	Ratio of the convex hull (CH) of region X by the area of CH(X)	Convexity is calculated using a ratio of eigenvalues (e.g., inertia axes of coordinates) and describes how the outline is curved outwards.	Rosin, 2005
Eccentricity Bounding Box	$Eccentricity = \frac{A}{B}$	Ratio of the length of the maximum chord A to the maximum chord B which is perpendicular to A	The eccentricity bounding box is the measure of the aspect ratio. The ratio of the length of the major axis to the minor axis, specifically the length vs. width ratio.	Rosin, 2005
Elongation	$s(n) = \frac{\sqrt{\lvert a(n) \rvert^2 + \lvert b(n) \rvert^2}}{\sqrt{\lvert a(1) \rvert^2 + \lvert b(1) \rvert^2}}$	N is the number of points on the boundary. The sequences a(n) and b(n) are the complex Fourier coefficients. They are used to derive a set of descriptors s(n) that are invariant to translation, rotation, and scaling.	Calculates the elongation of a shape	Rosin, 2005
Rectangularity	$\frac{area(X)}{area(MBR)}$	Ratio of the area of region X to the area of its minimum bounding rectangle (MBR)	Calculates how closely an object resembles a rectangle.	Rosin, 2005
Solidity	$Solidity = \frac{contour\ area}{convex\ hull\ area}$	Calculates the ratio of the shape area and the convex hull area	Measures the density of an object. A value of 1 signifies a solid object and a value of less than one will signify an object having an irregular boundary (e.g., contains holes).	Rosin, 2005

Landmark Configuration Analysis

LCA involves a computer-aided program placing predetermined points on the outline's critical defining features, where the computer then calculates the pairwise Euclidean distances between every pair of points using a matrix (Richtsmeier, et al., 1992; Richtsmeier, et al., 2002). Numerous studies have defined landmarks on fish to study their morphology. However, due to the diverse body shapes of deep-sea fishes, for this study five commonly used landmarks that are easily recognizable and present on all species of fishes were chosen (following Loy et al., 2000, Elmer et al., 2010, Farre et al., 2016a). The five landmarks used in this study included: (1) snout tip; (2) anterior insertion of the dorsal fin; (3) dorsal and (4) ventral insertion of the caudal fin; and (5) anterior insertion of the pelvic fin (*Figure 9*). The x and y coordinates of each landmark were extracted by first using the digitizing program tpsUtil64 (Rohlf, 2015) to convert photographs to .tps files. Before placing landmarks on each fish's body, the number of pixels per centimeter (cm) of each image was manually set using the "set scale factor" function. The ratio of pixels to centimeters was set by placing a point on the zero-centimeter mark of a ruler and then tracing a straight line until the one-centimeter mark was reached. Setting the scale was completed manually and done one picture at a time to ensure that the scale was the same for each picture. Next, the landmarks were added manually to each specimen. The .tps file containing all the images from this study was created to allow for the manual digitization of each fish's body with the program tpsDig232. The digitized points were converted to each landmark (x, y) coordinates within the fish body structure. The same procedure was followed for digitizing landmarks on every specimen's body to minimize human error in the digitizing process (Dhingra et al., 2019). Once each landmarks (x, y) coordinates were collected, a .tps file containing all the landmarks was created and uploaded into the program MorphoJ, version 1.07a, which allows for the computer-aided geometric morphometric analysis of two- and three-dimensional landmark data (Klingenberg, 2011).

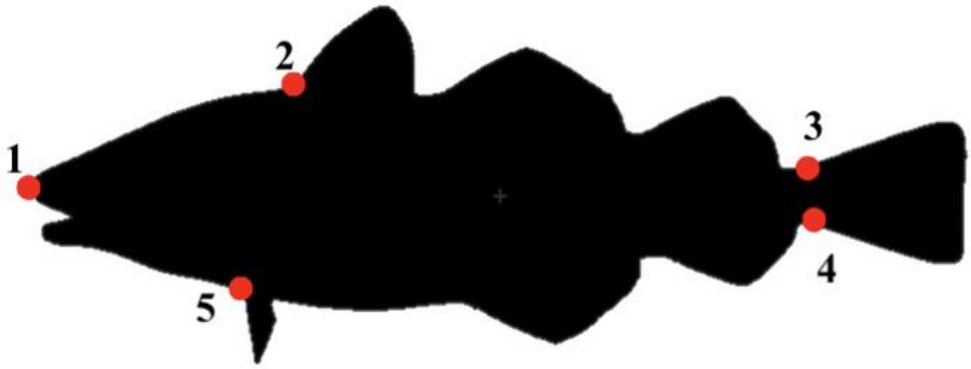

Figure 9 - Five landmark points used during landmark configuration analysis: the snout tip (1); the anterior insertion of the first dorsal fin (2); the dorsal and ventral insertion of the caudal fin (3 and 4); and the insertion of the pelvic fin (5). Figure adapted from Caillon et al (2018).

After the landmark coordinates were collected a Procrustes fit aligned by principal axes was run to extract shape information from the dataset by Procrustes superimposition. A Procrustes superimposition centers, aligns, and scales all specimens using the centroid of landmarks, then scales and rotates to minimize deviations of points from the average location of landmarks. The Procrustes Superimposition Alignment removes an object's size, position, and rotation (Gower, 1975), allowing for unbiased comparison of relative landmark locations between specimens by removing any differences in the mean landmark locations. Once the alignment was completed, the outliers within the data were assessed using Mahalanobis distance as an additional validation step. The Mahalanobis distance (i.e., squared distance metric that finds the distance between a point and a distribution) uses covariance between variables in order to find the distance between two points. Klingenberg (2011) suggested that the Mahalanobis distances, in the case of morphometric datasets, should be taken as an approximate guide. Many morphometric datasets do not conform to multivariate normal distributions and long-tailed distributions are rather common. Due to the variety of species assessed during this study, there was an extensive range of body shapes. Following Klingenberg (2011), outliers were visually assessed by comparing the theoretical and observed distribution of the observation values. Any individuals falling outside the main distribution were considered strong deviations from the dataset and were excluded.

After the validation steps were completed, multiple figures were created to represent the configuration of all landmarks and visualize the results. Wireframe figures (i.e., a set of lines

connecting the landmarks) were first created to confirm that the landmarks were correctly placed in the digitizing process. Transformation grids were created to compare the differences in landmark locations between each individual within each taxonomic and functional group, and warped outline drawings were created to compare each landmark to the group average. These figures were created for each individual to visually assess the placement of landmarks on a spatial plane. Finally, numerous multivariate analyses were run to compare similarities and differences between landmarks of individuals (see the *Multivariate Analyses* section below).

Outline Analysis

Preparation for outline analysis involved two major steps. The first step was editing photographs using the free image manipulation software GNU Image Manipulation Program (GIMP, ver. 2.10.14; GIMP Development Team 2020). GIMP was used to isolate specimens from each image's background to remove pixel noise (i.e., variations in image brightness or color) or any other visual distortion of the pixels. Once the pixel noise was removed, the specimen's outline was manually traced using the path tool in GIMP and then converted to a black mask. The background of the image was then converted to white to create a clear separation of pixels from the specimen and background of the image. The outline created from the analysis is a closed polygon produced by pixels placed on the (x, y) coordinate plane (*Figure 10*; Bonhomme et al., 2014). The second image preparation step was cropping silhouettes created in GIMP. The silhouettes were manually cropped using a batch cropping ROI (region of interest) macro in ImageJ software (Strock, 2021).

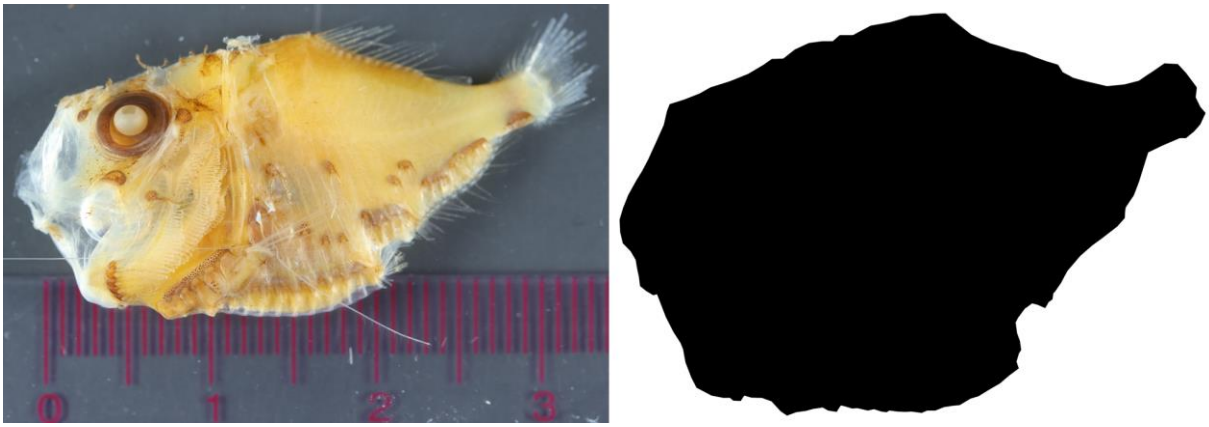

Figure 10 - Left image represents the original photograph of the individual PC012 (i.e., the twelfth specimen of the species Polyipnus clarus). The right image represents the silhouette of the individual PC012 created in GIMP.

Momocs (Modern Morphometrics; Bonhomme et al., 2014; Claude, 2008; R Development Core Team, 2013) is an image-analysis package for R (ver. 4.0.2; R Core Team, 2020), that is used to identify and extract outlines of complex shapes. Momocs was used to quantify the outline of the fishes being studied using the Elliptic Fourier Analysis (EFA; Bonhomme et al., 2014). Fourier-based approaches are powerful tools used to extract geometric information from outlines (Dhingra et al., 2019). Fourier-based approaches work based on the Fourier series, where complex periodic functions are decomposed into simpler trigonometric functions (i.e., sine and cosine). Sine and cosine waves have frequencies that are integer multiples or harmonics of one another. Within each harmonic, there are levels that are made up of four coefficients that respond to the effects of the cosine and sine on the x-axis (coefficients A and B) and the y-axis (coefficients C and D) of the 2D plot. The bodies of stomiiform fishes can be represented by these periodic functions because if a closed outline is traced, a reference point will periodically and repeatedly be crossed, making a closed outline a periodic function (*Figure 10;* Bonhomme et al., 2014), and allowing the geometry of the closed outline (the "shape") of the stomiiform fishes to be quantified. In EFA, the first (higher-order) harmonics extract the gross shape of an outline. As additional (lower-order) harmonics are added, they are able to describe increasingly fine-scale sinuosities in the outline (Bonhomme et al., 2014; Dhingra et al., 2019), but can lead to overfitting if allowed to generate a perfect fit. To avoid this issue, the number of harmonics required to best fit each outline to 90%, 95%, and 99% accuracy were estimated and compared using the process described below.

Silhouettes were uploaded into the Momocs package using the "import_jpg" function and compiled to create "coordinate outline matrices" (i.e., coo; a group of extracted outlines). During this step, each of the outlines were measured, scaled, and centered. Using the "stack" and "panel" functions the outlines were placed in panels and stacked on top of each other to compare their body shapes visually. Additionally, outlines were smoothed to remove excess noise from the outlines. Deviations from each outline's centroid size (i.e., center) were plotted and visually assessed. The number of harmonics producing the best-fitting outlines (at 90-99% accuracy) were determined for each specimen using reconstructed shapes and Ptolemy figures (Dhingra et al., 2019). Finally, the principal components corresponding to the Fourier harmonics for the best-

fitting outlines were extracted from each specimen and analyzed using multivariate analyses in Primer v7 software (*Multivariate Analyses* section below).

Multivariate Analyses

The multivariate analyses for the three morphometric methods were analyzed in PRIMER ver. 7 (Clarke & Gorley, 2015) with PERMANOVA. Principal Components Analyses (PCA) were conducted using SIMs, LCA, and outline analyses to compare major shape variations among individuals to identify which variables (indicators and landmarks) correlated with different taxonomic and functional groups.

Multiple analyses of similarities (ANOSIM) tests were conducted to determine whether significant differences of body shape could be detected between each taxon at species, genus, and family levels and also between each ecological traits type (DVM type, daytime depth distribution, and morphotype group; Clarke & Gorley, 2015). The prediction of taxonomic identity was used to test the effectiveness of computer-aided morphometric tools. ANOSIM analyses were conducted for all three morphometric methods and were used to isolate the effect each factor had on body shape (Somerfield et al., 2021a). ANOSIMs were run as one-way, unordered, crossed designs with 999 permutations, and resulted in an R statistic and a p-value that were interpreted together. A p-value that was less than 0.05 indicated there were significant differences between groups. The R statistic ranges from -1 to 1, with positive values indicating greater separation between groups than within groups, and negative R values indicating more separation within groups than between groups. Values close to zero typically indicate no strong group structuring is present (Somerfield et al., 2021b). Correlation matrices visualizing the ANOSIM results were created using the package corrplot in R (ver. 4.0.2; Wei & Simko, 2017; R Core Team, 2020). Tests on traits were accompanied with similarity percentages (SIMPER) analyses where significant ANOSIM results occurred to identify the shape indicators, harmonics, and landmarks that were most responsible for the dissimilarity between body shapes.

Finally, a Procrustes ANOVA was used to assess statistical hypotheses describing patterns of shape variation and covariation for a set of Procrustes shape variables for LCA (Marcy et al., 2018). The hypothesis being tested was if the body shape extracted from the Procrustes landmarks of stomiiform fishes changed with functional traits and taxonomy. It was

hypothesized that the body shape of stomiiform fishes differs based on their taxonomic rank and ecological characteristics. Procrustes ANOVAs and ANOSIMs are similar tests to one another, however, a Procrustes ANOVA was used to assess the Procrustes average distances among specimen landmarks.

Predictive Power

Canonical Analysis of Principal Coordinates (CAP) was conducted in PRIMER ver. 7 (Clarke & Gorley, 2015) to assess whether the different morphometric analyses used within this study could correctly predict various taxonomic resolutions and ecological traits that describe the identity of individuals. The taxonomic resolutions were used to test the efficacy of the different morphometric methods. The ecological traits used as predictive power include morphotypes, DVM types, and daytime depth distributions. A CAP was conducted separately for SIMs, outline analysis, and LCA to evaluate the predictive power of each method.

Results

A total of 216 fishes from 23 species were successfully photographed and used in this study (*Table 1*). However, due to the preservation techniques, damage from capture, and curvature of specimens, only body shape was included in the three morphometric analyses, as the remaining morphological features (i.e., fins and barbels) could not be consistently imaged. Therefore, the image analysis techniques used would not have been accurate.

Testing vs. Taxonomy

Shape Indicator Measurements

Seven of the fifteen SIM equations were excluded from this study due to the covariation between the SIMs. The eight SIMs and their equations used within this study are listed in *Table 2*.

PC 1 and PC 2 together explained 75.7% of the cumulative variance in the data, with Eccentricity Bounding Box (EBB; correlation = -0.459) and Elongation (EL; correlation = 0.459), creating the strongest correlation along PC 1. Rectangularity (REC; correlation = -0.674) and Solidity (SOL; correlation = -0.620) correlated most strongly with PC 2 (*Figure 16*). The EBB (i.e., length and width ratio; *Table 2*) and EL (i.e., the lengthening of an object; *Table 2*) of individuals were responsible for the largest shape variation along PC 1. Species that exhibited higher EBB measurements (e.g., *Argyropelecus aculeatus* and *Polyipnus clarus)* had lower EL values, and vice versa (e.g., *Stomias affinis and Chauliodus sloani*) had the lowest EBB. The length and width of stomiiform fishes had the strongest effect on PC 1 (*Figure 16(a)).*

As expected, the ANOSIM results showed significant effects of taxonomy (i.e., species, genus, family) on stomiiform fishes body morphology (p = 0.001; *Table 3*). Genus was observed to significantly effect SIMs (ANOSIM: Global R = 0.614; p = 0.001; *Table 3*) and formed the strongest groupings (*Figure 16(b)*). The genera of *Maurolicus* and *Sternoptyx* formed the largest amount of pairwise perfect separation between groupings (Pairwise ANOSIM: R = 1.0; p = 0.001; *Figure 13*; *Figure 14*; *Figure 16(b)*). *Chauliodus*, *Photostomias*, and *Pollichthys* individuals formed more separation within their groups than in between groupings (Pairwise ANOSIM results are shown in *Figure 13* and *Figure 14*). The differences of body morphology among genera were driven by caliper size (SIMPER: 5.38-25.78% dissimilarity), centroid size

(SIMPER: 1.68-7.13% dissimilarity), and Haralick circularity (SIMPER: 0.01-0.02 % dissimilarity).

Of the three taxonomic resolutions assessed, species had the second largest effect on body morphology (ANOSIM: Global R = 0.601; p = 0.001; *Table 3*). *Argyropelecus aculeatus*, *Cyclothone alba*, *Sternoptyx diaphana*, and *Sternoptyx pseudobscura* were species that formed the strongest intra-specific groupings (Pairwise ANOSIM: R = 1.0; p = 0.001; *Figure 11*; *Figure 12*; *Figure 16(a)*). *Argyropelecus* spp., *Cyclothone* spp., *Vinciguerria* spp., *Chauliodus sloani*, *Photostomias guernei*, and *Pollichthys mauli* formed the strongest inter-specific groupings (Pairwise ANOSIM results are shown in *Figure 11* and *Figure 12*). Additionally, *Cyclothone pallida* and *Sigmops elongatus* individuals formed no differences between or among their groupings (Pairwise ANOSIM: R = 0; p = 0.417; *Figure 16(a)*) and were indistinguishable from other fishes' by body shape. The SIMPER results showed the three SIMs contributing the most to dissimilarity between stomiiform fish body shapes: 1) caliper size (SIMPER: 6.03-25.76% dissimilarity), 2) centroid size (SIMPER: 1.82-7.73% dissimilarity), and 3) Haralick circularity (SIMPER: 0.01-0.03% dissimilarity), which are associated with elongated and circular bodies.

Family had a significant effect on SIMs (Global R = 0.408; p = 0.001; *Table 3*). Families Gonostomatidae and Phosichthyidae formed insignificant intra-specific groupings (Pairwise ANOSIM: R = 1.0; p = 0.001; *Figure 15*; *Figure 16(c)*). As expected, the significance of SIMs improved with increasing taxonomic rank. Similarly, to species and genus the SIMs that contributed the most to dissimilarity within body morphology were caliper size (SIMPER: 11.50-18.98% dissimilarity), centroid size (SIMPER: 3.45-5.05% dissimilarity), and Haralick circularity (SIMPER: 0.00-0.02% dissimilarity). Overall, the stomiiform fishes body morphology formed groupings between their taxonomic ranks driven by differences in caliper size, centroid size, and Haralick circularity.

Table 3 - Global ANOSIM results from taxonomic rank assessment of shape indicator measurements using a Bray Curtis matrix. Pairwise groupings were tested as unordered factors. The bolded R statistics and their corresponding p-values are those that were significant on the p-value ($p \leq 0.05$).

Taxonomic Rank	Global R Statistic	p-value
Species	**0.601**	**0.001**
Genus	**0.614**	**0.001**
Family	**0.408**	**0.001**

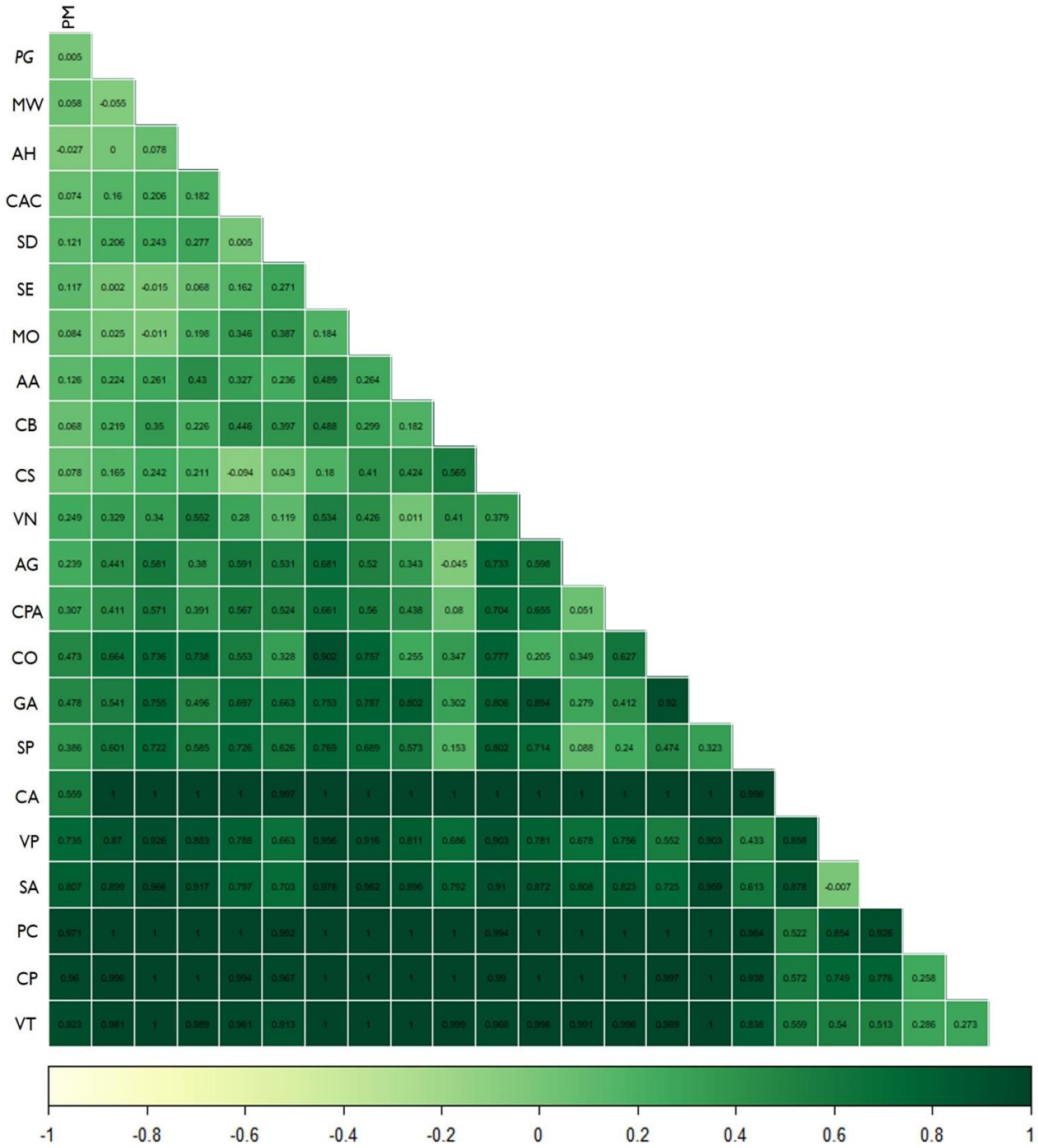

Figure 11 - Correlation matrix of ANOSIM R statistics from species assessment of shape indicator measurements using a Bray Curtis matrix. Pairwise groupings were tested as unordered factors. The colored squares represented the significance of the values. The darker colored squares represented higher R statistics and the lighter colored squares represented lower values. Species and genus identifiers followed descriptions in Table 1.

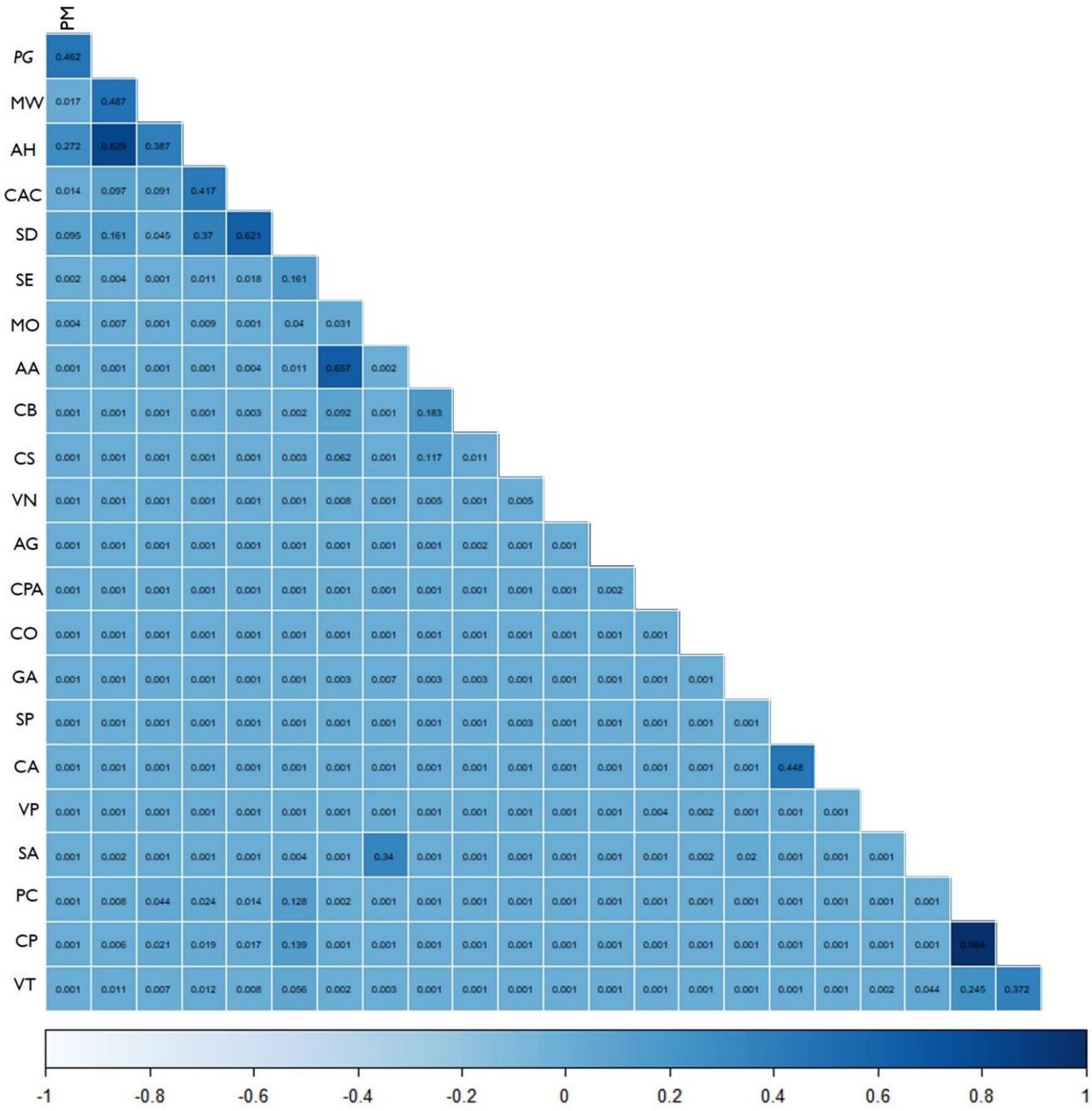

Figure 12 - Correlation matrix of ANOSIM p-values from species assessment of shape indicator measurements using a Bray Curtis matrix. Pairwise groupings were tested as unordered factors. The colored squares represented the significance of the values. The darker colored squares represented higher p-values and the lighter colored squares represented lower values. Significant p-values are those that had a value less than 0.05. Species and genus identifiers followed descriptions in Table 1.

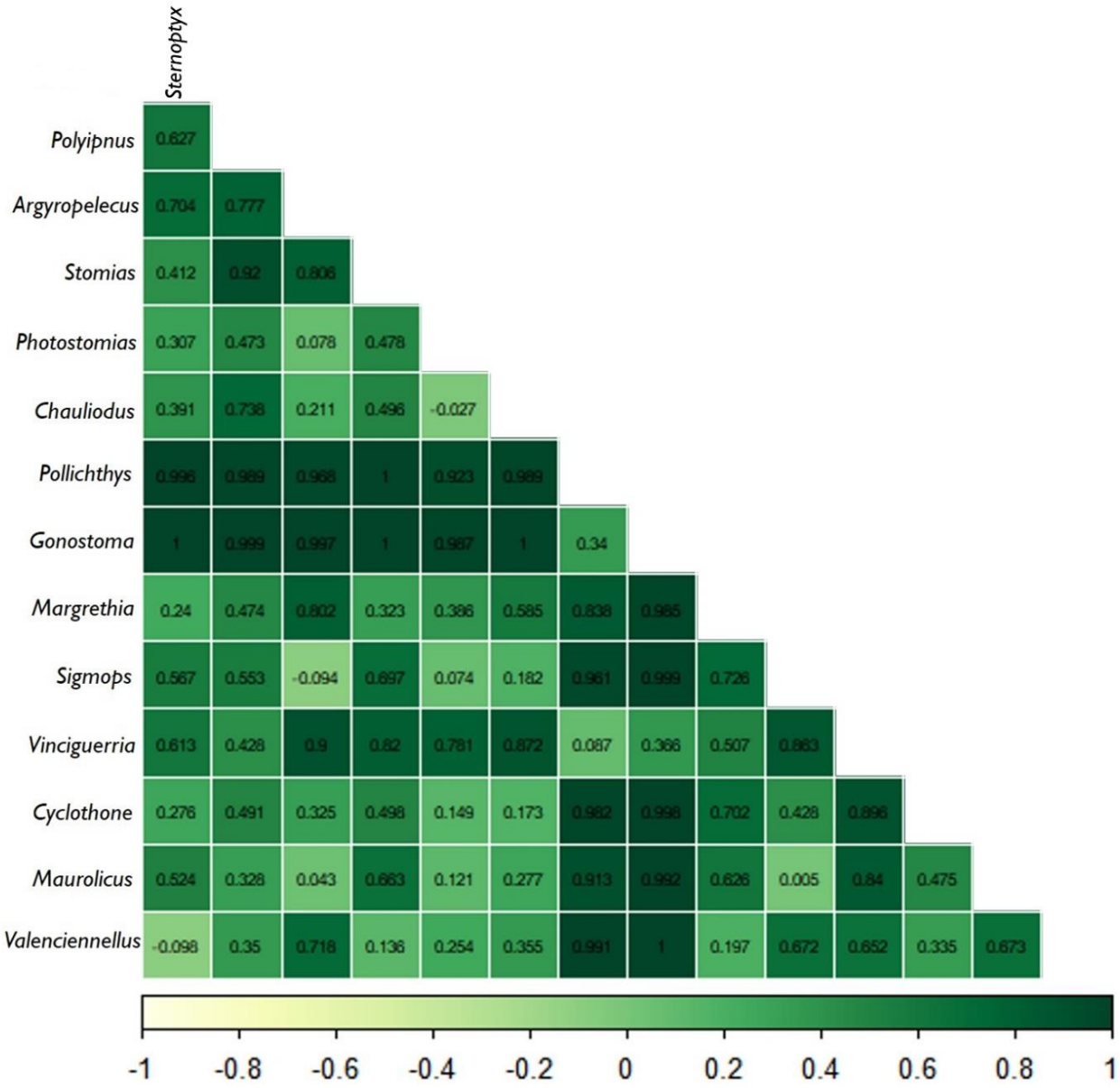

Figure 13 - Correlation matrix of ANOSIM R statistics from genus assessment of shape indicator measurements using a Bray Curtis matrix. Pairwise groupings were tested as unordered factors. The colored squares represented the significance of the values. The darker colored squares represented higher R statistics and the lighter colored squares represented lower values.

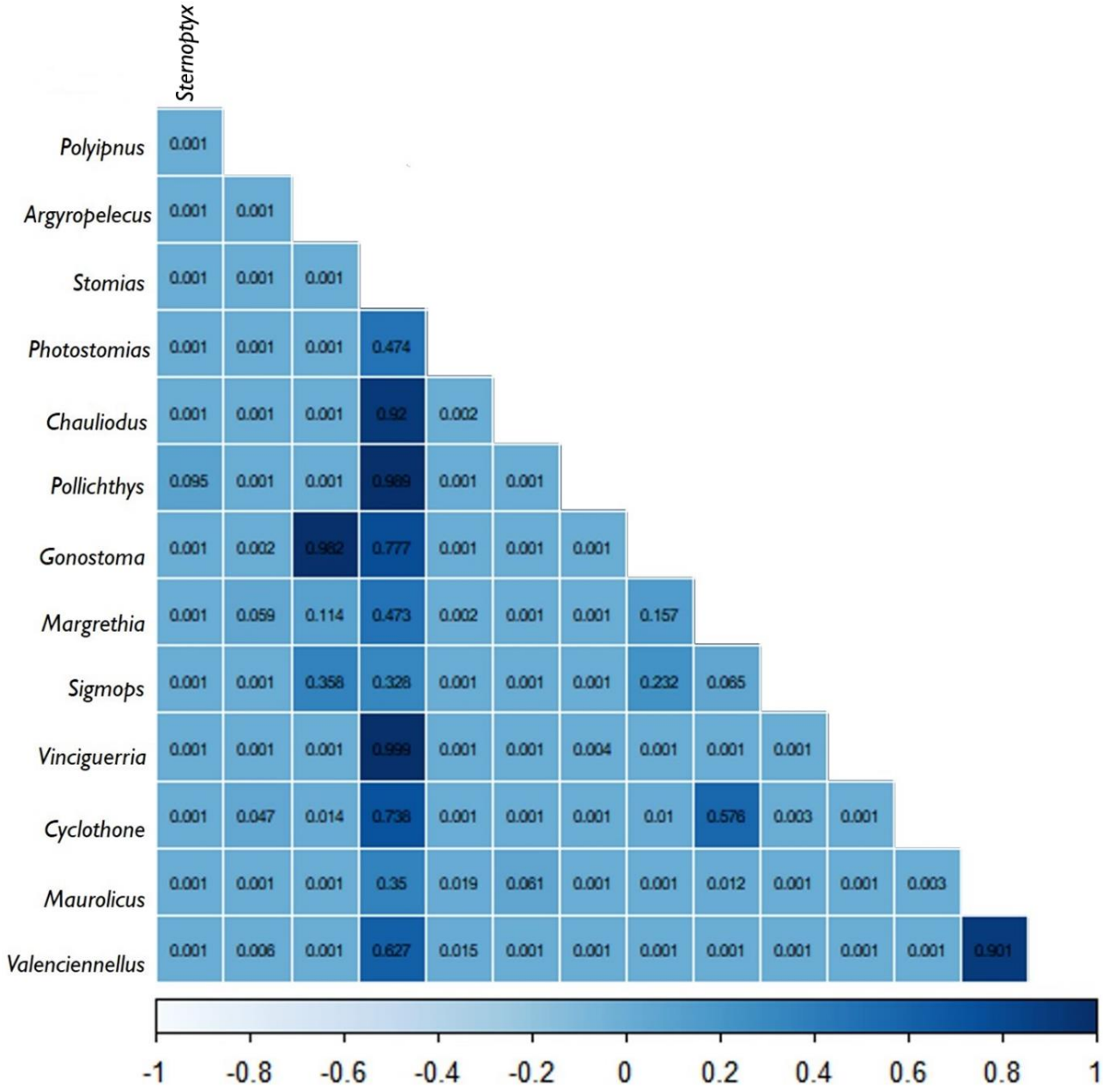

Figure 14 - Correlation matrix of ANOSIM p-values from genus assessment of shape indicator measurements using a Bray Curtis matrix. Pairwise groupings were tested as unordered factors. The colored squares represented the significance of the values. The darker colored squares represented higher p-values and the lighter colored squares represented lower values. Significant p-values are those that had a value less than 0.05.

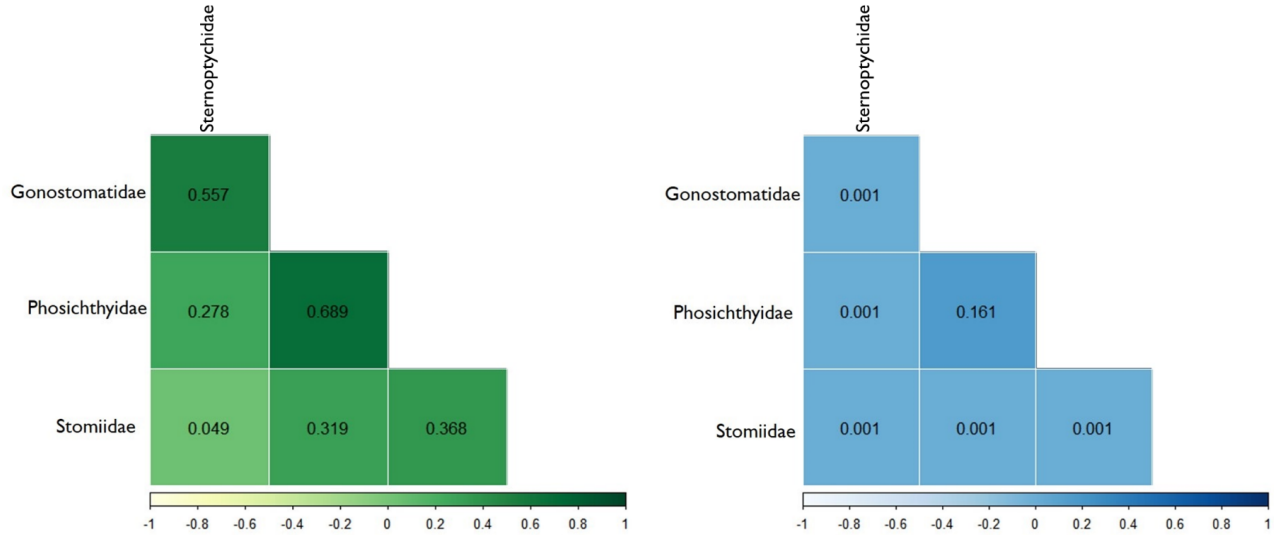

Figure 15 - Correlation matrix of ANOSIM results from family assessment of shape indicator measurements using a Bray Curtis matrix. Pairwise groupings were tested as unordered factors. Figure A represents the R statistic values and Figure B represents the corresponding p-values. The colored squares represented the significance of the values. The darker colored squares represented higher R statistics and p-values and the lighter colored squares represented lower values. Significant p-values are those that had a value less than 0.05.

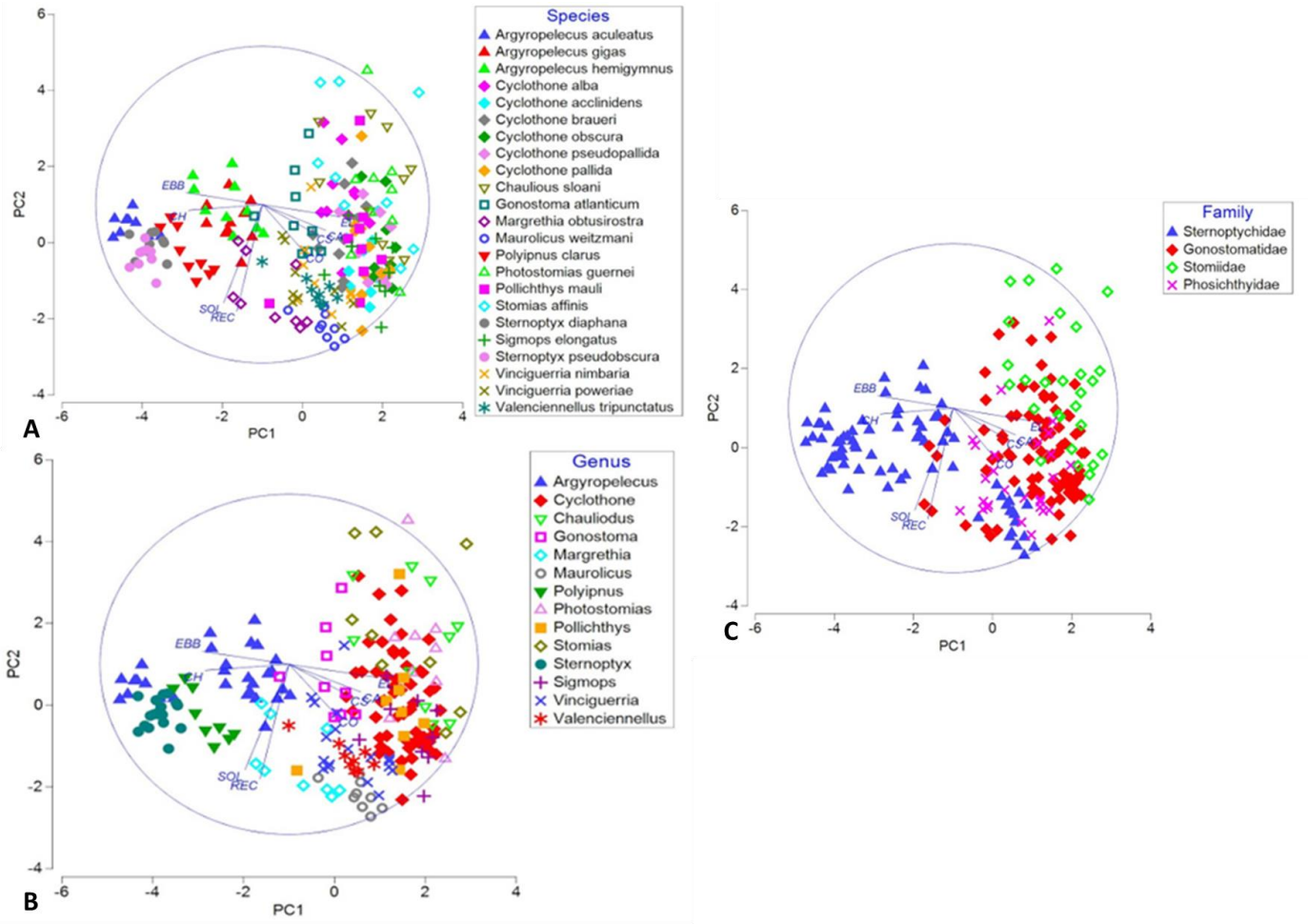

Figure 16 - Normalized principal component analysis of species (a), genus (b), and family (c) through shape indicator measurements. PC 1 explained 52.4% of the variance within the data, and PC 2 explained 23.2% of the variance within the data. Caliper size (CA), centroid size (CS), Haralick circularity, (CH), convexity (CO), eccentricity bounding box (EBB), elongation (EL), rectangularity (REC), and solidity (SOL). All genera were represented by a different symbol shape.

Landmark Configuration Analysis

Using the Mahalanobis distance, the landmarks for all 216 individuals were assessed for outliers. The species assessed within this study exhibited a large variety of body shapes. No observations were found to have deviated from the mean, therefore no landmarks were excluded from this study.

A principal component shape changes, or "wireframe" analysis, (*Figure 17*) was conducted within MorphoJ and represented the mean landmark outline calculated from the Procrustes superimposition of all fishes from this study's sample set. The wireframe analysis represented how the landmark locations changed along PC 1 (x-axis) and PC 2 (y-axis). Overall, for PC 1 and PC 2 landmark five (i.e., insertion of the pelvic fin; *Figure 9*) showed the most variation between species (i.e., the longest line/deviation from the mean landmark positions). The landmark with the second-largest shape change for PC1 was landmark one (i.e., the snout tip; *Figure 9*), followed by landmark two (i.e., the anterior insertion of the first dorsal fin), landmark three (i.e., the dorsal insertion of the caudal fin), and finally, landmark four (i.e., ventral insertion of the caudal fin) for all species. Overall, landmark five showed the largest variation along PC 1 and PC2 from the average body shape of fishes assessed in this study. The largest differences between PC 1 and PC 2 were the landmarks following the largest shape change (i.e., landmark five). Where PC 1 landmark changes from the largest to smallest variations: 1) landmark five; 2) landmark one; 3) landmark two; 4) landmark three; and 5) landmark four, and PC 2 changes were as follows: 1) landmark five; 2) landmark two; 3) landmark one; 4) landmark four; and 5) landmark three (*Figure 23*). Similarly to SIMs results, landmark changes involving the length or elongation of an individual resulted in the greatest changes.

Additionally, a PCA conducted within PRIMER (Clarke & Gorley, 2015) assessed the variation of body shape (through LCA) with regards to an individual's taxonomy (*Figure 23*). PC 1 and PC 2 together explained 72.8% of the cumulative variance in the data. Outliers were removed from the analysis to ensure they were not affecting the results of the PCA. There were no significant differences found with the PCA results when they were removed, and therefore, were included. The y-coordinate homologous landmarks Y1 and Y4 (correlation = -0.453), and Y3 (correlation = -0.457) had the highest absolute values for PC 1. The x-coordinate landmark of

X1 (correlation = 0.302) and the y-coordinate landmark Y4 (correlation = 0.196) had the highest absolute values for PC 2. The shape of stomiiform fish landmarks had the greatest change between individuals along the y-axis for PC 1 and PC 2. The position of the snout tip (i.e., landmark one) and the dorsal and ventral insertion of the caudal fin (i.e., landmarks 3 and 4) were the landmarks that showed the greatest change when compared to taxonomy.

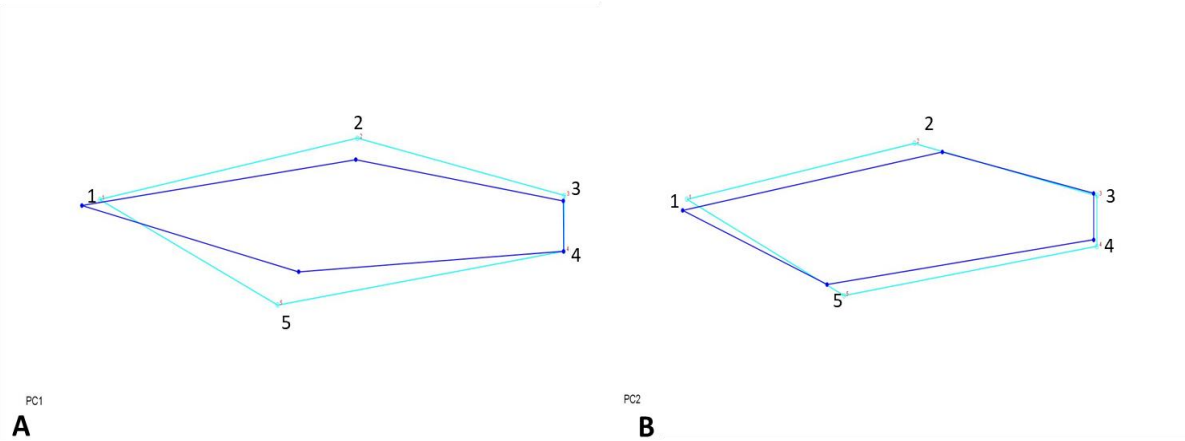

Figure 17 - Principal component analysis on the Procrustes superimposition. The wireframe figures represented the outline of stomiiform fishes body shapes, where the dark blue outline represented the mean outline, and the light blue outline represented the shape variation of the principal components. Figure A depicted the shape changes of PC 1 and Figure B depicted the shape changes of PC 2.

Species had a significant effect on landmark placement (ANOSIM: Global R = 0.551; p = 0.001; *Figure 23(a)*; *Table 4*). Perfect separation was observed when *Sternoptyx diaphana* and *Sternoptyx pseudobscura* individuals were compared to other species from different families (ANOSIM: R = 1.0; p = 0.001; *Figure 18*; *Figure 19*). The three highest contributing landmark coordinates to dissimilarity between body shapes were X4 (SIMPER: 1.16-2.85% dissimilarity), X3 (SIMPER: 1.80-2.08% dissimilarity), and X1 (SIMPER: 0.66-2.26% dissimilarity). The x-coordinates contributed more to the dissimilarity of species within this study.

A significant effect of genus on landmarks was observed (ANOSIM: Global R = 0.609; p = 0.001; *Figure 23(b)*; *Table 4)*. The genera of *Photostomias* and *Sternoptyx* individuals resulted in perfect separation between genera, making them more distinct from one another (Pairwise ANOSIM: R = 1.0; P = 0.001; *Figure 20*; *Figure 21*). Similar to species, the three highest landmark coordinates contributing to dissimilarity were X4 (SIMPER: 1.27-3.28% dissimilarity), X3 (SIMPER: 1.21-3.30 % dissimilarity), and X2 (SIMPER: 1.12-2.67 % dissimilarity).

Family had a significant effect on landmarks (ANOSIM: Global R = 0.390; p = 0.001; *Figure 23(c)*; *Table 4*) Sternoptychidae and Stomiidae formed the strongest groupings between families (Pairwise ANOSIM: R = 0.672; p = 0.001; *Figure 22*). Gonostomatidae and Phosichthyidae families formed the weakest groupings (Pairwise ANOSIM: R = 0.163; p = 0.002). The landmark coordinates that contributed the most to separation between body shapes were X2 (SIMPER: 0.87-2.91% dissimilarity), X3 (SIMPER: 1.82-2.83% dissimilarity), and X4 (SIMPER: 1.62-2.87% dissimilarity).

The centroid size and body shape of the average Procrustes landmarks significantly differed with the taxonomic rank of an individual (p = <0.0001; *Tables 5-6*).

Table 4 - Global ANOSIM results from taxonomic rank assessment of landmark configuration analysis using a Bray Curtis matrix. Pairwise groupings were tested as unordered factors. The bolded R statistics and their corresponding p-values are those that were significant on the p-value ($p \leq 0.05$).

Taxonomic Rank	Global R Statistic	p-value
Species	**0.551**	**0.001**
Genus	**0.609**	**0.001**
Family	**0.39**	**0.001**

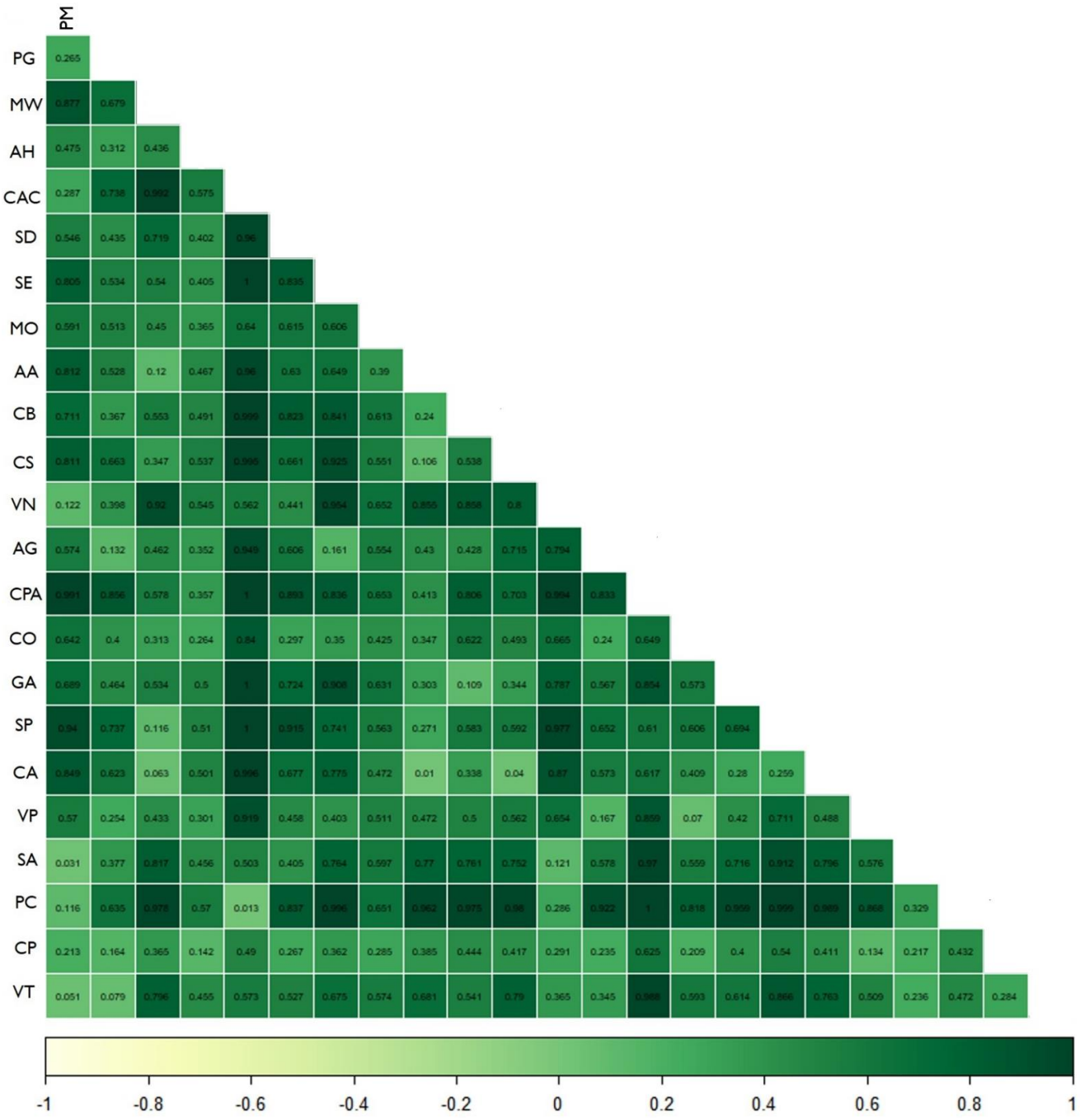

Figure 18 - Correlation matrix of ANOSIM R statistics from species assessment of landmark configuration analysis using a Bray Curtis matrix. Pairwise groupings were tested as unordered factors. The colored squares represented the significance of the values. The darker colored squares represented higher R statistics and the lighter colored squares represented lower values. Species and genus identifiers followed descriptions in Table 1.

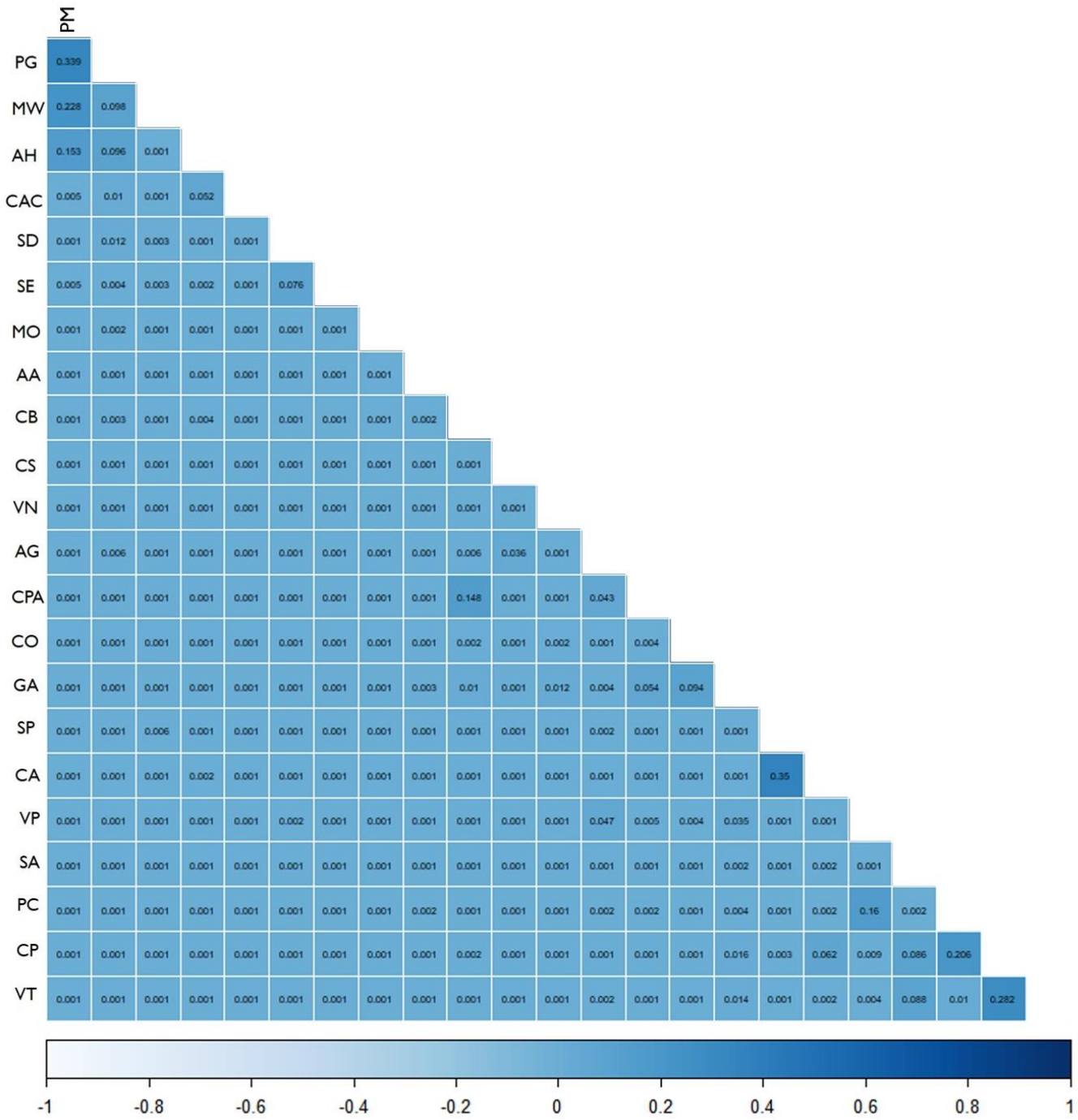

Figure 19 - Correlation matrix of ANOSIM p-values from species assessment of landmark configuration analysis using a Bray Curtis matrix. Pairwise groupings were tested as unordered factors. The colored squares represented the significance of the values. The darker colored squares represented higher p-values and the lighter colored squares represented lower values. Significant p-values are those that had a value less than 0.05. Species and genus identifiers followed descriptions in Table 1.

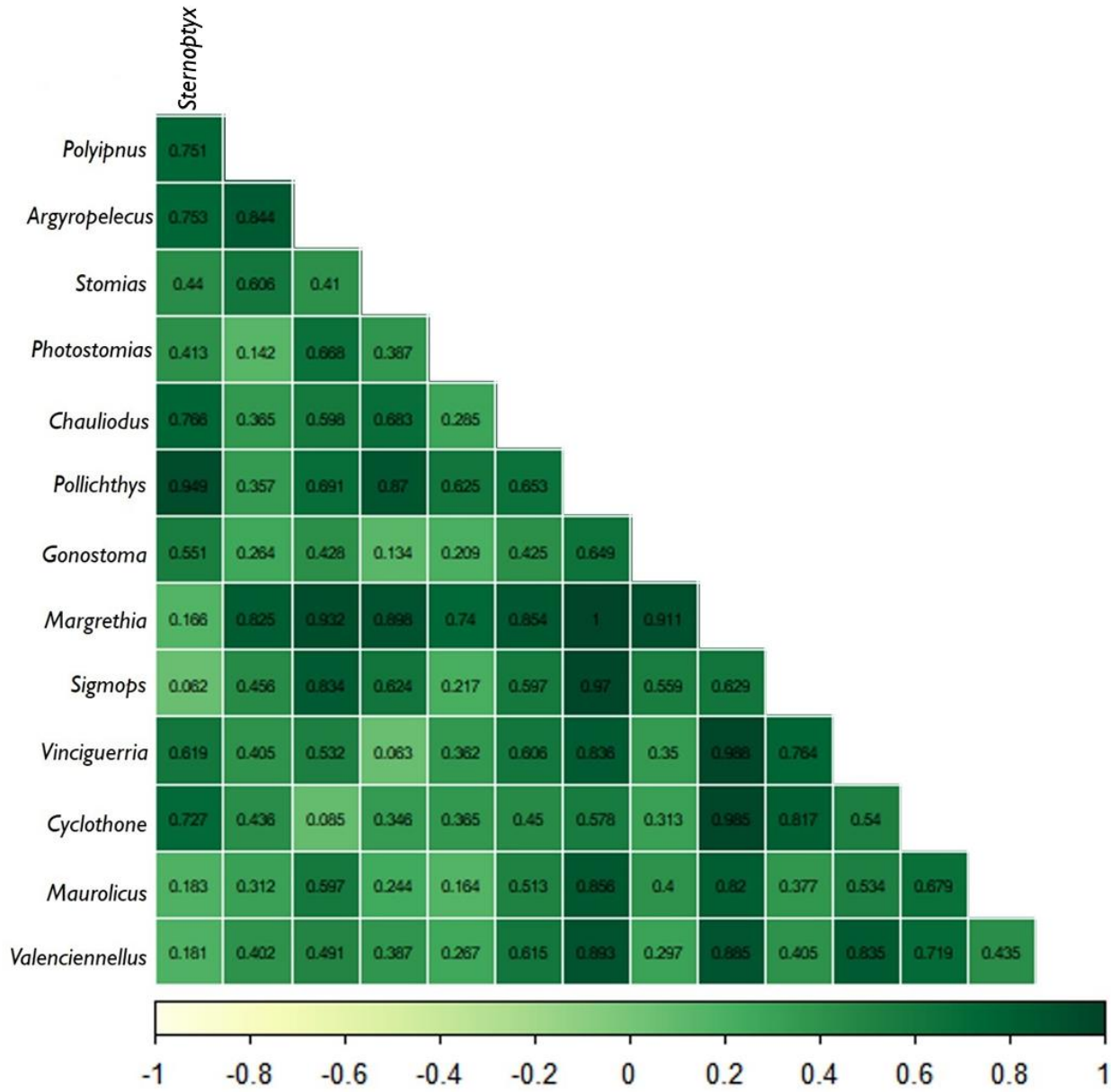

Figure 20 - Correlation matrix of ANOSIM R statistics from genus assessment of landmark configuration analysis using a Bray Curtis matrix. Pairwise groupings were tested as unordered factors. The colored squares represented the significance of the values. The darker colored squares represented higher R statistics and the lighter colored squares represented lower values.

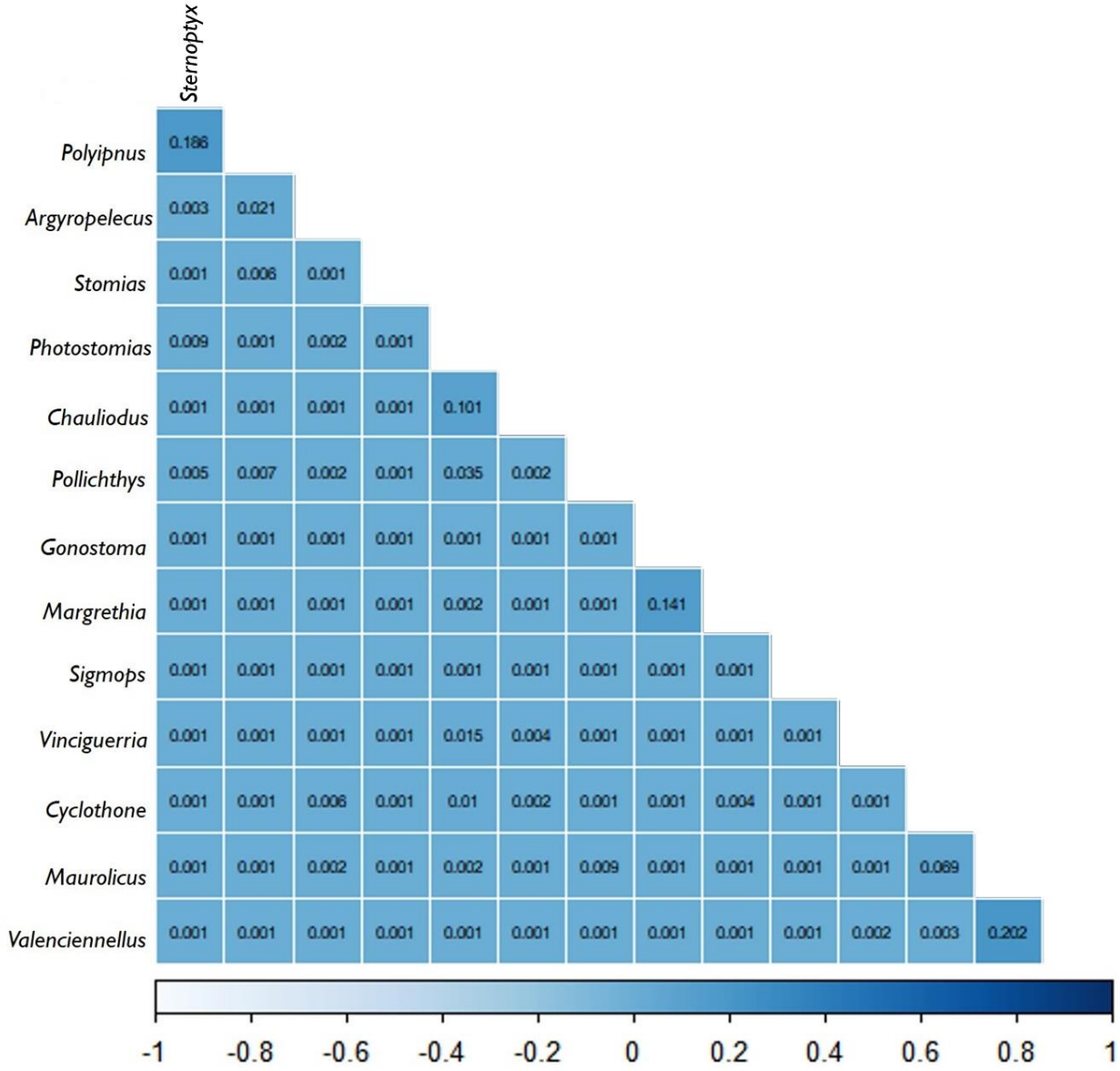

Figure 21 - Correlation matrix of ANOSIM p-values from genus assessment of landmark configuration analysis using a Bray Curtis matrix. Pairwise groupings were tested as unordered factors. The colored squares represented the significance of the values. The darker colored squares represented higher p-values and the lighter colored squares represented lower values. Significant p-values are those that had a value less than 0.05.

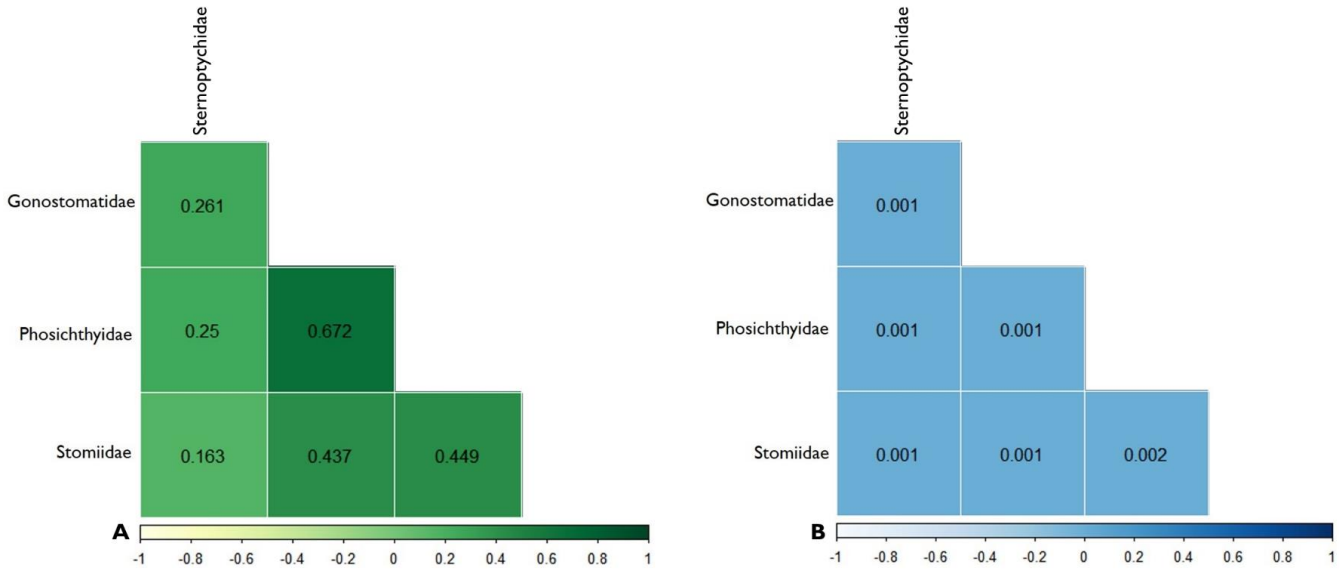

Figure 22 - Correlation matrix of ANOSIM results from family assessment of landmark configuration analysis using a Bray Curtis matrix. Pairwise groupings were tested as unordered factors. Figure A represents the R statistic values and Figure B represents the corresponding p-values. The colored squares represented the significance of the values. The darker colored squares represented higher R statistics and p-values and the lighter colored squares represented lower values. Significant p-values are those that had a value less than 0.05.

Table 5 - Procrustes ANOVA of Centroid Size

Effect	SS	MS	df	F	P (param.)
Family	394.795	131.598	3	14.86	<0.0001
Genus	542.812	41.755	13	21.91	<0.0001
Species	329.580	17.346	19	9.18	<0.0001
Residuals	364.801	1.890	193		

Table 6 - Procrustes ANOVA of Body Shape

Effect	SS	MS	df	F	P (param.)	Pillai tr.
Family	7.356	0.409	18	8.16	<0.0001	3.14
Genus	12.878	0.165	78	126.70	<0.0001	3.41
Species	11.352	0.099	114	82.83	<0.0001	3.38
Residuals	1.392	0.001	1158			

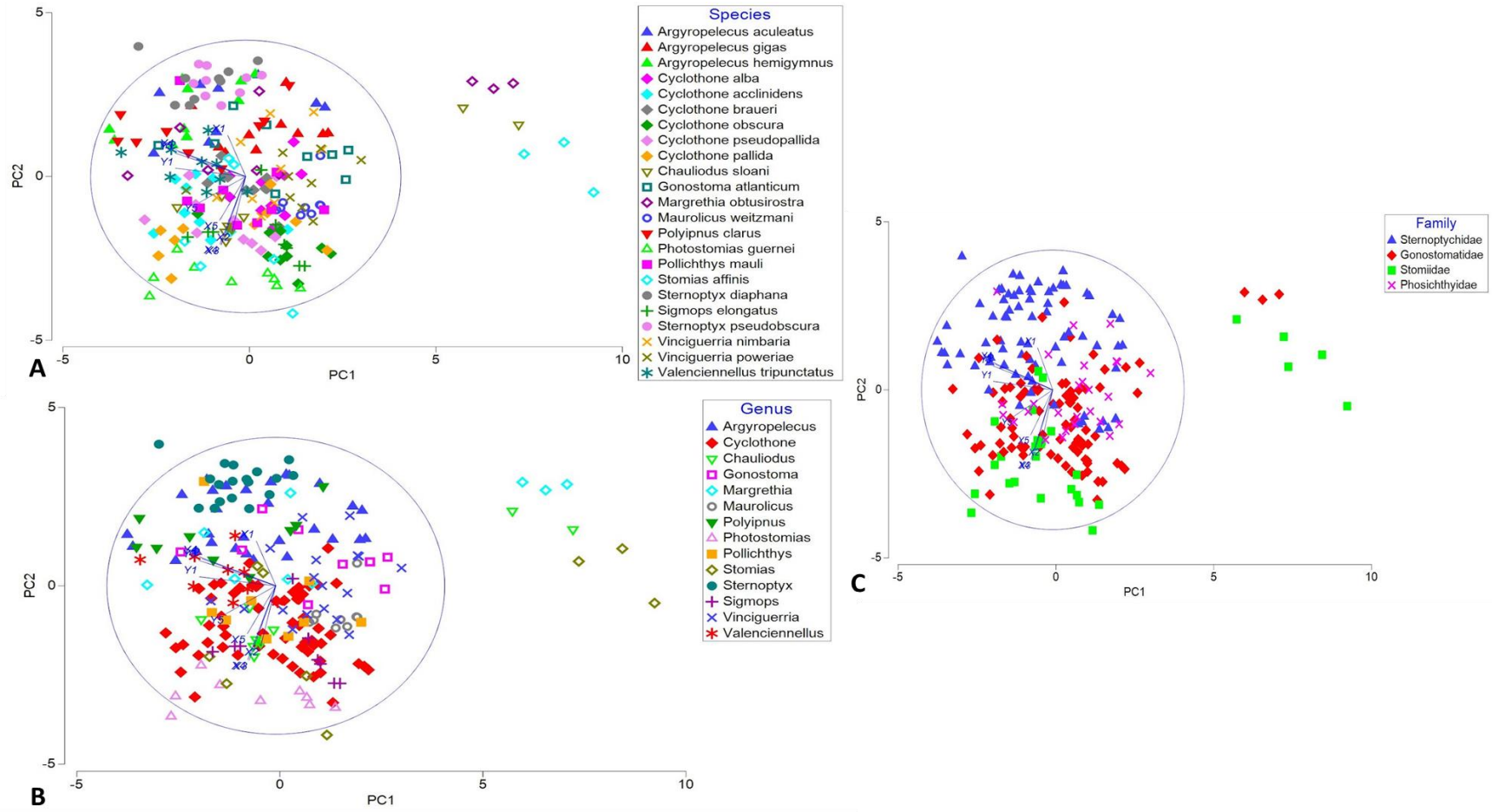

Figure 23 - Normalized principal component analysis of species (a), genus (b), and family (c) through landmark configuration analysis. PC 1 explained 40.2% of the variance within the data, and PC 2 explained 32.6% of the variance within the data. X-coordinate of landmark one (X1), Y-coordinate of landmark one (Y1), X-coordinate of landmark two (X2), Y-coordinate of landmark two (Y2), X-coordinate of landmark three (X3), Y-coordinate of landmark three (Y3), X-coordinate of landmark four (X4), Y-coordinate of landmark four (Y4), X-coordinate of landmark five (X5), Y-coordinate of landmark five (Y5). All genera were represented by a different shaped symbol.

Outline Analysis

The fish outlines were described to 99% accuracy using eleven harmonic coefficients defined by Elliptical Fourier Analysis (*Figure 24*). I opted not to use 100% accuracy (12 harmonic coefficients) due to the risk of overfitting the outlines. The reconstructed shapes using 11 harmonic coefficients can be viewed in *Figures 25-26*.

A PCA conducted within R using the Momocs package (ver. 4.0.2; R Core Team, 2020) used 11 EFA harmonics to compare stomiiform fish body shapes. PC 1 and PC 2 together explained 81% of the cumulative variance in the shape data. PCs 1-11 represented 99% of the cumulative variance in the data (*Figures 32-34*) and were extracted for multivariate analyses in PRIMER v7 software.

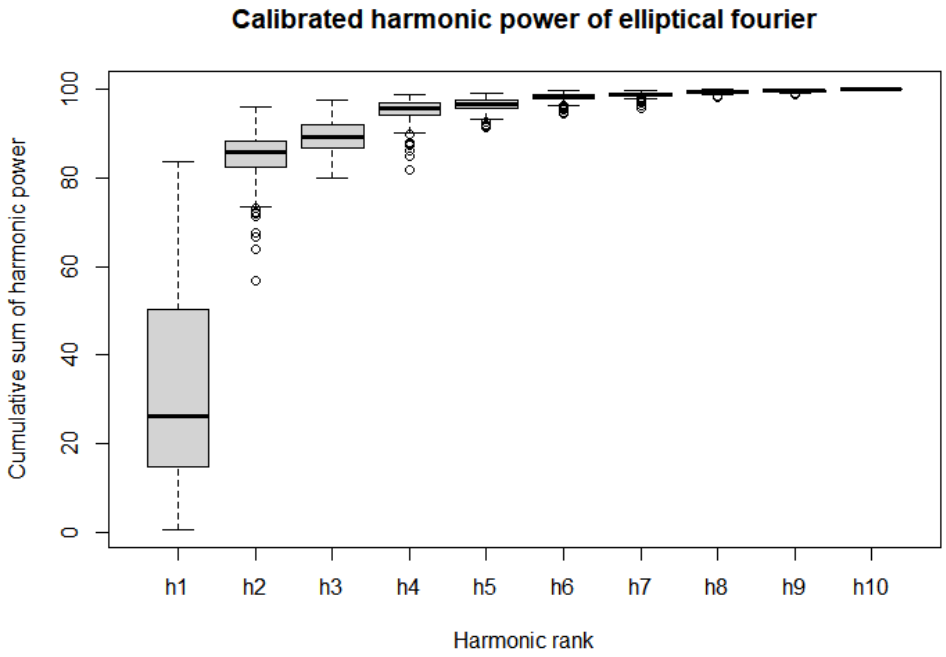

Figure 24 - Box and whisker plot of calibrated harmonic power for the elliptical Fourier analysis.

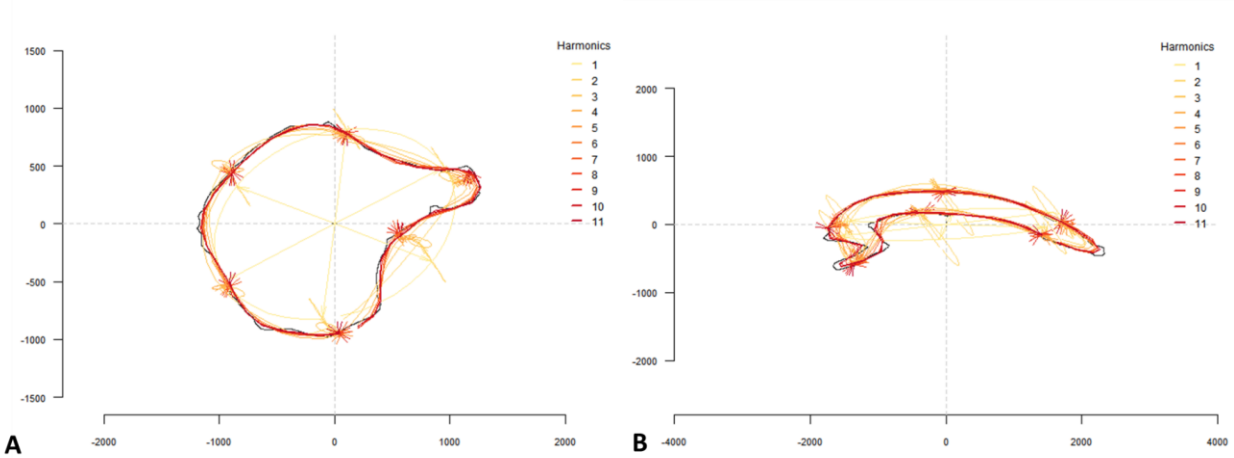

Figure 25 - Ptolemy figures of the species Argyropelecus aculeatus and Photostomias guernei. Figure A represented 11 harmonics quantifying 99% of the cumulative harmonic power for Argyropelecus aculeatus individuals. Figure B represented 11 harmonics quantifying 99% of the cumulative harmonic power for Photostomias guernei individuals. The scale of each figure were estimated as the magnitude of the semi-major axis of the ellipse as defined by the first harmonic.

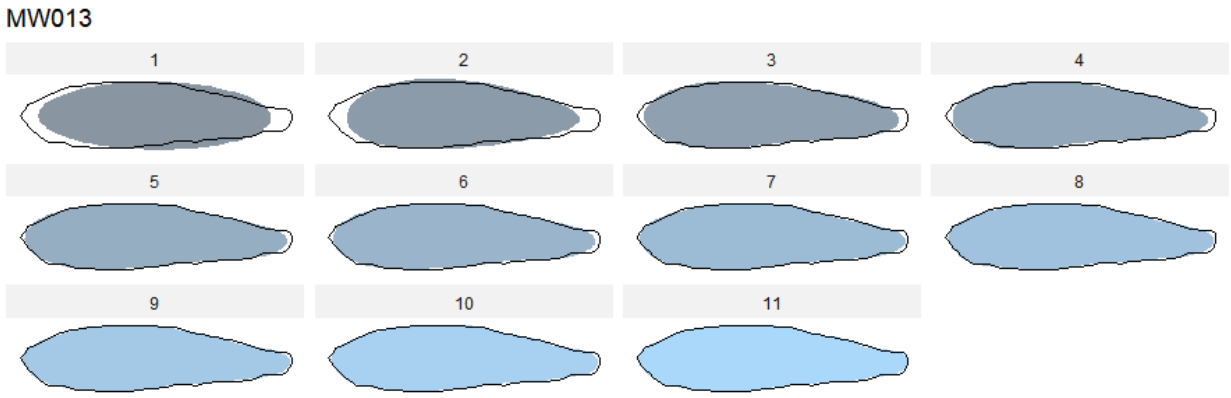

Figure 26 - Example showing the shape each harmonic represented when quantifying a Maurolicus weitzmani outline. 11 harmonics were chosen to retain 99% of the cumulative harmonic power. The gray and blue shapes were the quantified outline with increasing numbers of Fourier harmonics.

Taxonomic comparisons (i.e., species, genus, family) showed significant effects on the body shape of stomiiform fishes (ANOSIM: p = 0.001; *Table 7*). Overall, species significantly affected an individual's shape based on EFA (ANOSIM: Global R = 0.296; p = 0.001; *Figure 27*; *Figure 28*; *Figure 32*), however, pairwise comparisons between *Cyclothone* spp., *Argyropelecus* spp., and *Chauliodus sloani* individuals formed weaker inter-specific groupings (Pairwise

ANOSIM results are shown in *Figure 27* and *Figure 28*). Unlike the ANOSIM results from SIMs and LCA, no pairwise species comparisons resulted in perfect separation.

Genus had a significant effect on an individual's harmonics (ANOSIM: Global R = 0.387; p = 0.001; *Figure 29*; *Figure 30*; *Figure 33)*. *Cyclothone*, *Pollichthys*, *Gonostoma*, and *Margrethia* resulted in statistically insignificant groupings defined by their genera (p > 0.05; Pairwise ANOSIM results are shown in *Figure 29* and *Figure 30*).

A significant effect of family on body shapes was observed (ANOSIM: Global R = 0.192; p = 0.001; *Figure 34; Table 7*). Relatively strong group separation was observed between Stomiidae and Gonostomatidae families (Pairwise ANOSIM: R = 0.372; p = 0.001; *Figure 31*). The pairwise comparisons between Sternoptychidae and Phosichthyidae (Pairwise ANOSIM: R = -0.025; p = 0.675; *Figure 31*) and Gonostomatidae and Phosichthyidae (Pairwise ANOSIM: R = -0.04; p = 0.717; *Figure 31*) revealed insignificant groupings.

Table 7 - Global ANOSIM results from taxonomic rank assessment of outline analysis using a Bray Curtis matrix. Pairwise groupings were tested as unordered factors. The bolded R statistics and their corresponding p-values are those that were significant on the p-value (p≤0.05).

Taxonomic Rank	Global R Statistic	p-value
Species	**0.296**	**0.001**
Genus	**0.387**	**0.001**
Family	**0.192**	**0.001**

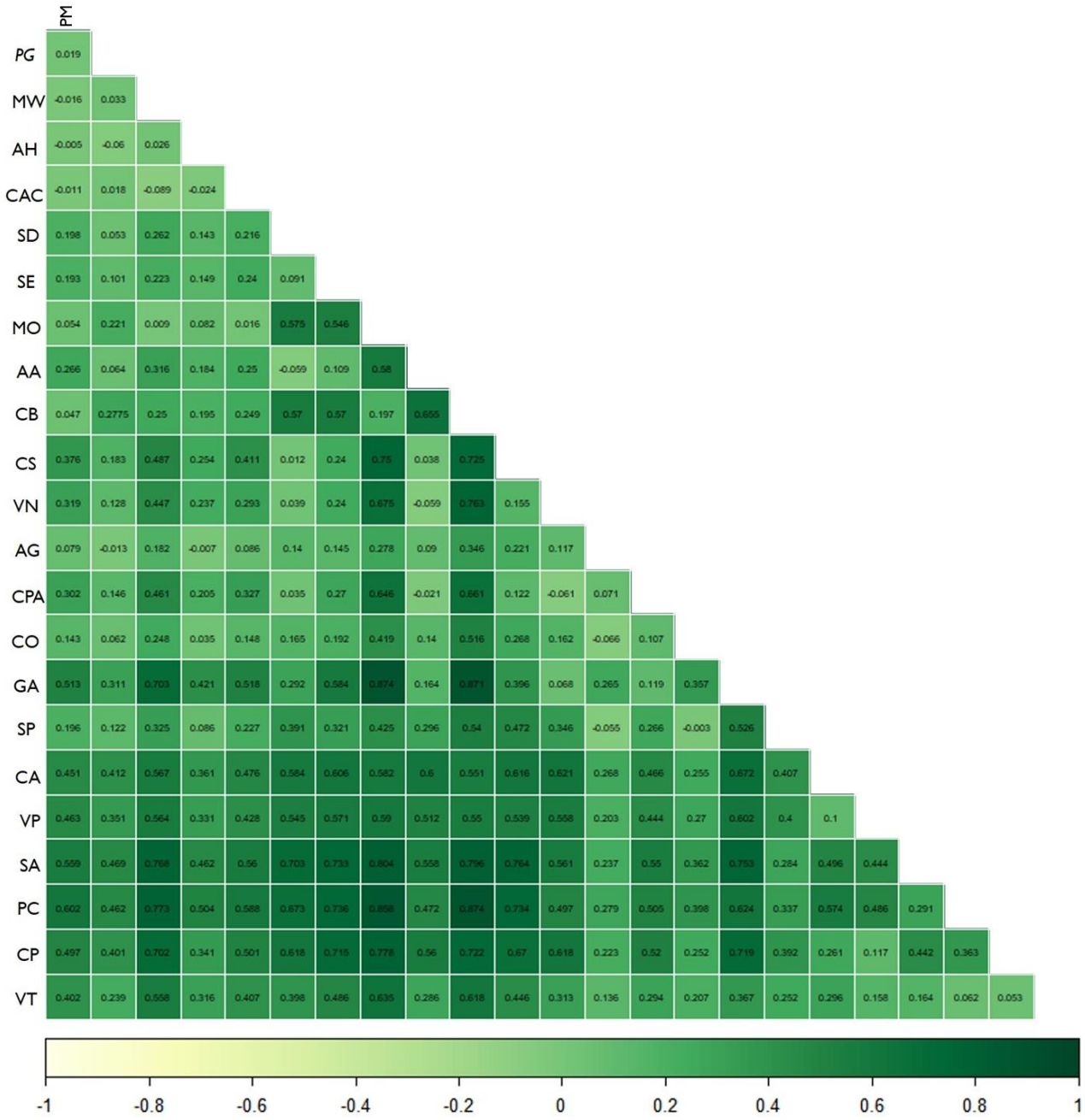

Figure 27 - Correlation matrix of ANOSIM R statistics from species assessment of outline analysis using a Bray Curtis matrix. Pairwise groupings were tested as unordered factors. The colored squares represented the significance of the values. The darker colored squares represented higher R statistics and the lighter colored squares represented lower values. Species and genus identifiers followed descriptions in Table 1.

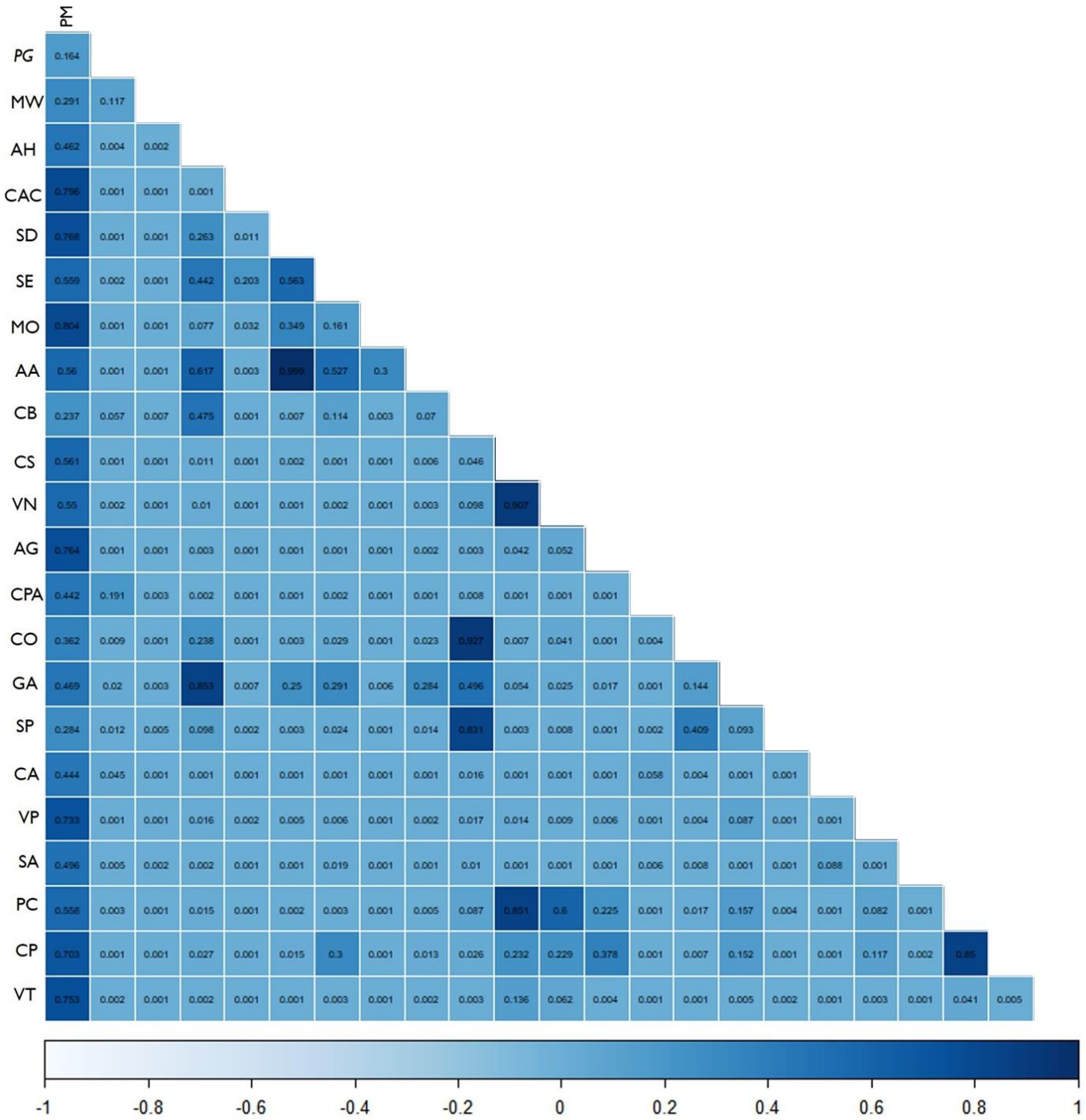

Figure 28 - Correlation matrix of ANOSIM p-values from species assessment of outline analysis using a Bray Curtis matrix. Pairwise groupings were tested as unordered factors. The colored squares represented the significance of the values. The darker colored squares represented higher p-values and the lighter colored squares represented lower values. Significant p-values are those that had a value less than 0.05. Species and genus identifiers followed descriptions in Table 1.

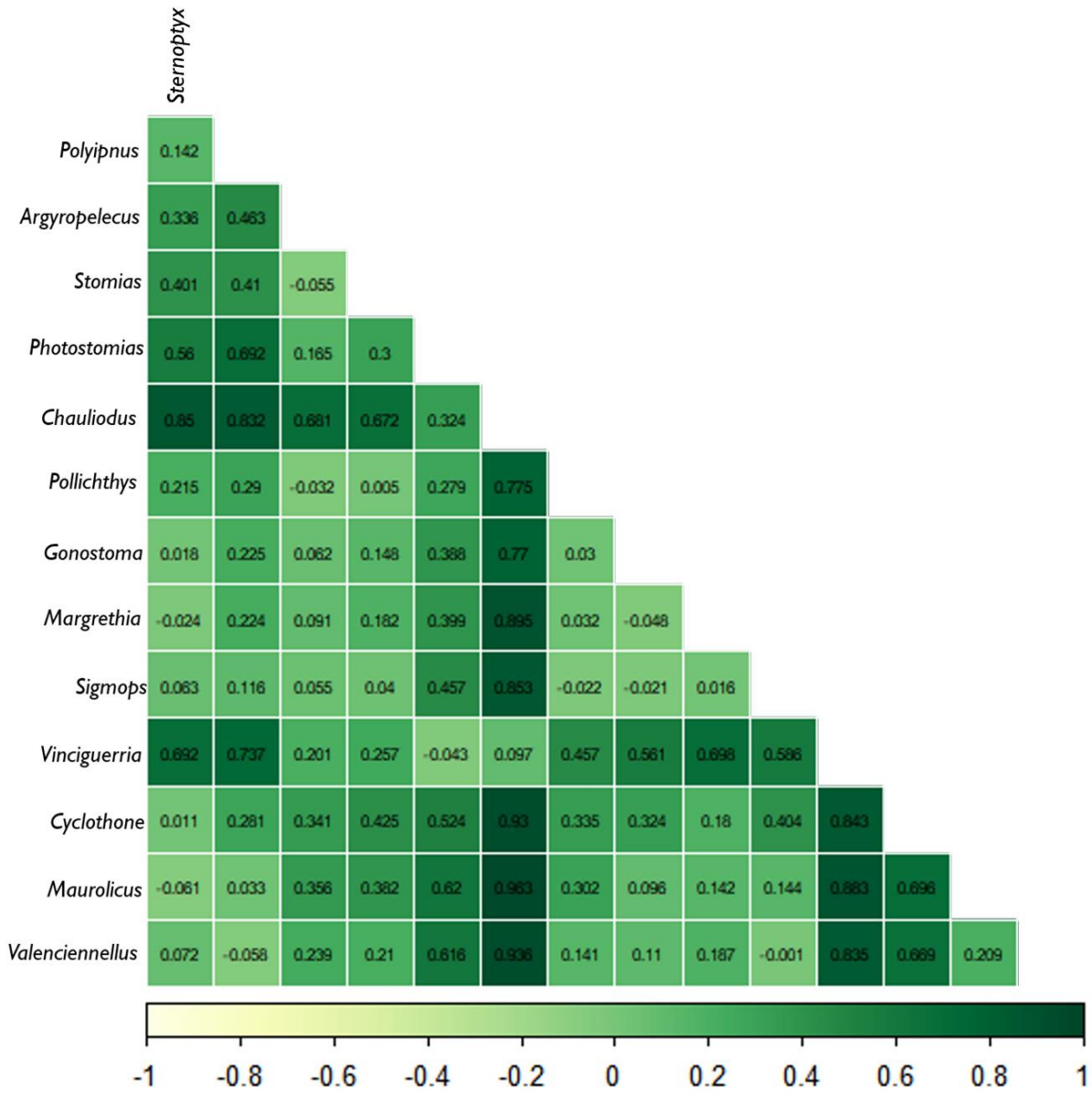

Figure 29 - Correlation matrix of ANOSIM R statistics from genus assessment of outline analysis using a Bray Curtis matrix. Pairwise groupings were tested as unordered factors. The colored squares represented the significance of the values. The darker colored squares represented higher R statistics and the lighter colored squares represented lower values.

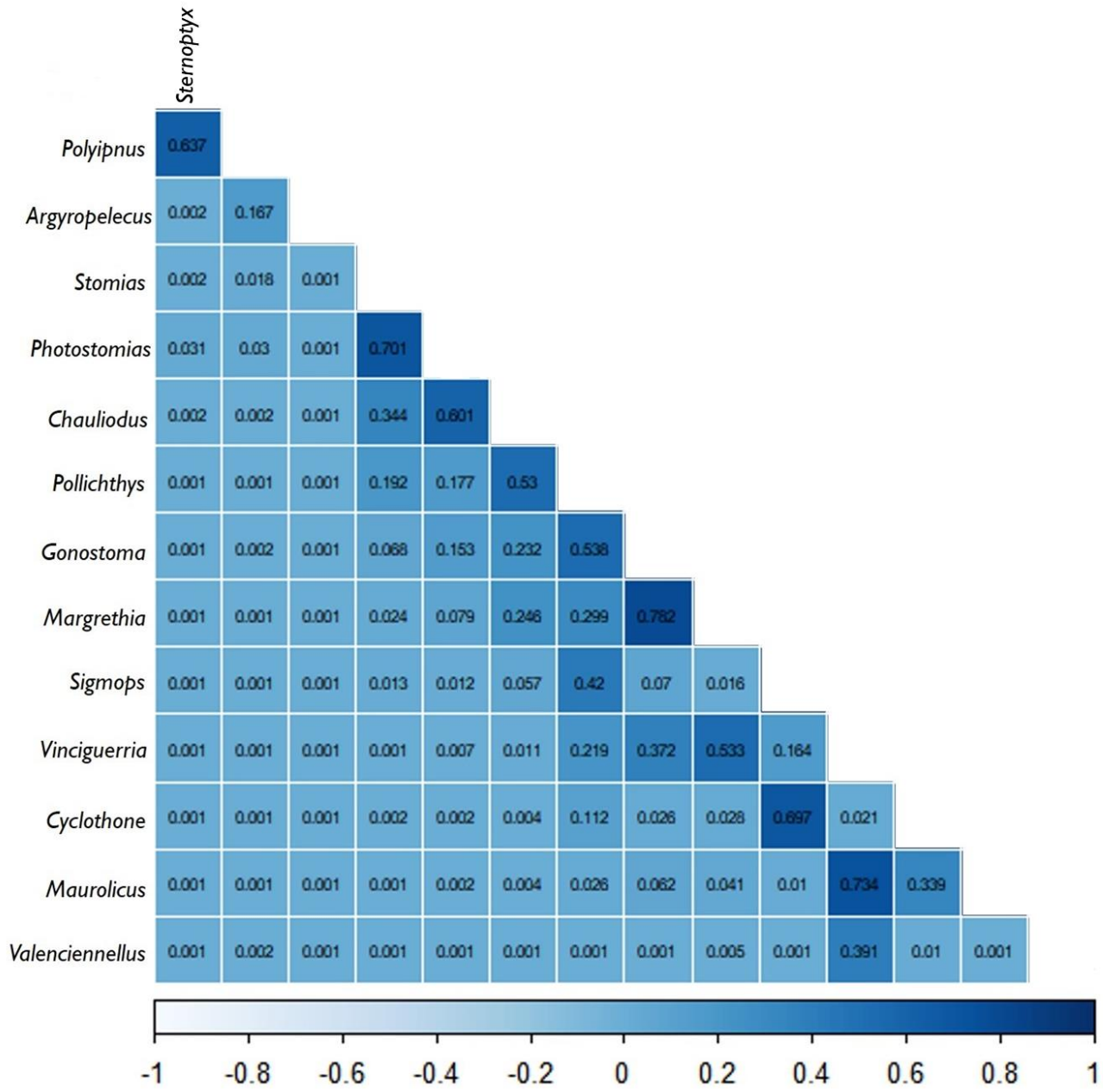

Figure 30 - Correlation matrix of ANOSIM p-values from genus assessment of outline analysis using a Bray Curtis matrix. Pairwise groupings were tested as unordered factors. The colored squares represented the significance of the values. The darker colored squares represented higher p-values and the lighter colored squares represented lower values. Significant p-values are those that had a value less than 0.05.

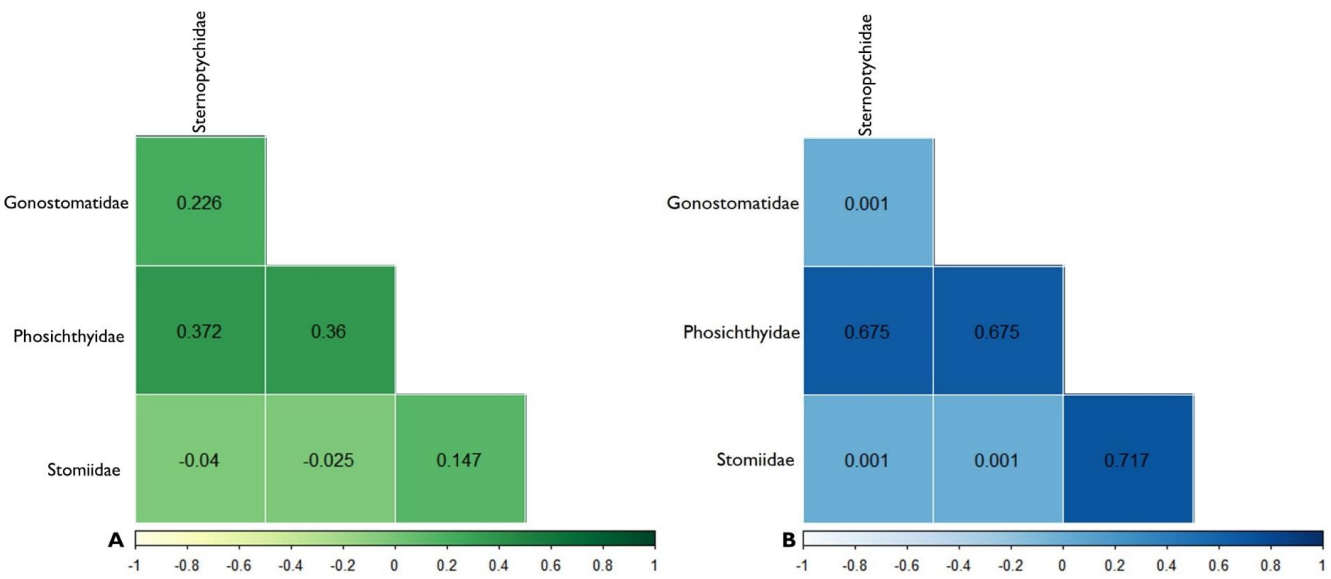

Figure 31 - Correlation matrix of ANOSIM results from family assessment of outline analysis using a Bray Curtis matrix. Pairwise groupings were tested as unordered factors. Figure A represents the R statistic values and Figure B represents the corresponding p-values. The colored squares represented the significance of the values. The darker colored squares represented higher R statistics and p-values and the lighter colored squares represented lower values. Significant p-values are those that had a value less than 0.05.

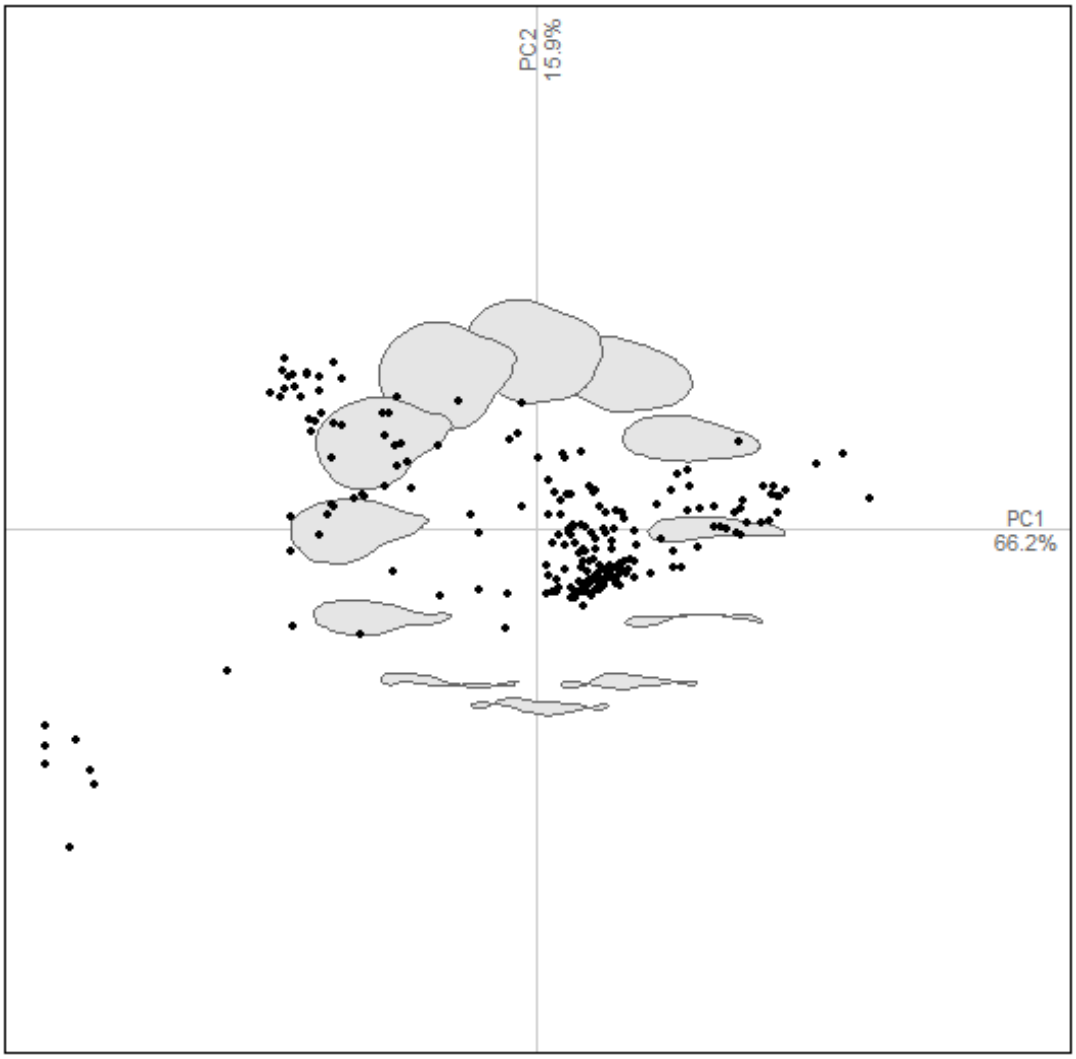

Figure 32 - Normalized PCA-ordinations of body shape among the 23 stomiiform fish species. Numbers next to the axis labels indicated the percentage of explained variation in morphology for that axis in a given ordination (PC 1 = 66% and PC 2 = 16%). Points that fell within the minimum convex polygons represented the realized morphology of body shape for each species. Gray body shape silhouettes depicted the full continuum of morphospace among all species as calculated using harmonic coefficients through EFA.

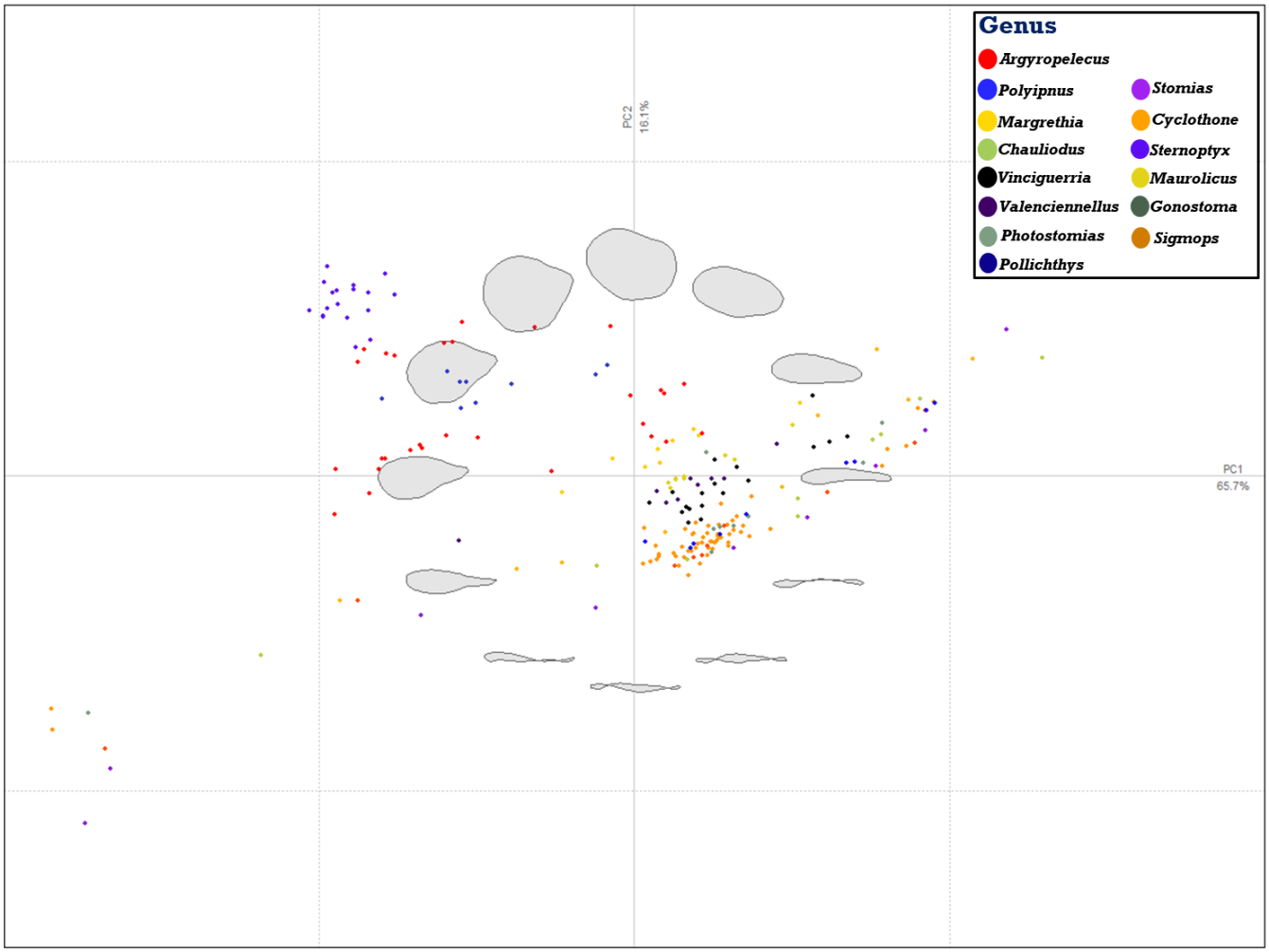

Figure 33 - Normalized PCA-ordinations of body shape among stomiiform fish genera. Numbers next to the axis labels indicated the percentage of explained variation in morphology for that axis in a given ordination (PC 1 = 66% and PC 2 = 16%). Points that fell within the minimum convex polygons represented the realized morphology of body shape for all genera. The Stomiiform genera included: 1) Argyropelecus, 2) Cyclothone, 3) Chauliodus, 4) Gonostoma, 5) Margrethia, 6) Maurolicus, 7) Polyipnus, 8) Photostomias, 9) Pollichthys, 10) Stomias, 11) Sternoptyx, 12) Sigmops, 13) Vinciguerria, and 14) Valenciennellus. Gray body shape silhouettes depicted the full continuum of morphospace among all genera for each individual as calculated using harmonic coefficients through EFA.

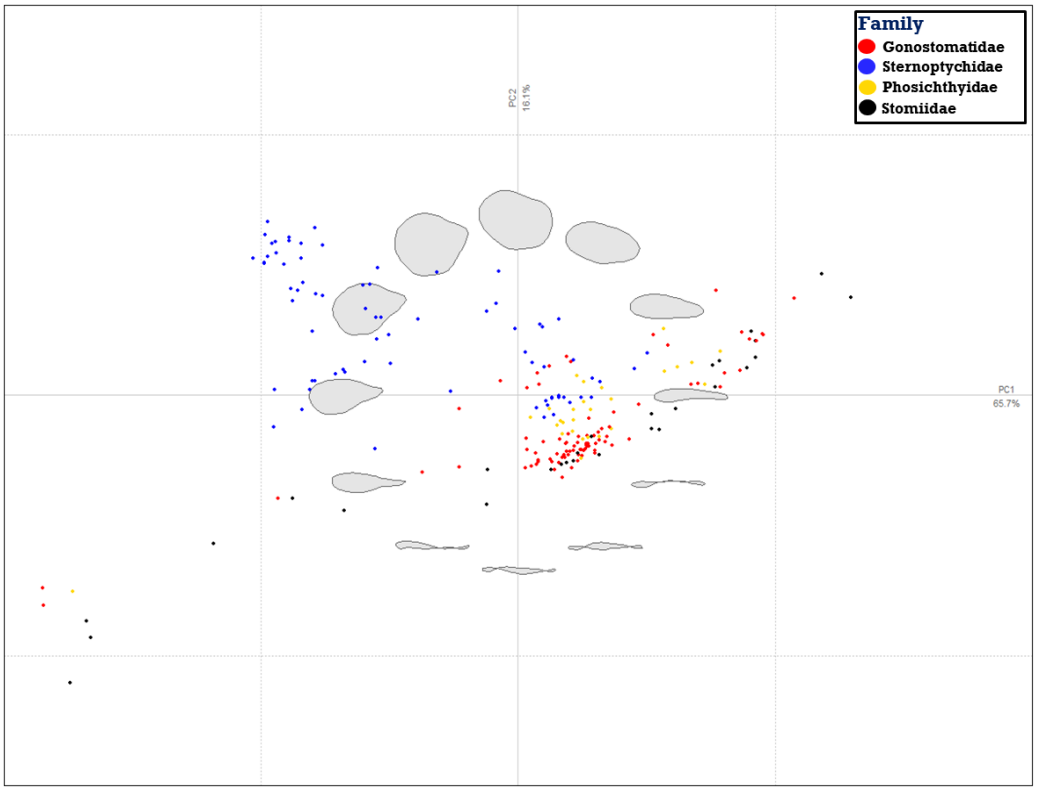

Figure 34 - Normalized PCA-ordinations of body shape among stomiiform fish families. Numbers next to the axis labels indicated the percentage of explained variation in morphology for that axis in a given ordination (PC 1 = 66% and PC 2 = 16%). Points that fell within the minimum convex polygons represented the realized morphology of body shape for each family. The Stomiiform families included: 1) Sternoptychidae, 2) Phosichthyidae, 3) Gonostomatidae, and 4) Stomiidae. Gray body shape silhouettes depicted the full continuum of morphospace among all families for each individual as calculated using harmonic coefficients through EFA.

Predicting Taxonomic Identity

Predicting Species

CAP analysis showed that LCA data were able to predict species identity 58% of the time among the present sample set (*Figure 35(a)*). SIMs were the second-best at predicting species identity (44%; *Figure 35(b)*), and outline analyses were not as good a predictor at species level as LCA and SIMs were (32%; *Figure 35(c)*). The confusion matrix summarizing LCA, SIMs, and outline analyses predictive performance of species is listed in *Tables 8-10*.

Predicting Genus

When identifying individuals to their genus, LCA had the highest percentage (79%) of individuals correctly identified (*Figure 36(a)*), outline analysis had the second-best predictive power (54%; *Figure 36(c)*), and SIMs were the worst predictors (52%; *Figure 36(b)*). The confusion matrix of genus prediction performance is listed in *Table 11*.

Table 8 - Confusion matrix of normalized CAP predictions at species level for landmark configuration analysis. Species and genus identifiers followed descriptions in Table 1.

Original Group	AA	AG	AH	CA	CAC	CB	CO	CP	CPA	CS	GA	MO	MW	PC	PG	PM	SA	SD	SE	SP	VN	VP	VT	Total	% Correct
AA	3	2	2	0	0	0	0	0	0	0	0	0	0	2	0	0	0	0	0	0	0	0	0	9	33%
AG	2	5	2	0	0	0	0	0	0	0	1	0	0	0	0	0	0	0	0	0	0	0	0	10	50%
AH	2	1	7	0	0	0	0	0	0	0	0	0	0	0	0	0	0	0	0	0	0	0	0	10	70%
CA	0	0	0	7	0	2	1	0	0	0	0	0	0	0	0	0	0	0	0	0	0	0	0	10	70%
CAC	0	0	0	0	6	2	0	0	2	0	0	0	0	0	0	0	0	0	0	0	0	0	0	10	60%
CB	0	0	0	2	1	5	0	0	1	0	0	0	0	0	0	0	0	0	1	0	0	0	0	10	50%
CO	0	0	0	1	0	0	6	1	2	0	0	0	0	0	0	0	0	0	0	0	0	0	0	10	60%
CP	0	0	0	1	1	1	1	4	2	0	0	0	0	0	0	0	0	0	0	0	0	0	0	10	40%
CPA	0	0	0	3	0	0	1	3	3	0	0	0	0	0	0	0	0	0	0	0	0	0	0	10	30%
CS	0	0	0	0	0	0	0	0	0	9	0	1	0	0	0	0	0	0	0	0	0	0	0	10	90%
GA	0	1	0	0	0	0	0	0	0	0	6	0	0	0	0	0	0	0	0	0	1	1	0	9	67%
MO	0	0	0	0	0	1	0	1	0	0	0	2	2	0	0	0	0	0	0	0	1	1	1	9	22%
MW	0	0	0	0	0	0	0	0	0	0	0	1	8	0	0	0	0	0	0	0	0	0	0	9	89%
PC	1	0	2	0	0	0	0	0	0	0	0	0	0	6	0	0	0	0	0	0	0	0	0	9	67%
PG	0	0	0	0	0	0	0	0	0	0	0	0	0	0	9	0	0	0	0	0	0	0	0	9	100%
PM	0	0	0	0	0	0	0	0	0	0	0	0	0	0	0	6	0	0	0	0	2	0	1	9	67%
SA	0	0	0	0	0	0	0	0	0	0	1	0	0	0	0	0	7	0	0	0	1	0	0	9	78%
SD	0	0	2	0	0	0	0	0	0	0	0	0	0	0	0	0	0	3	0	4	0	0	0	9	33%
SE	0	0	0	0	1	0	1	0	0	0	1	0	0	0	0	0	0	0	6	0	0	0	0	9	67%
SP	0	0	0	0	0	0	0	0	0	0	0	1	0	0	0	0	0	6	0	2	0	0	0	9	22%
VN	0	0	0	1	0	0	0	0	0	0	0	1	1	0	0	1	0	0	1	0	4	0	0	9	44%
VP	0	0	0	0	0	0	0	0	0	0	2	1	1	0	0	1	0	0	0	0	1	3	0	9	33%
VT	0	0	0	0	0	0	0	0	0	0	1	0	0	0	0	0	0	0	0	0	0	0	8	9	89%

Table 9 - Confusion matrix of normalized CAP predictions at species level for shape indicator measurements. Species and genus identifiers followed descriptions in Table 1.

Original Group	AA	AG	AH	CA	CAC	CB	CO	CP	CPA	CS	GA	MO	MW	PC	PG	PM	SA	SD	SE	SP	VN	VP	VT	Total	% Correct
AA	9	0	0	0	0	0	0	0	0	0	0	0	0	0	0	0	0	0	0	0	0	0	0	9	100%
AG	0	7	2	0	0	0	0	0	0	0	0	0	0	1	0	0	0	0	0	0	0	0	0	10	70%
AH	0	3	7	0	0	0	0	0	0	0	0	0	0	0	0	0	0	0	0	0	0	0	0	10	70%
CA	0	0	0	4	1	0	0	0	0	2	2	0	0	0	0	0	1	0	0	0	0	0	0	10	40%
CAC	0	0	0	0	6	0	0	1	1	0	0	0	0	0	1	0	0	0	1	0	0	0	0	10	60%
CB	0	0	0	1	2	2	0	0	0	2	2	0	0	0	0	1	0	0	0	0	0	0	0	10	20%
CO	0	0	0	0	1	0	4	1	1	0	0	0	0	0	2	0	1	0	0	0	0	0	0	10	40%
CP	0	0	0	1	3	0	3	1	0	0	0	0	0	0	1	0	1	0	0	0	0	0	0	10	10%
CPA	0	0	0	1	3	0	1	0	0	1	0	0	0	0	0	1	0	0	3	0	0	0	0	10	0%
CS	0	0	0	0	0	0	0	0	0	2	1	0	0	0	3	2	1	0	1	0	0	0	0	10	20%
GA	0	0	0	1	0	2	0	0	0	0	5	0	0	0	0	0	0	0	0	0	1	0	0	9	56%
MO	0	0	0	0	0	0	0	0	0	0	2	3	3	0	0	0	0	0	0	0	1	0	0	9	33%
MW	0	0	0	0	0	0	0	0	0	0	0	0	8	0	0	0	0	0	0	0	0	0	1	9	89%
PC	1	0	0	0	0	0	0	0	0	0	0	0	0	5	0	0	0	2	0	1	0	0	0	9	56%
PG	0	0	0	0	1	0	1	0	0	4	0	0	0	0	2	0	1	0	0	0	0	0	0	9	22%
PM	0	0	0	0	0	2	0	1	0	1	0	1	0	0	0	0	0	0	4	0	0	0	0	9	0%
SA	0	0	0	3	0	0	1	0	0	1	0	0	0	0	2	0	1	0	1	0	0	0	0	9	11%
SD	1	0	0	0	0	0	0	0	0	0	0	0	0	0	0	0	0	8	0	0	0	0	0	9	89%
SE	0	0	0	0	0	0	2	0	1	0	0	0	0	0	0	2	0	0	3	0	1	0	0	9	33%
SP	0	0	0	0	0	0	0	0	0	0	0	0	0	0	0	0	0	1	0	8	0	0	0	9	89%
VN	0	0	0	0	0	0	0	0	0	0	2	1	1	0	0	0	0	0	1	0	1	2	1	9	11%
VP	0	0	0	0	0	0	0	0	0	0	2	1	3	0	0	0	0	0	0	0	0	3	0	9	33%
VT	0	0	0	0	0	0	0	0	0	0	1	0	0	0	0	0	0	0	0	0	1	0	7	9	78%

Table 10 - Confusion matrix of normalized CAP predictions at species level for outline analysis. Species and genus identifiers followed descriptions in Table 1.

Original Group	AA	AG	AH	CA	CAC	CB	CO	CP	CPA	CS	GA	MO	MW	PC	PG	PM	SA	SD	SE	SP	VN	VP	VT	Total	% Correct
AA	6	0	0	0	0	0	0	0	0	0	0	0	0	3	0	0	0	0	0	0	0	0	0	9	67%
AG	0	6	3	0	0	0	0	0	0	0	0	0	0	1	0	0	0	0	0	0	0	0	0	10	60%
AH	1	2	6	0	0	0	0	0	0	0	0	0	0	0	0	0	0	0	0	0	0	0	1	10	60%
CA	0	0	0	0	0	0	3	2	2	0	1	0	0	0	1	0	0	0	1	0	0	0	0	10	0%
CAC	0	0	0	0	0	1	2	4	2	1	0	0	0	0	0	0	0	0	0	0	0	0	0	10	0%
CB	0	0	0	0	1	1	0	2	3	0	1	0	0	0	0	0	0	0	0	0	1	0	1	10	10%
CO	0	0	0	2	0	2	2	2	1	0	0	0	0	0	1	0	0	0	0	0	0	0	0	10	20%
CP	0	0	0	0	1	2	1	3	3	0	0	0	0	0	0	0	0	0	0	0	0	0	0	10	30%
CPA	0	0	0	0	1	1	3	2	2	0	0	0	0	0	0	0	0	0	0	0	1	0	0	10	20%
CS	0	0	0	1	0	2	1	0	1	0	0	0	0	0	1	0	1	0	1	0	1	0	1	10	0%
GA	0	0	0	0	0	0	0	0	0	1	1	0	0	0	1	1	1	0	1	0	0	0	3	9	11%
MO	0	1	0	0	0	0	0	0	0	0	0	2	4	0	0	0	0	0	0	0	0	1	1	9	22%
MW	0	0	0	0	0	0	0	0	0	0	0	0	7	0	0	0	0	0	0	0	0	2	0	9	78%
PC	2	1	0	0	0	0	0	0	0	0	0	1	0	5	0	0	0	0	0	0	0	0	0	9	56%
PG	0	0	1	2	1	0	0	0	0	0	3	0	0	0	0	0	2	0	0	0	0	0	0	9	0%
PM	0	0	0	1	0	1	2	0	1	0	0	0	1	0	0	0	1	0	2	0	0	0	0	9	0%
SA	0	0	0	1	0	0	0	1	0	1	1	0	0	0	4	0	1	0	0	0	0	0	0	9	11%
SD	0	0	0	0	0	0	0	0	0	0	0	0	0	0	0	0	0	8	0	1	0	0	0	9	89%
SE	0	0	0	0	0	1	1	1	0	1	0	0	0	0	2	0	0	0	1	0	0	0	2	9	11%
SP	0	0	0	0	0	0	0	0	0	0	0	0	0	0	0	0	0	0	0	9	0	0	0	9	100%
VN	0	0	0	0	0	2	0	0	1	0	0	0	0	0	0	0	0	0	0	0	2	3	1	9	22%
VP	0	0	0	0	0	0	0	0	0	0	0	0	4	0	0	0	0	0	0	0	5	0	0	9	0%
VT	0	1	0	0	0	0	0	0	0	0	0	0	0	0	0	0	0	0	0	0	0	0	8	9	89%

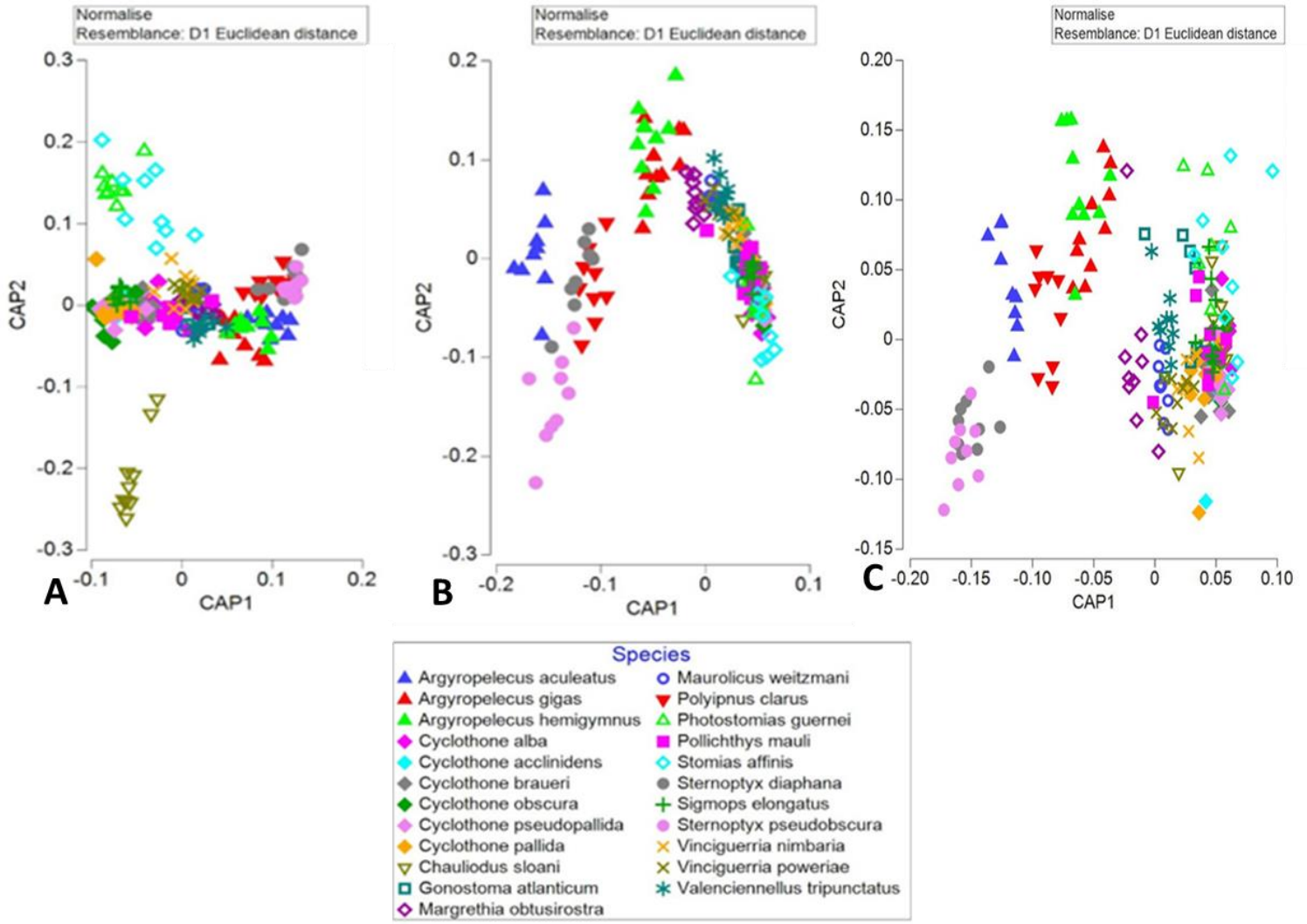

Figure 35 – Normalized metric CAP of all individuals using the landmark configuration analysis method (A), shape indicator measurements (B), and outline analysis (C), grouped by species. Each genus is represented by a different symbol shape.

Table 11 - Confusion matrix of the normalized CAP predictions at genus level. Genera are represented by a two-letter code: 1) AR=Argyropelecus; 2) CY=Cyclothone; 3) CH=Chauliodus; GO=Gonostoma; 4) MA=Margrethia; 5) MU=Maurolicus; 6) PO=Polyipnus; 7) PH=Photostomias; 8) PL=Pollichthys; 9) ST=Stomias; 10) SE = Sternoptyx; 11) SI=Sigmops; 12) VI=Vinciguerria; 13) VT=Valenciennellus.

	Original Group	**AR**	**CY**	**CH**	**GO**	**MA**	**MU**	**PO**	**PH**	**PL**	**ST**	**SE**	**SI**	**VI**	**VT**	**Total**	**% Correct**
SIMs	*Argyropelecus*	25	0	0	0	1	0	3	0	0	0	0	0	0	0	29	86%
	Cyclothone	0	24	5	6	0	0	0	3	4	6	0	11	1	0	60	40%
	Chauliodus	0	0	2	1	0	0	0	3	2	1	0	1	0	0	10	20%
	Gonostoma	0	0	0	6	0	0	0	0	0	1	0	0	1	1	9	67%
	Margrethia	0	0	0	1	4	1	0	0	0	0	0	0	1	2	9	44%
	Maurolicus	0	0	0	0	0	8	0	0	0	0	0	0	0	1	9	89%
	Polyipnus	3	0	0	0	0	0	6	0	0	0	0	0	0	0	9	67%
	Photostomias	0	1	4	0	0	0	0	1	0	2	0	1	0	0	9	11%
	Pollichthys	0	2	1	0	1	0	0	0	2	0	0	3	0	0	9	22%
	Stomias	0	1	0	1	0	0	0	3	0	3	0	1	0	0	9	33%
	Sternoptyx	0	0	0	0	0	0	4	0	0	0	14	0	0	0	18	78%
	Sigmops	0	0	1	0	0	0	0	0	2	0	0	5	1	0	9	56%
	Vinciguerria	0	0	0	2	3	4	0	0	0	0	0	1	6	2	18	33%
	Valenciennellus	0	0	0	0	1	1	0	0	0	0	0	0	1	6	9	67%

(Table 11. Cont.)

	Original Group	AR	CY	CH	GO	MA	MU	PO	PH	PL	ST	SE	SI	VI	VT	Total	% Correct
LCA	*Argyropelecus*	20	0	0	4	0	0	5	0	0	0	0	0	0	0	29	69%
	Cyclothone	0	54	0	0	0	0	0	0	0	0	0	6	0	0	60	69%
	Chauliodus	0	0	9	0	1	0	0	0	0	0	0	0	0	0	10	90%
	Gonostoma	1	0	0	8	0	0	0	0	0	0	0	0	0	0	9	89%
	Margrethia	0	2	0	0	3	1	0	0	0	0	0	0	2	1	9	33%
	Maurolicus	0	0	0	0	1	8	0	0	0	0	0	0	0	0	9	89%
	Polyipnus	2	0	0	0	0	0	7	0	0	0	0	0	0	0	9	78%
	Photostomias	0	0	0	0	0	0	0	9	0	0	0	0	0	0	9	100%
	Pollichthys	0	0	0	0	1	0	0	0	6	0	0	0	1	1	9	67%
	Stomias	0	0	0	1	0	0	0	0	0	7	0	0	1	0	9	78%
	Sternoptyx	2	0	0	0	1	0	0	0	0	0	15	0	0	0	18	83%
	Sigmops	0	0	0	1	0	0	0	0	0	0	0	8	0	0	9	89%
	Vinciguerria	0	0	0	3	1	3	0	0	1	0	0	1	9	0	18	50%
	Valenciennellus	0	0	0	1	0	0	0	0	0	0	0	0	0	8	9	89%
Outline	*Argyropelecus*	16	0	0	0	1	0	9	0	0	0	1	0	0	2	29	55%
	Cyclothone	0	46	3	2	0	0	0	1	1	0	0	2	4	1	60	77%
	Chauliodus	0	2	0	0	0	0	0	1	1	1	0	3	1	1	10	0%
	Gonostoma	0	0	0	1	0	0	0	1	0	1	0	1	1	4	9	11%
	Margrethia	0	0	0	0	2	4	0	1	0	0	0	0	1	1	9	22%
	Maurolicus	0	0	0	0	0	7	0	0	0	0	0	0	2	0	9	78%
	Polyipnus	2	0	0	0	0	0	6	0	0	0	1	0	0	0	9	67%
	Photostomias	1	1	2	3	0	0	0	0	0	2	0	0	0	0	9	0%
	Pollichthys	0	5	0	0	0	1	0	0	0	1	0	2	0	0	9	0%
	Stomias	0	2	1	0	0	0	0	5	0	1	0	0	0	0	9	11%
	Sternoptyx	0	0	0	0	0	0	0	0	0	0	18	0	0	0	18	100%
	Sigmops	0	3	1	0	0	0	0	2	0	0	0	2	1	0	9	22%
	Vinciguerria	0	2	0	0	0	4	0	0	0	0	0	0	11	1	18	61%
	Valenciennellus	0	0	0	1	0	1	0	0	0	0	0	0	0	7	9	78%

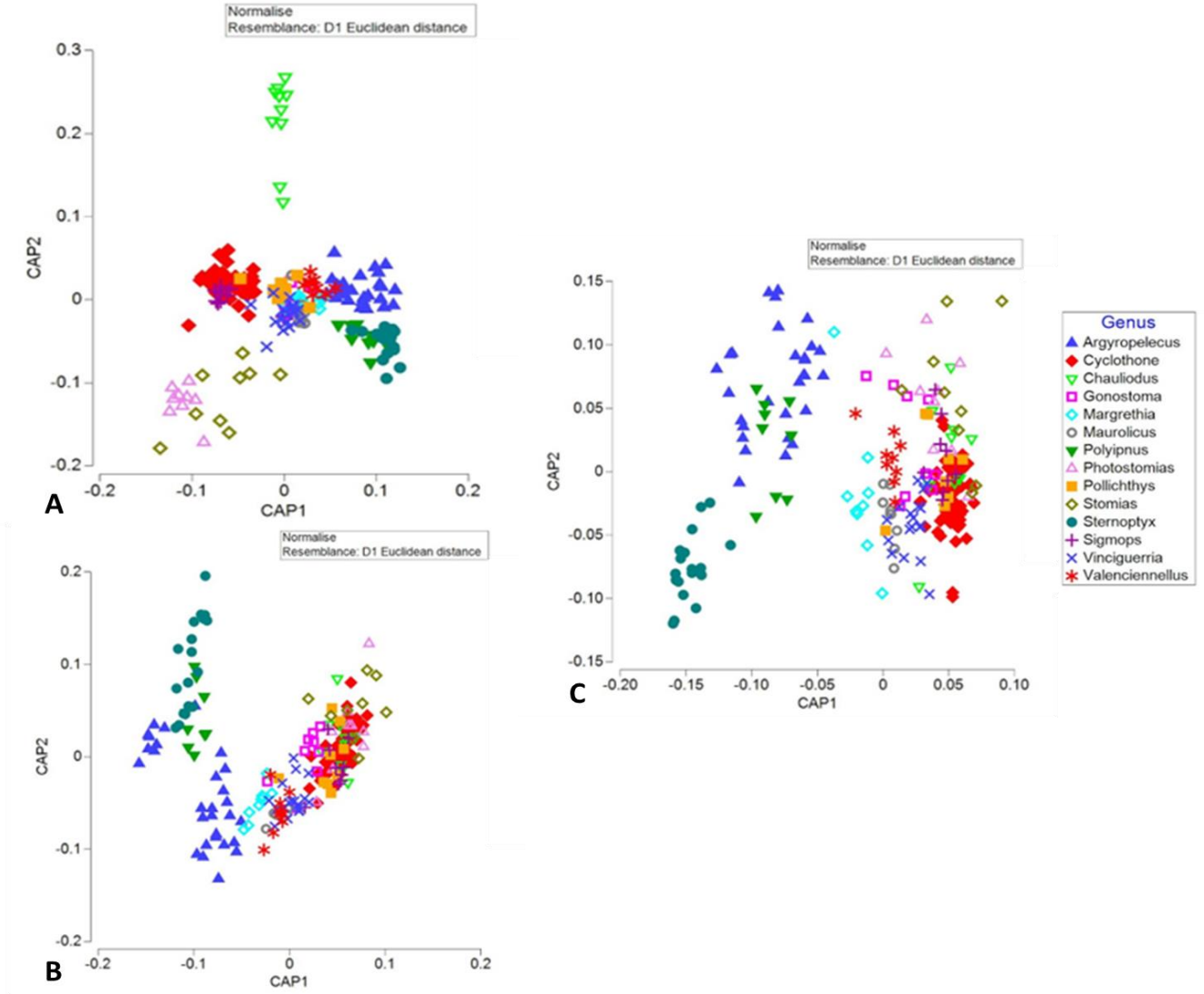

Figure 36 – Normalized metric CAP of all individuals using the landmark configuration analysis method (a), shape indicator measurements (b), and outline analysis (c), grouped by genus.

Predicting Family

When identifying individuals to their families, LCA had the highest percentage (81%) of individuals correctly identified (*Figure 37(a)*), and SIMs had the second-highest predictive power (68%; *Figure 37(b)*). Of the three morphometric techniques, outline analyses were not as precise a predictor (66%) as LCA and SIMs (*Figure 37(c)*). The confusion matrix of family prediction performance from the three morphometric methods used are listed in *Table 12*. The outlier (i.e., Sternoptychidae individual) of *Figure 37(a)* was removed and the CAP analysis was repeated to compare the results, ensuring they were not affected. No significant differences were observed after the outlier was removed, and therefore, was included within the analyses.

Table 12 - Confusion matrix of the normalized CAP predictions at family level.

	Original Group	**Sternoptychidae**	**Gonostomatidae**	**Stomiidae**	**Phosichthyidae**	**Total**	**% Correct**
SIMs	Sternoptychidae	57	0	0	17	74	77%
	Gonostomatidae	3	52	18	14	87	60%
	Stomiidae	0	11	17	0	28	61%
	Phosichthyidae	0	6	2	19	27	70%
LCA	Sternoptychidae	58	1	0	15	74	78%
	Gonostomatidae	4	72	0	11	87	83%
	Stomiidae	0	4	22	2	28	79%
	Phosichthyidae	2	2	0	23	27	85%
Outline	Sternoptychidae	57	0	0	17	74	77%
	Gonostomatidae	2	50	15	20	87	57%
	Stomiidae	1	8	17	2	28	61%
	Phosichthyidae	0	8	1	18	27	67%

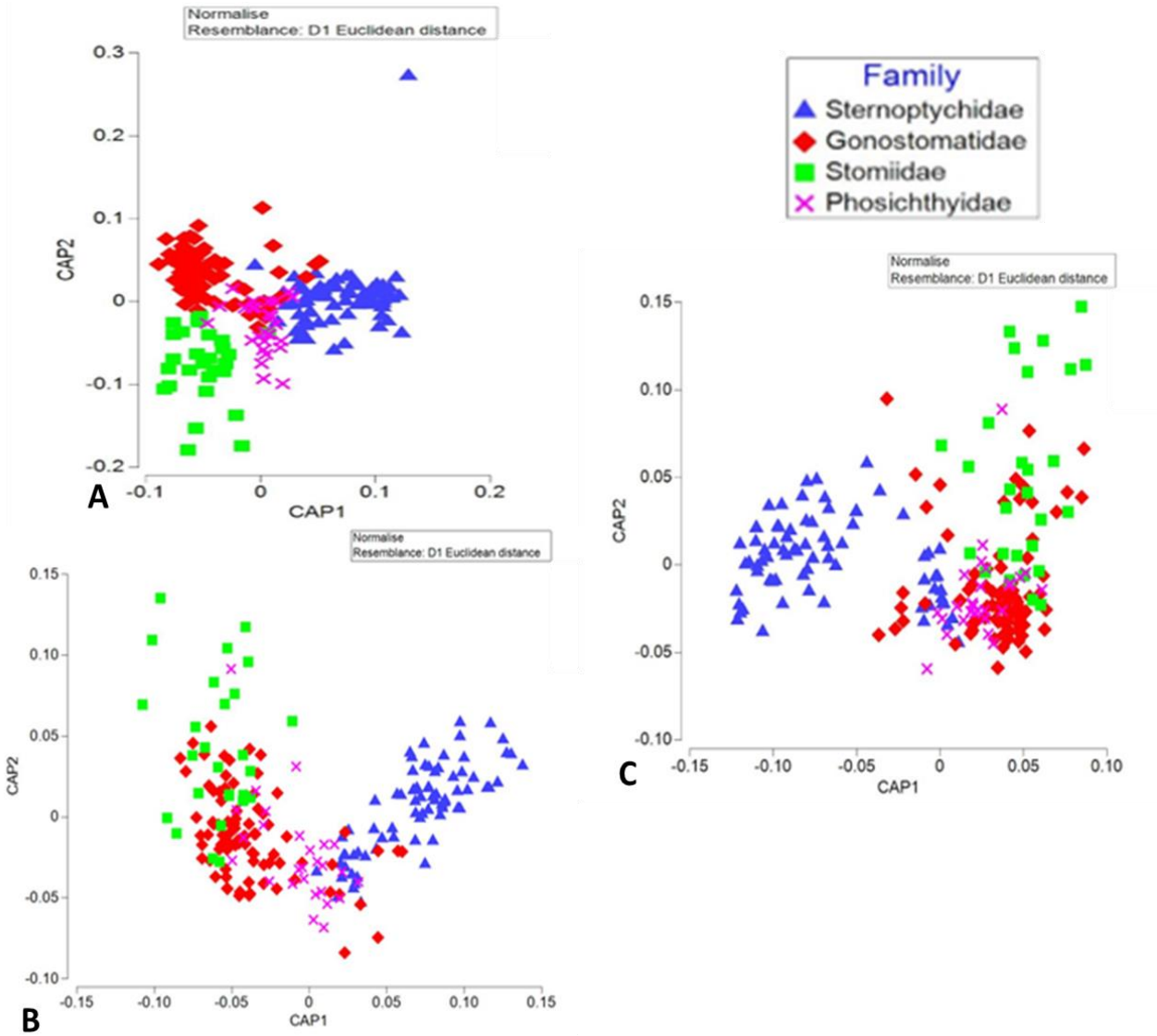

Figure 37 – Normalized metric CAP of all individuals using the landmark configuration analysis (a), shape indicator measurements (b), and outline analysis (c), grouped by family.

Testing vs. Traits

Shape Indicator Measurements (SIMs)

Strong group separation was observed between morphotypes (ANOSIM: Global R = 0.706; p = 0.001; *Figure 41(a); Table 13*). All morphotypes were significantly different from each other (p = 0.001; *Figure 39*), where morphotype C (i.e., laterally compressed and short body shape) was especially distinct from morphotypes A (i.e., elongated body shape) and B (i.e., compressed and elongated body shape). While morphotypes A and B were the most similar (albeit different; Pairwise ANOSIM results are shown in *Figure 39*). Differences between morphotypes were driven mainly by caliper size (SIMPER: 12.42-21.64% dissimilarity), centroid size (SIMPER: 3.72-5.68% dissimilarity), Haralick circularity (SIMPER: 0.02-2.04% dissimilarity), and eccentricity bounding box (SIMPER: 0.00-0.21% dissimilarity).

A significant relationship between DVM types on SIMs was observed (ANOSIM: Global R = 0.076; p-value: 0.001; *Figure 41(b)*; *Table 13*). All pairwise comparison p-values between groups were also statistically significant (<0.050). Complete migrators and partial migrators formed the strongest intra-specific groupings (Pairwise ANOSIM: R = 0.114; p = 0.001; *Figure 38*), and non-migrators and partial migrators formed the weakest groupings (Pairwise ANOSIM: R = 0.114; p = 0.001; *Figure 38*). The SIMs that contributed the most to dissimilarity between body shapes for the DVM types were: 1) caliper size (SIMPER: 14.06-15.10% dissimilarity); 2) centroid size (SIMPER: 4.04-4.27% dissimilarity); and 3) Haralick circularity (SIMPER: 0.00-0.01% dissimilarity).

Overall, daytime depth distributions exhibited significant effects on SIMs (ANOSIM: Global R = 0.066; p = 0.039; *Figure 41(c)*; *Table 13*), however, there were some insignificant pairwise groupings (p > 0.05; *Figure 40*). The daytime depths of 600-1000 m to 600-1200 m, 1000-1500 m to 600-1200 m, 200-1200 m to 600-1200 m, and 0-600 m to 600-1200 m showed perfect separation between groups (Pairwise ANOSIM: R = 1.0; p = 0.001; *Figure 40*), and these daytime depths included five species. The highest contributing SIMs were caliper size (SIMPER: 5.90-19.24% dissimilarity), centroid size (SIMPER: 1.74-4.26% dissimilarity), and Haralick circularity (SIMPER: 0.01-0.03% dissimilarity).

Table 13 - Global ANOSIM results from the ecological traits assessment of shape indicator measurements using a Bray Curtis matrix. Pairwise groupings were tested as unordered factors. The bolded R statistics and their corresponding p-values are those that were significant on the p-value ($p \leq 0.05$).

Ecological Trait	Global R Statistic	p-value
Morphotypes	**0.706**	**0.001**
DVM types	**0.076**	**0.001**
Daytime depths	**0.066**	**0.039**

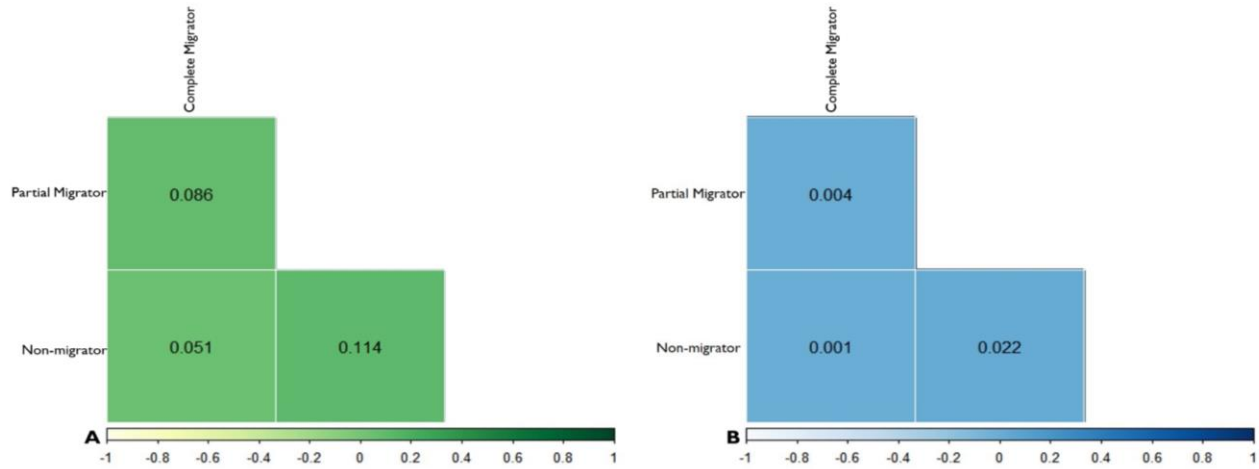

Figure 38 - Correlation matrix of ANOSIM results from DVM types assessment of shape indicator measurements using a Bray Curtis matrix. Pairwise groupings were tested as unordered factors. Figure A represents the R statistic values and Figure B represents the corresponding p-values. The colored squares represented the significance of the values. The darker colored squares represented higher R statistics and p-values and the lighter colored squares represented lower values. Significant p-values are those that had a value less than 0.05.

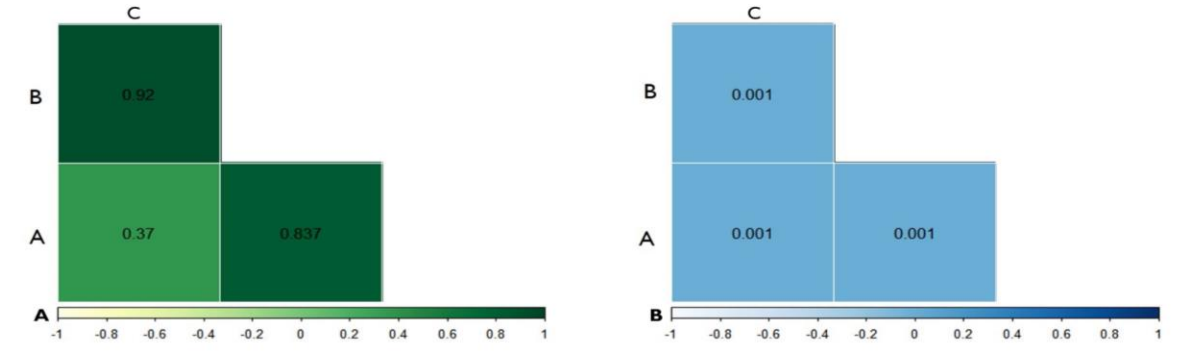

Figure 39 - Correlation matrix of ANOSIM results from morphotypes assessment of shape indicator measurements using a Bray Curtis matrix. Pairwise groupings were tested as unordered factors. Figure A represents the R statistic values and Figure B represents the corresponding p-values. The colored squares represented the significance of the values. The darker colored squares represented higher R statistics and p-values and the lighter colored squares represented lower values. Significant p-values are those that had a value less than 0.05.

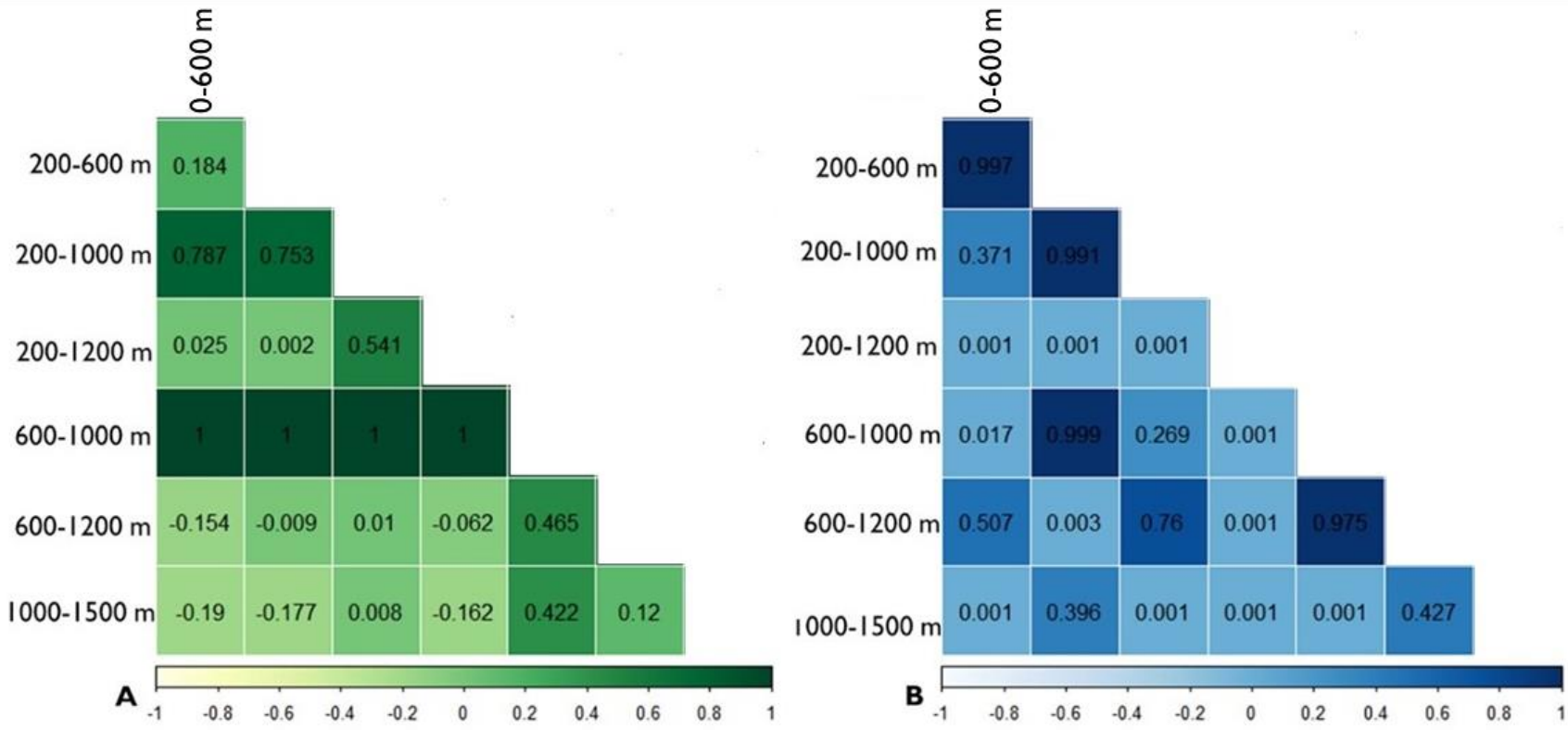

Figure 40 - Correlation matrix of ANOSIM results from daytime depths assessment of shape indicator measurements using a Bray Curtis matrix. Pairwise groupings were tested as unordered factors. Figure A represents the R statistic values and Figure B represents the corresponding p-values. The colored squares represented the significance of the values. The darker colored squares represented higher R statistics and p-values and the lighter colored squares represented lower values. Significant p-values are those that had a value less than 0.05.

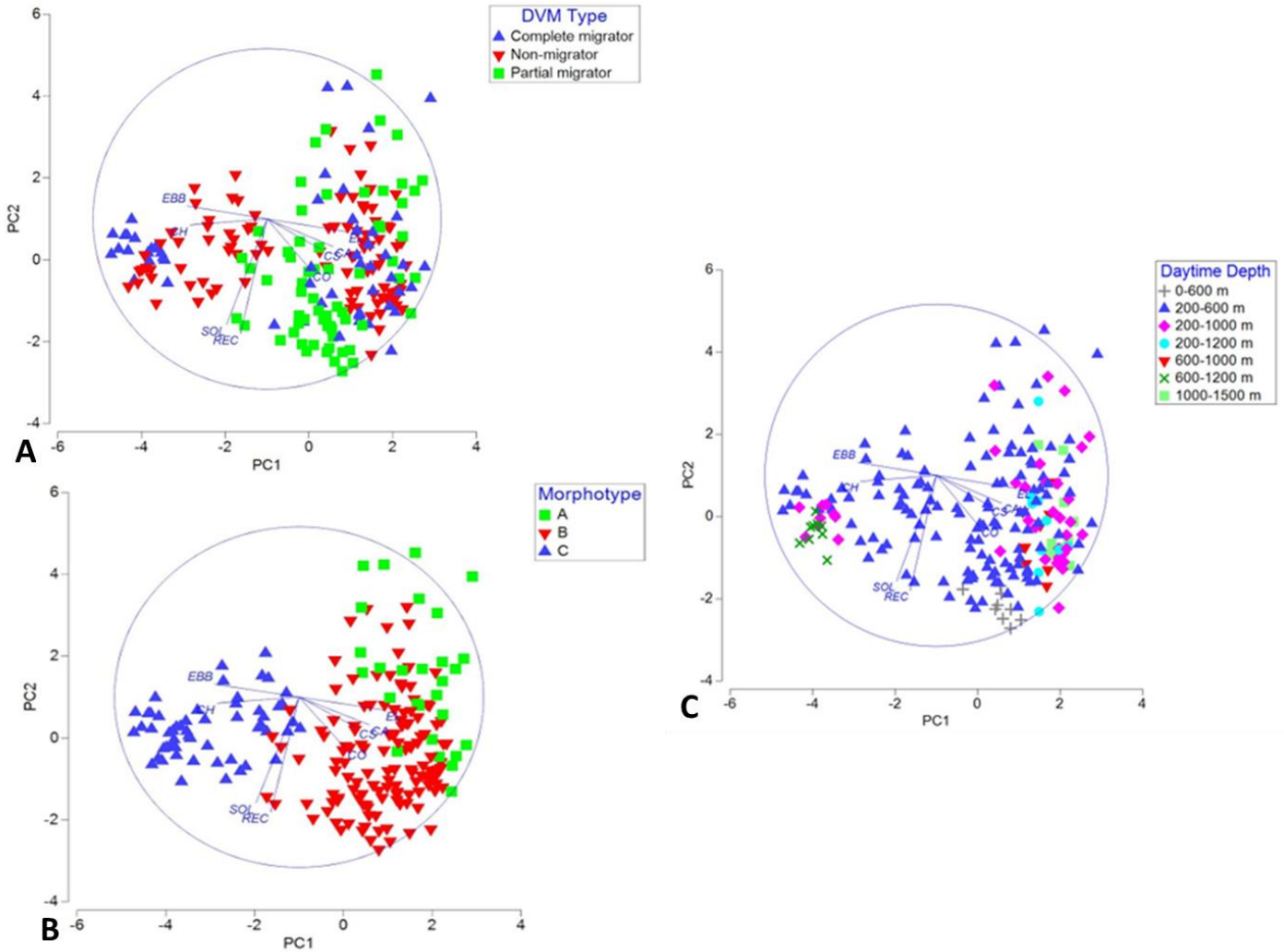

Figure 41 - Normalized principal component analysis of DVM types (a), Morphotypes (b), and Daytime depths (c) through shape indicator measurements. PC 1 explained 52.4% of the variance within the data, and PC 2 explained 23.2% of the variance within the data. Caliper size (CA), centroid size (CS), Haralick circularity (CH), convexity (CO), eccentricity bounding box (EBB), elongation (EL), rectangularity (REC), and solidity (SOL).

Landmark Configuration Analysis

Of the three ecological traits analyzed, the landmark body shape of stomiiform fishes had no significant relationships with daytime depths, although the p-value was close to 0.05 (ANOSIM: Global R = 0.061; p = 0.065; *Figure 45(c)*; *Table 14*). Additionally, daytime depths and DVM types were combined into a new factor to assess the interaction between the two factors. The combination of these two factors increased the relationship between body shapes and daytime depths but it decreased the significance of the relationship between body shapes and DVM types. As a result, the variables were assessed independently.

Significant differences in shape were identified between DVM types (ANOSIM: Global R = 0.108; p = 0.001; *Figure 45(a)*; *Table 14*). The greatest separation was observed between complete migrators and non-migrators (Pairwise ANOSIM: R = 0.137; p = 0.001; *Figure 42)*, and the lowest between complete migrators and partial migrators (Pairwise ANOSIM: R = 0.035; p = 0.021; *Figure 42*). The five landmark x-coordinates (i.e., X1, X2, X3, X4, and X5) contributed some to the differences (dissimilarity) between body shapes. Overall, the highest contributing landmark coordinate was X3 (SIMPER: 19.50-20.19% dissimilarity), followed by X4 (SIMPER: 18.26-20.01% dissimilarity), X2 (SIMPER: 15.28-16.59 % dissimilarity), X5 (SIMPER: 9.28-15.61% dissimilarity), and X1 (SIMPER: 3.46-7.74% dissimilarity).

Strong separation was observed between the three morphotypes (ANOSIM: Global R = 0.706; p = 0.001; *Figure 45(b)*; *Table 14*), with all three groups significantly different to each other. Morphotype A and morphotype C showed the greatest separation (Pairwise ANOSIM: R = 0.766; p = 0.001; *Figure 43*), and morphotype B and morphotype A showed the least (Pairwise ANOSIM: R = 0.483; p = 0.001; *Figure 42*). The three highest contributing landmark coordinates were X2 (SIMPER: 8.00-23.67% dissimilarity), X3 (SIMPER: 17.40-20.97% dissimilarity), and X4 (SIMPER: 17.62-20.56% dissimilarity).

Outliers were observed within the PCA plots of the three ecological traits assessed. To ensure the outliers did not significantly impact the results, they were removed and the PCA's were run again. No overall changes to the results were observed when the outliers were removed from the analyses.

The landmark centroid size varied significantly with DVM types (ANOVA: p = 0.0153; *Table 15*) and morphotypes (ANOVA: p = <0.0001; *Table 15*). Shape of landmarks varied significantly with morphotypes (ANOVA: p = <0.0001; *Table 16*). No significant effects on the centroid size or shape from daytime depths were observed (ANOVA: p > 0.05; *Table 16*).

Table 14 - Global ANOSIM results from the ecological traits assessment of landmark configuration analysis using a Bray Curtis matrix. Pairwise groupings were tested as unordered factors. The bolded R statistics and their corresponding p-values are those that were significant on the p-value (p≤0.05).

Ecological Trait	Global R Statistic	p-value
Morphotypes	**0.547**	**0.001**
DVM types	**0.108**	**0.001**
Daytime depths	0.061	0.065

Table 15 - Procrustes ANOVA of Centroid Size

Effect	SS	MS	df	F	P (param.)
DVM Type	233.446	77.815	3	4.49	0.0153
Morphotype	401.769	200.884	2	24.91	<0.0001
Daytime depth	146.032	24.339	6	0.93	0.4976
Residuals	364.801	1.890	193		

Table 16 - Procrustes ANOVA of Body Shape

Effect	SS	MS	df	F	P (param.)	Pillai tr.
DVM Type	1.714	0.095	18	0.96	0.515	1.15
Morphotype	6.539	0.545	12	10.02	<0.0001	1.62
Daytime depth	3.619	0.101	36	1.02	0.452	1.48
Residuals	1.392	0.001	1158			

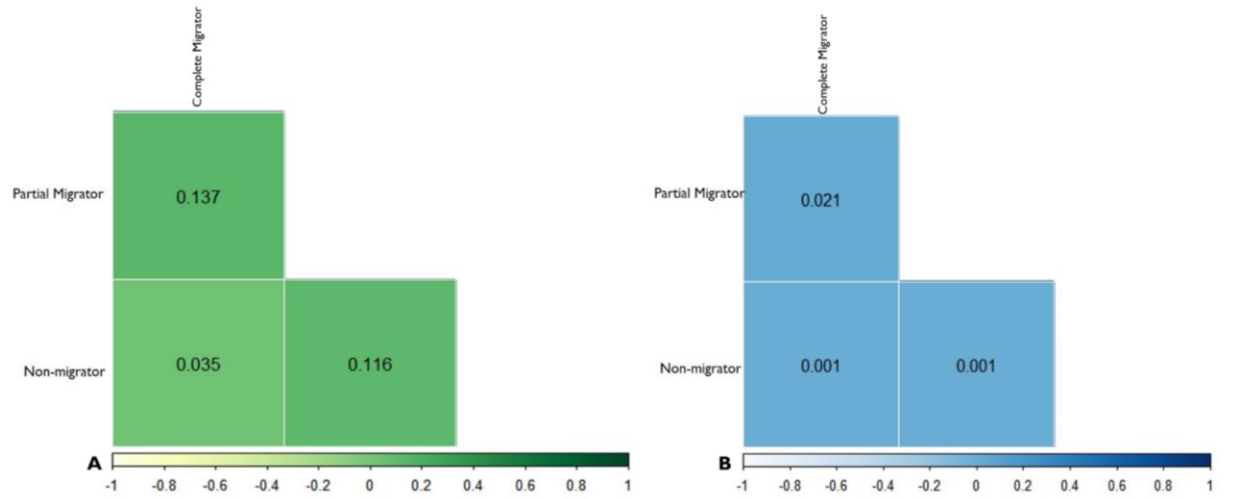

Figure 42 - Correlation matrix of ANOSIM results from DVM types assessment of landmark configuration analysis using a Bray Curtis matrix. Pairwise groupings were tested as unordered factors. Figure A represents the R statistic values and Figure B represents the corresponding p-values. The colored squares represented the significance of the values. The darker colored squares represented higher R statistics and p-values and the lighter colored squares represented lower values. Significant p-values are those that had a value less than 0.05.

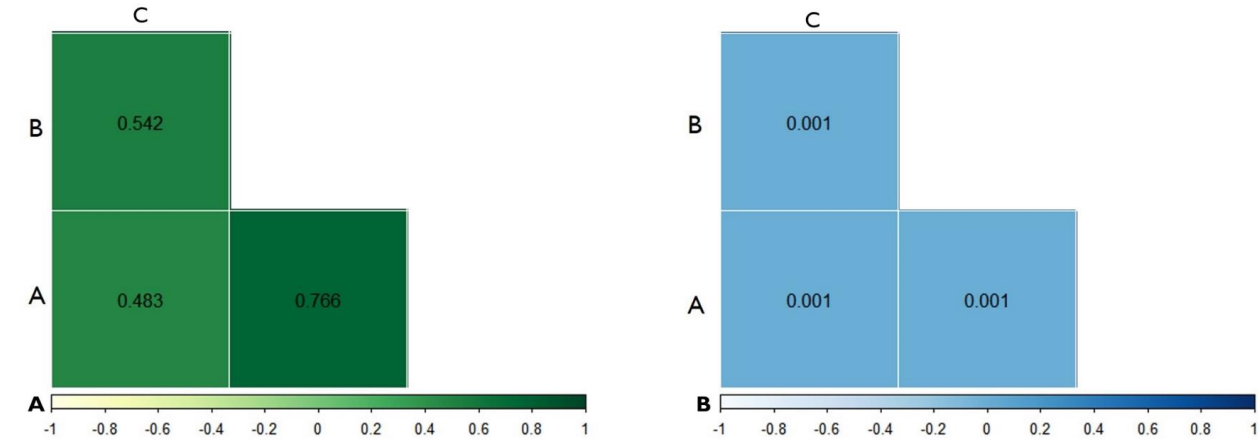

Figure 43 - Correlation matrix of ANOSIM results from morphotypes assessment of landmark configuration analysis using a Bray Curtis matrix. Pairwise groupings were tested as unordered factors. Figure A represents the R statistic values and Figure B represents the corresponding p-values. The colored squares represented the significance of the values. The darker colored squares represented higher R statistics and p-values and the lighter colored squares represented lower values. Significant p-values are those that had a value less than 0.05.

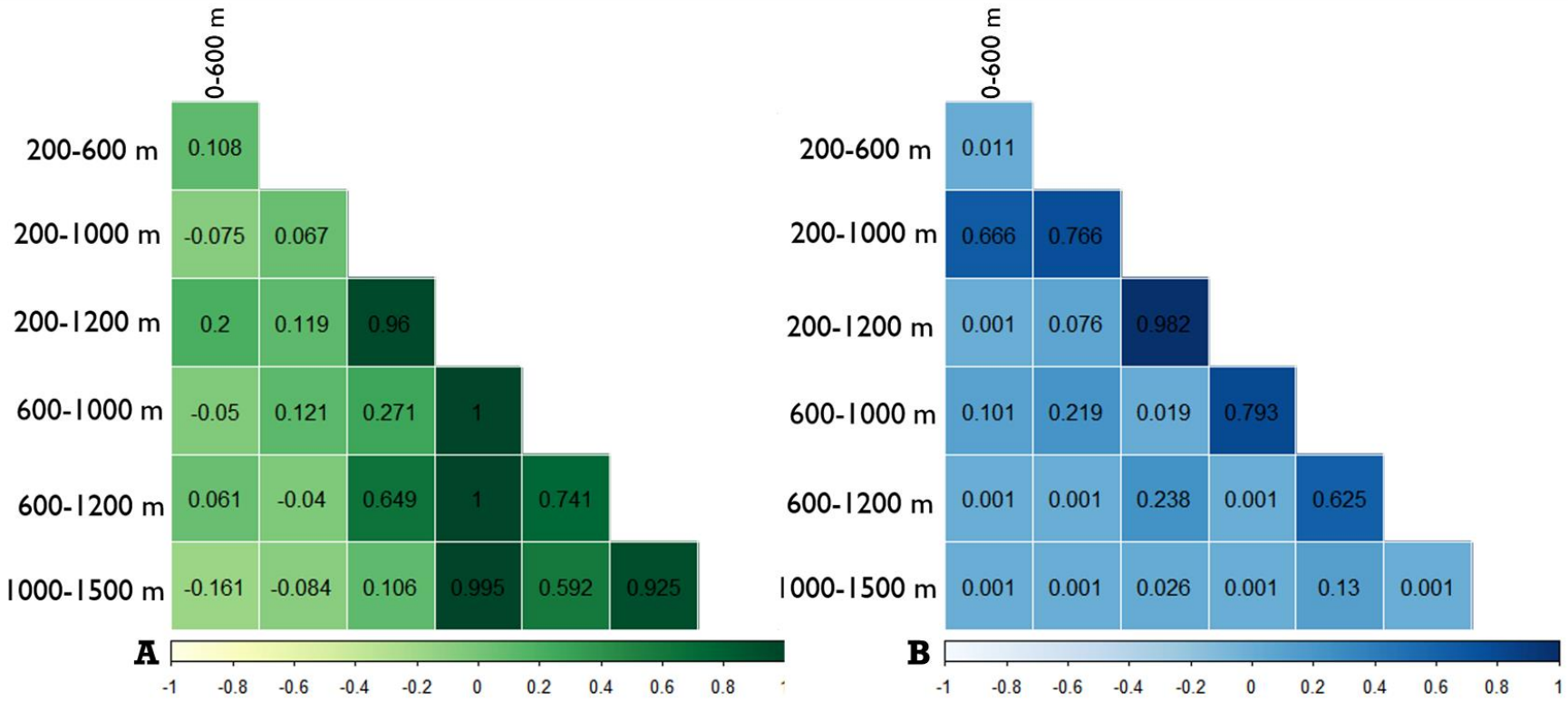

Figure 44 - Correlation matrix of ANOSIM results from daytime depths assessment of landmark configuration analysis using a Bray Curtis matrix. Pairwise groupings were tested as unordered factors. Figure A represents the R statistic values and Figure B represents the corresponding p-values. The colored squares represented the significance of the values. The darker colored squares represented higher R statistics and p-values and the lighter colored squares represented lower values. Significant p-values are those that had a value less than 0.05.

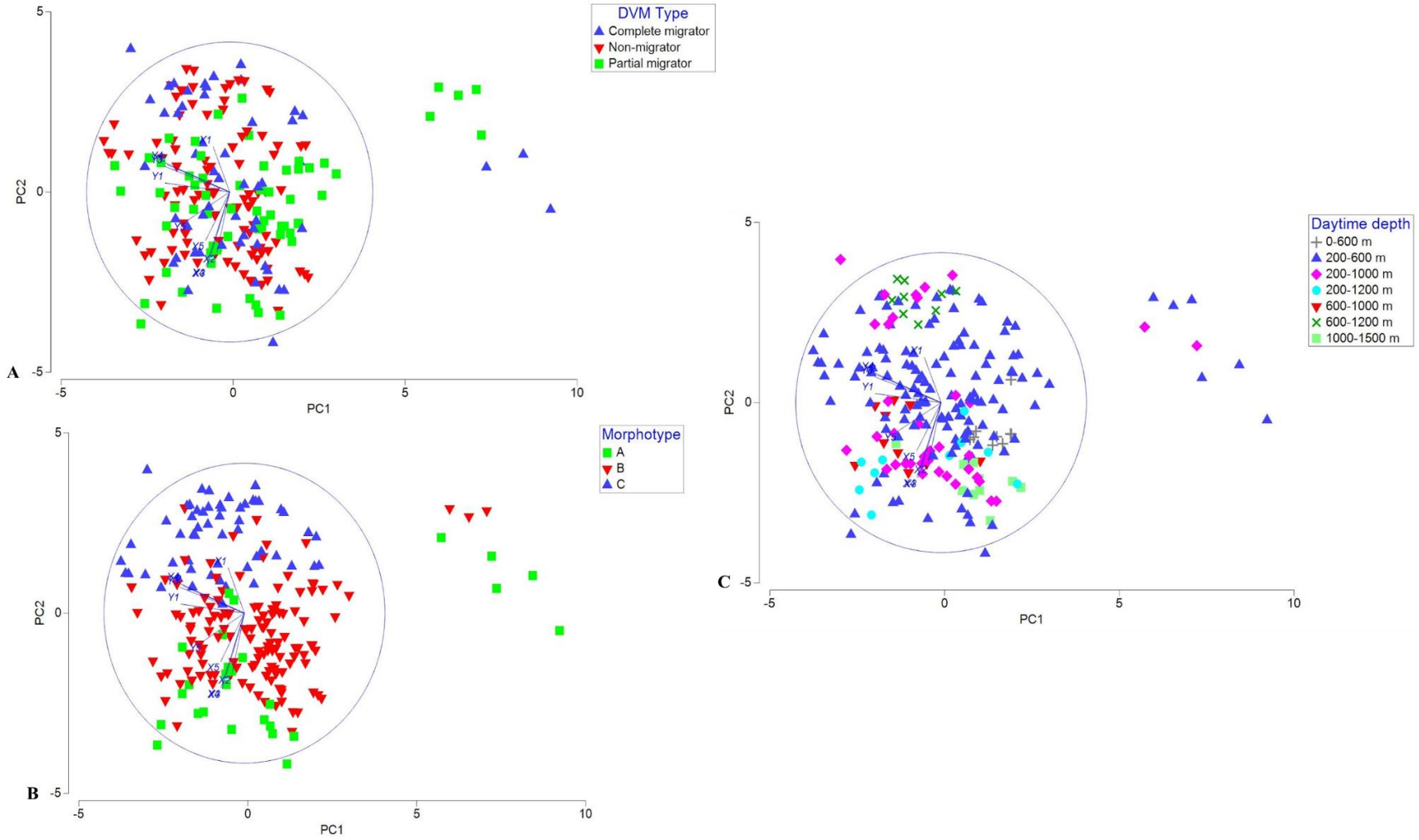

Figure 45 - Normalized principal component analysis of DVM type (A), Morphotype (B), and Daytime depth distributions (C) through landmark configuration analysis. PC 1 explained 40.2% of the variance within the data and PC 2 explained 32.6% of the variance within the data. X-coordinate of landmark one (X1), Y-coordinate of landmark one (Y1), X-coordinate of landmark two (X2), Y-coordinate of landmark two (Y2), X-coordinate of landmark three (X3), Y-coordinate of landmark three (Y3), X-coordinate of landmark four (X4), Y-coordinate of landmark four (Y4), X-coordinate of landmark five (X5), Y-coordinate of landmark five (Y5).

Outline Analysis

A significant relationship between DVM types on harmonics was observed (ANOSIM: Global R = 0.064; p = 0.001; *Table 17; Figure 49*). Within the DVM type pairwise comparisons, non-migrators and partial migrators had the strongest group separation (Pairwise ANOSIM: R = 0.089; p = 0.002; *Figure 46; Figure 49*), whereas complete migrators and non-migrators had the weakest separation (Pairwise ANOSIM: R = 0.05; p = 0.044; although the p-value was close to 0.05; *Table 49*).

Similarly to the other computer-aided morphometric techniques assessed, morphotypes had the highest R statistics of the three ecological traits (ANOSIM: Global R = 0.418; p = 0.001; *Table 17*; *Figure 47*; *Figure 50*). All pairwise morphotype group comparisons were statistically significant (p = 0.001). Morphotype C and Morphotype B were responsible for the largest separation between morphotypes (Pairwise ANOSIM: R = 0.493; p = 0.001; *Figure 50*). Morphotype C and Morphotype A had little effect on group separation (Pairwise ANOSIM: R = 0.32; p = 0.001; *Figure 50*). Morphotype B was responsible for strong separation between body shapes.

No significant relationship between daytime depths on harmonics were observed (ANOSIM: Global R = -0.136; p = 0.998; *Figure 48*; *Figure 51*; *Table 17*). The Pairwise ANOSIM results are shown in *Figure 51*.

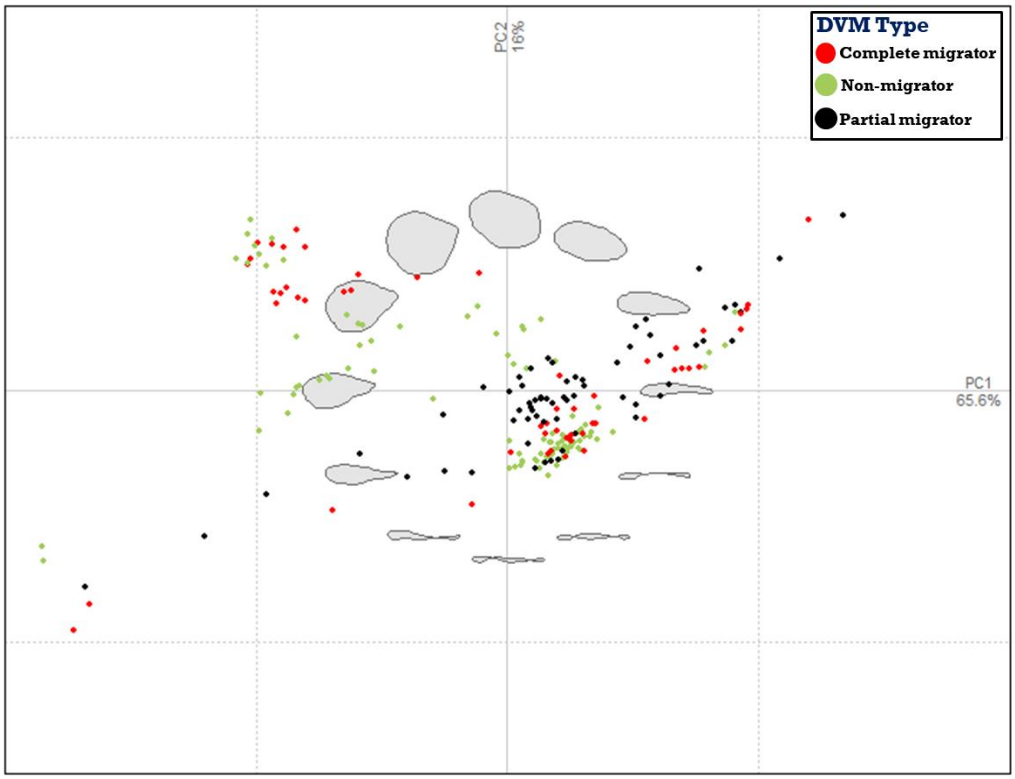

Figure 46 - Normalized PCA-ordinations of body shape among DVM types. Numbers next to the axis labels indicated the percentage of explained variation in morphology for that axis in a given ordination (PC 1 = 66% and PC 2 = 16%). Points that fell within the minimum convex polygons represented the realized morphology of body shape for each DVM type. The DVM types included: 1) Complete migrators, 2) non-migrators, and 3) partial migrators. Gray body shape silhouettes depicted the full continuum of morphospace among all DVM types for each species as calculated using harmonic coefficients through EFA.

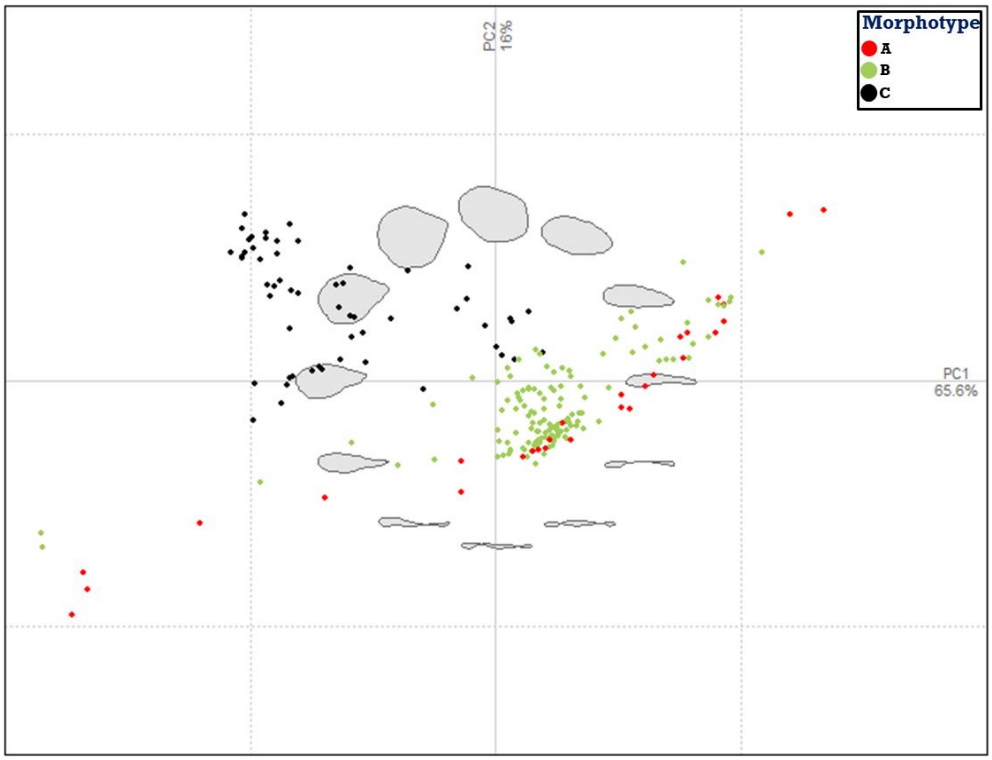

Figure 47 - Normalized PCA-ordinations of body shape among morphotypes. Numbers next to the axis labels indicated the percentage of explained variation in morphology for that axis in a given ordination (PC 1 = 66% and PC 2 = 16%). Points that fell within the minimum convex polygons represented the realized morphology of body shape for each morphotype. The morphotypes included: 1) A, 2) B, and 3) C (Sutton, 2003). Gray body shape silhouettes depicted the full continuum of morphospace among all morphotypes for each species as calculated using harmonic coefficients through EFA.

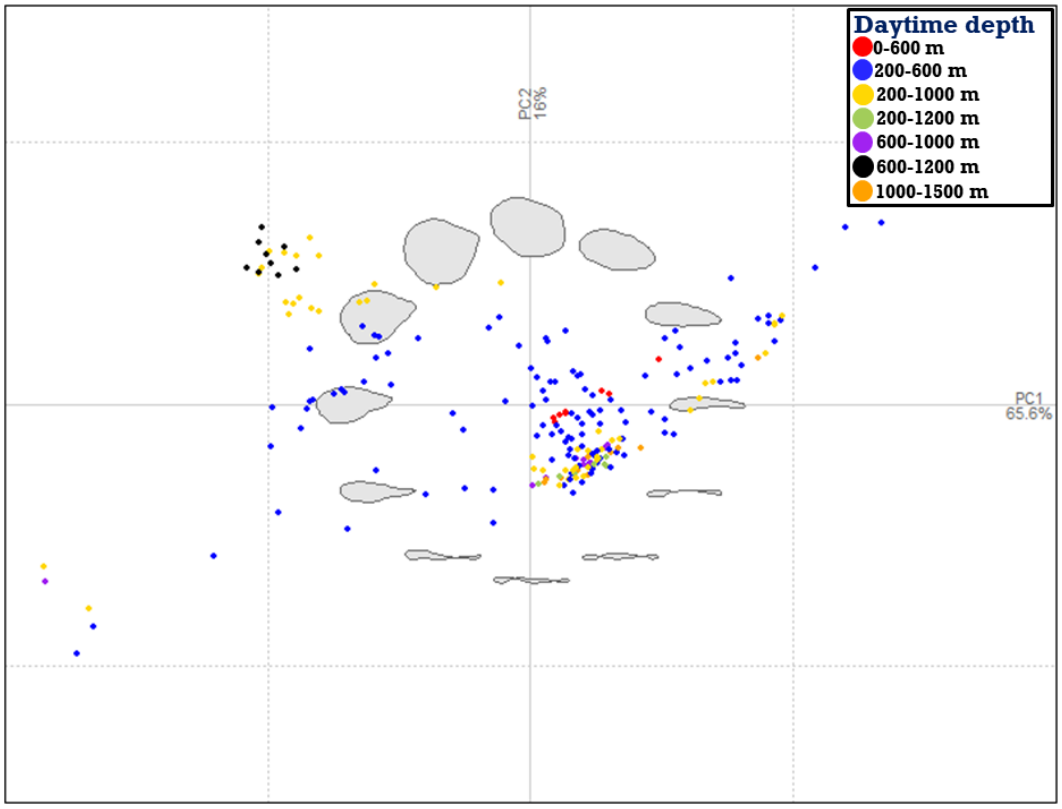

Figure 48 - Normalized PCA-ordinations of body shape among daytime depth distributions. Numbers next to the axis labels indicated the percentage of explained variation in morphology for that axis in a given ordination (PC 1 = 66% and PC 2 = 16%). Points that fell within the minimum convex polygons represented the realized morphology of body shape for each daytime depth. The daytime depth distributions included: 1) 0-600 m, 2) 200-600 m, 3) 200-1000 m, 4) 200-1200 m, 5) 600-1000 m, 6) 600-1200 m, and 7) 1000-1500 m. Gray body shape silhouettes depicted the full continuum of morphospace among all daytime depths for each species as calculated using harmonic coefficients through EFA.

Table 17 - Global ANOSIM results from the ecological traits assessment of outline analysis using a Bray Curtis matrix. Pairwise groupings were tested as unordered factors. The bolded R statistics and their corresponding p-values are those that were significant on the p-value ($p \leq 0.05$).

Ecological Trait	Global R Statistic	p-value
Morphotypes	**0.418**	**0.001**
DVM types	**0.064**	**0.001**
Daytime depths	-0.136	0.998

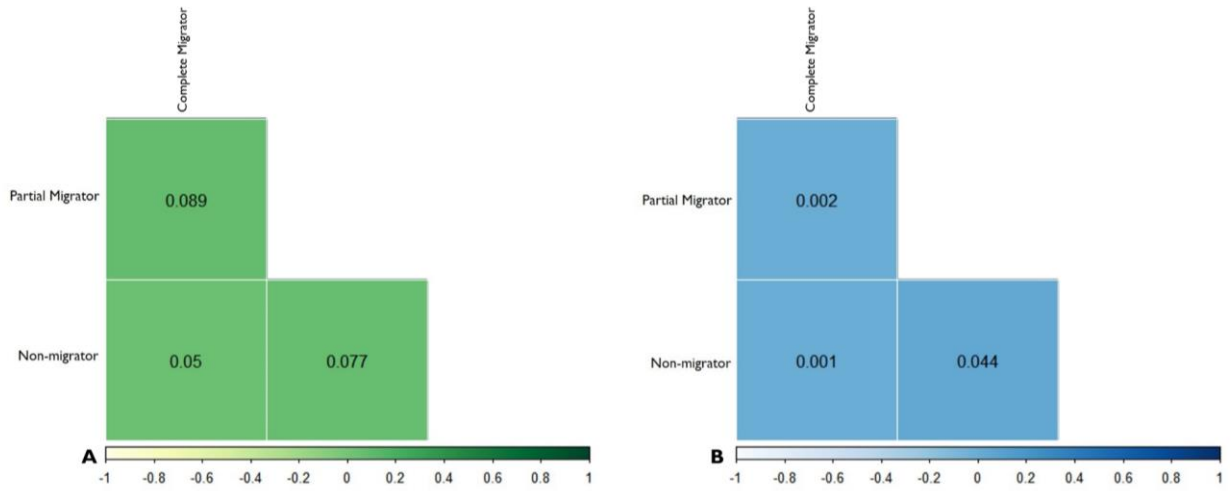

Figure 49 - Correlation matrix of ANOSIM results from DVM types assessment of outline analysis using a Bray Curtis matrix. Pairwise groupings were tested as unordered factors. Figure A represents the R statistic values and Figure B represents the corresponding p-values. The colored squares represented the significance of the values. The darker colored squares represented higher R statistics and p-values and the lighter colored squares represented lower values. Significant p-values are those that had a value less than 0.05.

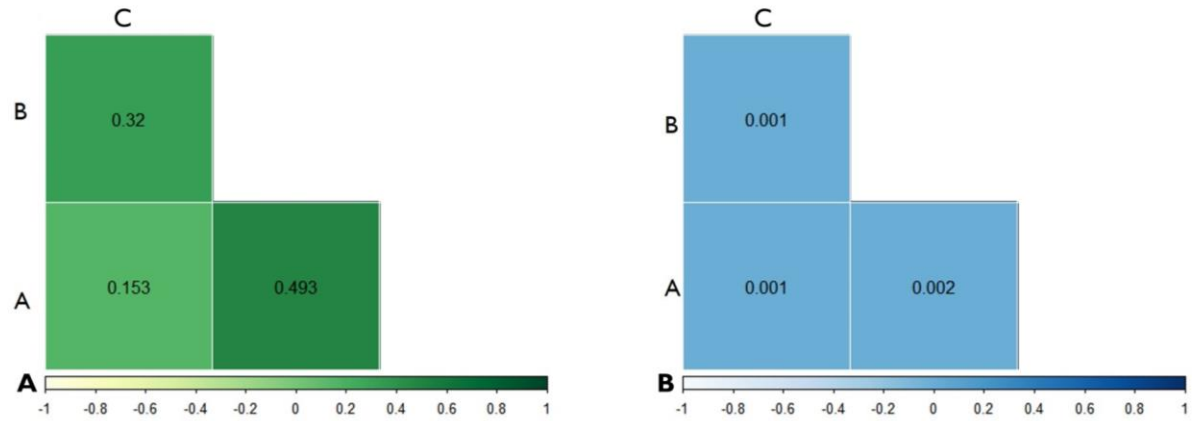

Figure 50 - Correlation matrix of ANOSIM results from morphotypes assessment of outline analysis using a Bray Curtis matrix. Pairwise groupings were tested as unordered factors. Figure A represents the R statistic values and Figure B represents the corresponding p-values. The colored squares represented the significance of the values. The darker colored squares represented higher R statistics and p-values and the lighter colored squares represented lower values. Significant p-values are those that had a value less than 0.05.

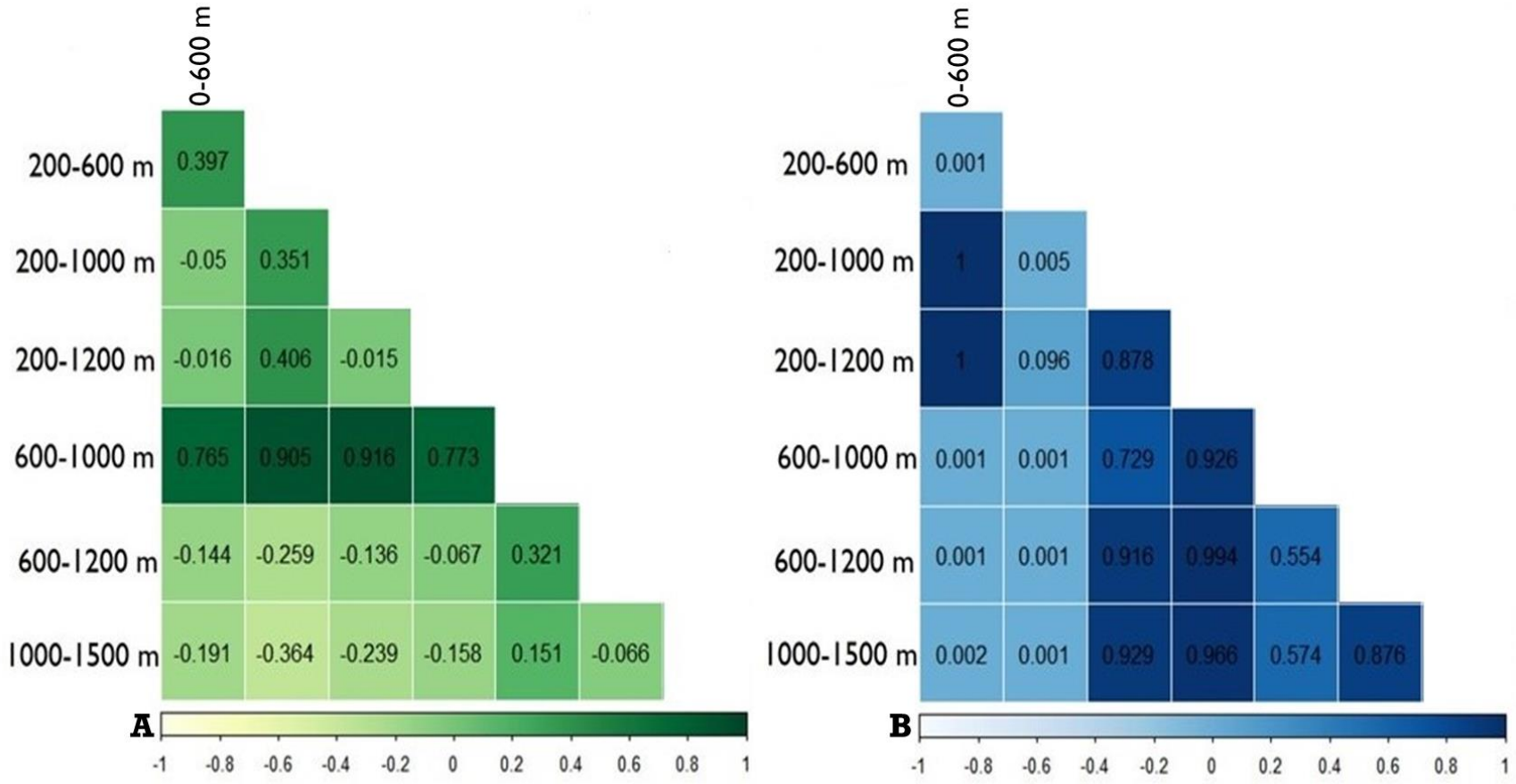

Figure 51 - Correlation matrix of ANOSIM results from daytime depths assessment of outline analysis using a Bray Curtis matrix. Pairwise groupings were tested as unordered factors. Figure A represents the R statistic values and Figure B represents the corresponding p-values. The colored squares represented the significance of the values. The darker colored squares represented higher R statistics and p-values and the lighter colored squares represented lower values. Significant p-values are those that had a value less than 0.05.

Predicting Traits

Predicting Morphotypes

When identifying individuals to their morphotypes, LCA had the highest percentage (95%) of individuals correctly identified (*Figure 52(a)*). Outline analyses had the second-best predictive power for Morphotypes (88%; *Figure 52(b)*), and SIMs were not as good a predictor as either LCA or outline analysis (85%; *Figure 52(c)*). Overall, morphotype predictions had the highest predictive power compared to the other morphometric techniques or ecological traits being analyzed. The confusion matrix of the normalized CAP for morphotypes is listed in *Table 18*. No significant differences were observed after the outlier (i.e., Sternoptychidae individual) was removed, and therefore, was included within the analyses.

Table 18 - Confusion matrix of the normalized CAP morphotype predictions

	Original Group	**C**	**B**	**A**	**Total**	**% Correct**
SIMs	C	56	0	0	56	100%
	B	0	108	24	132	82%
	A	0	8	20	28	71%
Outline	C	56	0	0	56	100%
	B	0	116	16	132	88%
	A	1	10	17	28	67%
LCA	C	54	2	0	56	96%
	B	0	129	3	132	98%
	A	0	5	23	28	82%

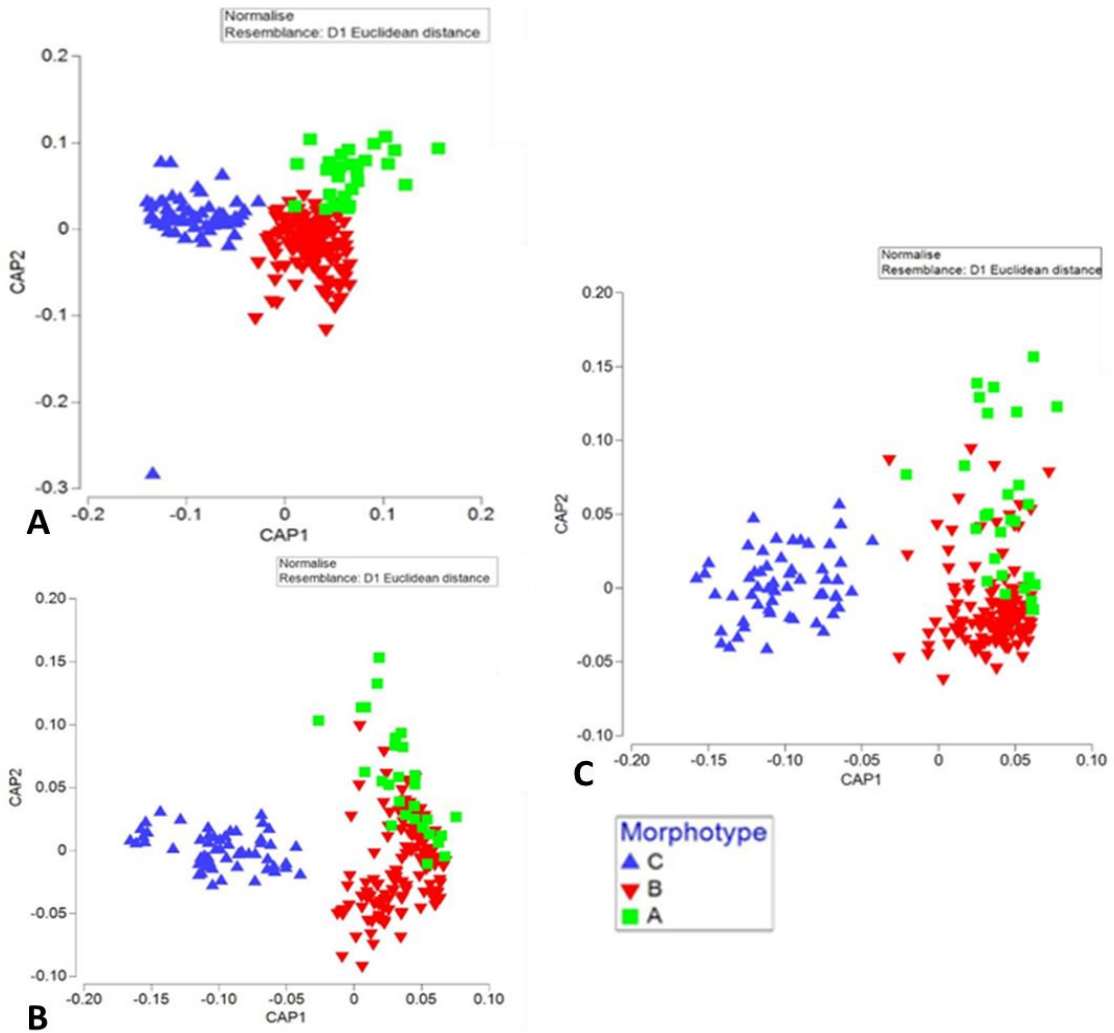

Figure 52 – Normalized metric CAP of all individuals using the landmark configuration analysis method (A), shape indicator measurements (B), and outline analysis (C), grouped by morphotypes.

Predicting DVM types

When identifying individuals by their DVM type, landmark configuration analysis had the highest percentage (65%) of individuals correctly identified (*Figure 53(a)*). Outline analysis had the second-best predictive power (56%) for DVM types (*Figure 53(b)*), and SIMs were not as good a predictor as LCA and outline analyses (48%; *Figure 53(c)*). The confusion matrix for the predictive performance of DVM types is listed in *Table 19*

Table 19 - Confusion matrix of normalized CAP DVM type predictions.

	Original Group	Complete migrator	Non-migrator	Partial migrator	Total	% Correct
SIMs	Complete migrator	21	14	19	54	39%
	Non-migrator	34	39	25	98	40%
	Partial migrator	9	11	44	64	69%
LCA	Complete migrator	25	21	8	54	46%
	Non-migrator	13	77	8	98	79%
	Partial migrator	16	10	38	64	59%
Outline	Complete migrator	22	10	22	54	41%
	Non-migrator	21	57	20	98	58%
	Partial migrator	11	11	42	64	66%

Predicting Daytime Depths

LCA and outline analysis had the highest percent of individuals correctly identified 58% of the time (*Figure 54(a)(b)*). SIMs were not as good a predictor as LCA and outline analyses (54%; *Figure 54(c)*). Three outliers were identified during outline analysis and were removed to compare if there were any significant differences in the data. No significant differences were observed and outliers were included within the CAP. The confusion matrix of the normalized CAP for predicting daytime depths from body shape is listed in *Table 20.*

Table 20 - Confusion matrix of the normalized CAP for daytime depth predictions.

	Original group	200-600 m	600-1000 m	1000-15000 m	200-1000 m	200-1200 m	0-600 m	600-1200 m	Total	% Correct
SIMs	200-600 m	75	6	5	18	2	19	5	130	58%
	600-1000 m	0	5	2	0	3	0	0	10	50%
	1000-1500 m	0	1	7	2	0	0	0	10	70%
	200-1000 m	6	6	3	11	10	0	2	38	29%
	200-1200 m	1	3	1	1	3	1	0	10	30%
	0-600 m	1	0	0	0	0	8	0	9	89%
	600-1200 m	0	0	0	1	0	0	8	9	89%
LCA	200-600 m	78	17	1	4	3	23	4	130	60%
	600-1000 m	0	8	1	0	1	0	0	10	80%
	1000-1500 m	0	1	6	0	3	0	0	10	60%
	200-1000 m	3	7	8	12	1	0	7	38	32%
	200-1200 m	0	3	1	0	6	0	0	10	60%
	0-600 m	0	0	0	1	0	8	0	9	89%
	600-1200 m	0	0	0	0	1	0	8	9	89%
Outline	200-600 m	120	0	0	7	0	3	0	130	92%
	600-1000 m	9	0	1	0	0	0	0	10	0%
	1000-1500 m	10	0	0	0	0	0	0	10	0%
	200-1000 m	37	0	1	0	0	0	0	38	0%
	200-1200 m	9	0	0	1	0	0	0	10	0%
	0-600 m	5	0	0	0	0	4	0	9	44%
	600-1200 m	8	0	0	0	0	0	1	9	11%

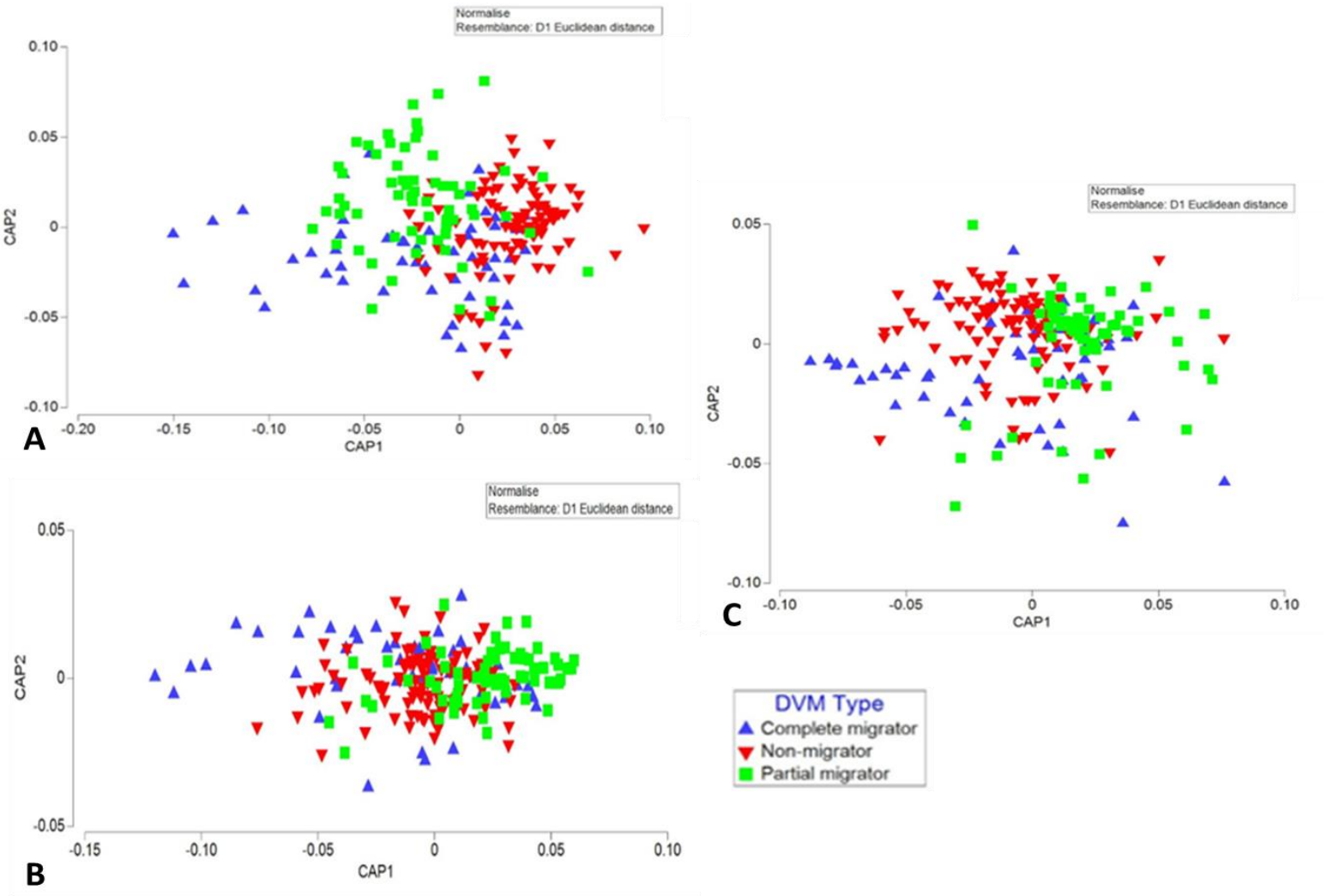

Figure 53 – Normalized metric CAP of all individuals using the landmark configuration analysis method (a), shape indicator measurements (b), and outline analysis (c), grouped by DVM types.

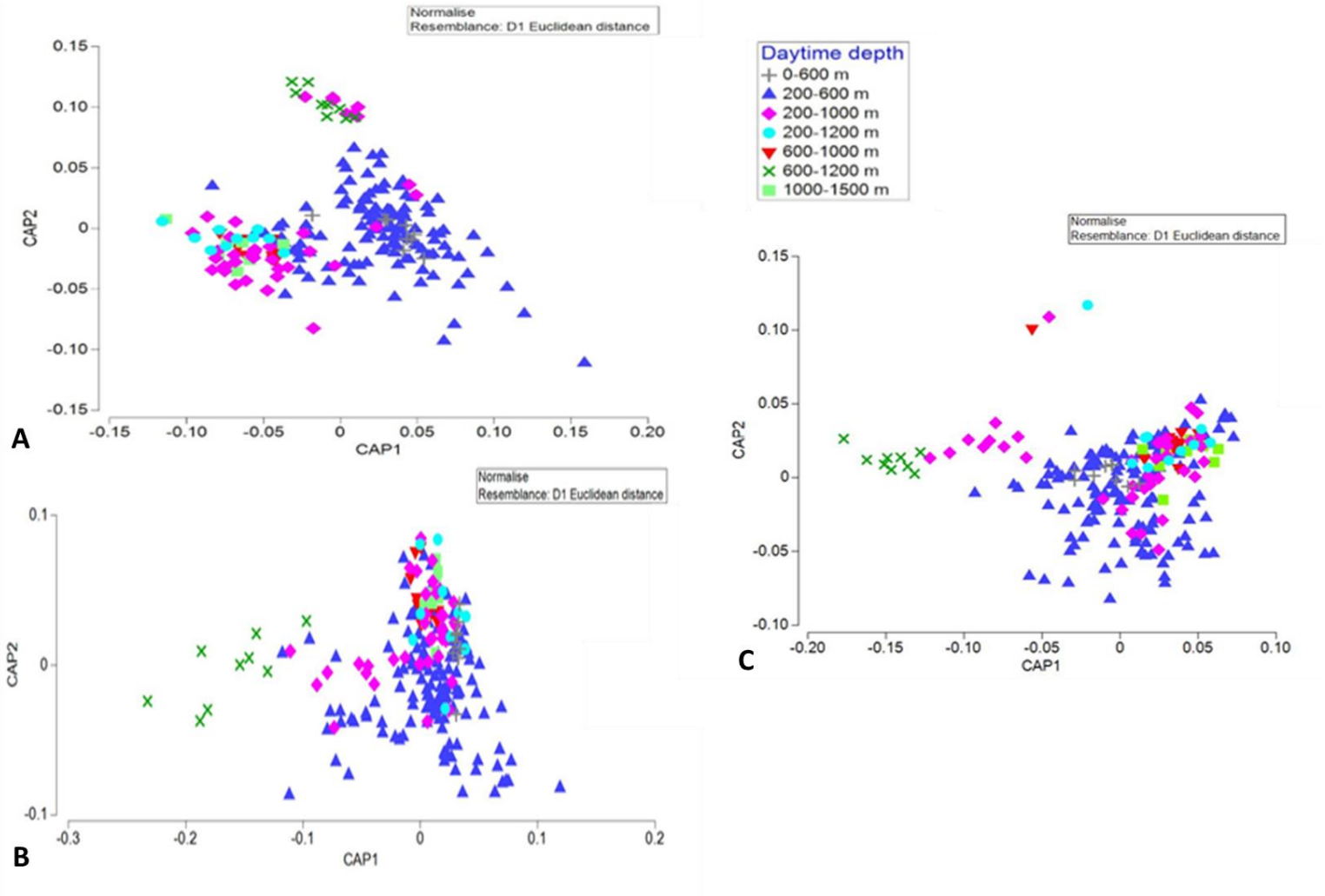

Figure 54 – Normalized metric CAP of all individuals using the landmark configuration analysis method (A), shape indicator measurements (B), and outline analysis (C), grouped by daytime depths.

Discussion

Fishes may vary in shape due to age, sex, geographic location, or phylogenetic relationship (Lawing & Polly, 2010). In many situations, assessing the shape variation among fishes can reveal insights into their functioning and the underlying mechanisms leading to certain variations in shape (Bonhomme et al., 2014). Here, I examined the relationship between the body shape of stomiiform fishes and their established traits by assessing the feasibility of three computer-aided morphometric tools. In the present study, computer-aided morphometric techniques were relatively successful in distinguishing between some taxa, but the extent of its success varied according to the taxa and the technique used. Functional traits associated with DVM and vertical distributions were generally significant, but showed similar variability across techniques and taxa. Despite this, the fact that this study was based exclusively on the lateral body shape of fixed specimens strongly suggests that these tools show considerable promise in future research.

Part 1: Body Shape vs. Taxonomy

In the present study, higher taxonomic ranks was more closely aligned with body morphology of stomiiform fishes than the other parameters examined. The greatest variation in the body shape of stomiiform fishes was observed when individuals were classified to their species and genus levels. The body shape of stomiiform fishes varied more within their families than between families.

Interestingly, the genus level showed the greatest separation of body morphology of the three taxonomic ranks. An explanation for better resolution at the genus level than at species and family levels may relate to the fact that some taxonomically important features of stomiiform fishes (e.g., photophores, fins, and gape size) were not included in the present study. The entire morphology of an individual is commonly used to classify them into their taxonomic resolutions; the lower the taxonomic rank the more morphological features, such as body shape, are shared between individuals. For example, stomiids are generally separated to species level by comparing their gape of mouth, teeth, elongated bodies, lateral photophore series, and barbels to other individuals (Sutton et al., 2020b). To further identify individuals to their species morphological features not common to all individuals (i.e., barbels) are used. Due to the exclusion of these specific morphological features the identification of individuals to species

level may not be possible based on simple body shape. Specifically, when individuals within the families Phosichthyidae and Stomiidae were compared to one another they showed the weakest separation between one another and were insignificant. Certain species within these families share similar body shapes, but differ with finer-scale morphological features. The stomiiform fishes' body shape may have allowed for individuals to be best distinguished down to genus levels, but further external morphological features (e.g., location/occurrence of photophores) may be needed to predict species for individuals whose body shapes are similar to one another.

Across all taxonomic ranks, *Sternoptyx* spp., *Argyropelecus* spp., and *Polyipnus* spp. (family Sternoptychidae) tended to exhibit the strongest separation between species, genera, and families. Of the three morphotypes, hatchetfishes (Sternoptychidae) exhibited circular and concave body forms that were very characteristic and should be easily identifiable in profile view, whereas the outlines comparing the genera of *Chauliodus*, *Photostomias*, and *Pollichthys* for example (which share elongated body shapes) were not as easily distinguishable.

Part 2: Body Shape vs. Traits

Morphotype traits and body shape had the most significant relationship as they both describe the morphology of stomiiform fishes. Morphotype C (i.e., laterally compressed and short bodies; "hatchet" type) and morphotype A (i.e., elongated bodies) formed the largest differences in body shapes for LCA and SIMs. For outline analysis, morphotype B (i.e., fairly compressed and elongated bodies) and morphotype C had the greatest differences in body shapes. For all three computer-aided morphometric techniques, morphotype A and morphotype B were the most similar. In this study, the three groups identified by Sutton (2003) were also distinguished as distinct groups. The elongation of stomiiform fishes was the main contributor to species distinction, which is similar to previous morphometric studies (e.g., Caillon et al., 2018; Martinez et al., 2021). It was unclear why outline analysis differed from the LCA and SIMs' strongest groupings of body shapes. An explanation may be found in the limitations of outline analysis (e.g., sensitivity to misalignment and human error during the imaging and digitization processes), which is discussed further below.

Body shape varied significantly with DVM type, but suggested group overlap between body shapes and DVM types, specifically when comparing partial migrators. The relationship

between body shapes on DVM types was a surprising observation because previous studies have described body shape as a reliable indicator of swimming behavior, which has some influence on a fish's feeding performance and location within the water column (Webb, 1984; Motta & Kotrschal, 1992; Wainwright & Richard, 1995). The greater number of partial migrators selected, and the similarity in body form between *Cyclothone* (non-migrator) and the other gonostomatids and phosichthyids (migrators) may have biased the DVM results from this study, but regardless, only small differences were observed. While previous studies have analyzed the advantages and disadvantages of deep-sea fish morphology, how their body shapes relate to their migration patterns is still not widely known (e.g., van Ginneken et al., 2005; Sébert et al., 2009). Stomiiform fishes exhibit a wide variety of morphologies and DVM types; however, it is possible that individuals grouped within the same taxon may not exhibit the same DVM patterns. Individuals within the *Argyropelecus* genus exhibit similar, laterally compressed body forms yet conduct different migration patterns. Within the GoM, *Argyropelecus gigas* and *Argyropelecus hemigymnus* individuals were identified as occurring at a depth of 200-600 m during both day and night (non-migrators), whereas *Argyropelecus aculeatus* individuals' core daytime depth distributions ranged between 200-1000 m, but migrated to the epipelagic during the night (complete migrators). Similarly, individuals within the same species may display asynchronous DVM patterns, such as *Chauliodus sloani* (Clarke, 1973; Sutton & Hopkins, 1996), suggesting that not all individuals are migrating each day. At the population level, individuals must be capable of conducting migrations (which may distinguish them from non-migrators), but they do not necessarily complete it every day (which might distinguish them from complete migrators). Historically, DVM types have been assigned at the population level and these classifications were used within this study. However, over time it has been observed that there is usually not a taxonomic group where all individuals migrate in the same way throughout life, so it may be more appropriate for DVM patterns to be analyzed within sub-population groups that account for these additional variables of importance. The choice of DVM type classifications used for this study may be a contributing factor to the inconclusive results observed in this study.

There were few significant relationships between the body shape of stomiiform fishes and their daytime depth distributions, and they were only identified by the SIMs. One explanation for the lack of influence on body shape was suggested by Moser (1981) who discussed that

differences in fish's vertical location could be mostly explained in relation to their morphological specializations for feeding and predator evasion strategies under different light regimes that reach their respective depth layers. The positioning a fish chooses within the water column may therefore be determined by behavioral traits and/or other non-measured adaptations, such as coloration, bioluminescence, and eye morphology more than body shape *per se*. Another explanation for the lack of influence body shape has on daytime depth distributions may be related to an individual's physiology. Pauly (2010) proposed that an individual's physiology (i.e., their metabolism, temperature, or oxygen consumption) can explain how fish regulate their DVM patterns to maintain an appropriate abiotic regime for their size and species. Additionally, the daytime depth distributions varied greatly between species and certain daytime depth ranges were occupied by more species than others (e.g., the daytime depth of 0-600 m was occupied by one species whereas the daytime depth of 200-600 m had thirteen species). Clarke and Gorley (2015) discussed that ANOSIM results may be biased by the number of individuals per variable being compared. As with the other ecological traits (e.g., DVM types), further functional testing would be required to support these hypotheses. Additional functional testing should include an analysis of the entire morphology of stomiiform fishes to fully exclude the body shape as a significant driver of daytime depth distributions.

Part 3: Evaluation of Computer-Aided Morphometric Techniques

Computer-aided morphometric techniques are considered suitable methods for exploring deep-sea fish morphological variability and for a rough assessment of ecological traits within and between individuals (Loy et al., 2001; Prosanta, 2006; Radinović & Kajtez, 2021). The use of computer-aided morphometric techniques has rapidly increased in the field of biological sciences (Slice, 2007; Polly, 2008; Lawing & Polly, 2010). Some examples include, assessing geographic variations, phylogeography, sexual dimorphism, and morphological integration. Olson and Miller (1958) pioneered the use of statistical correlations to test the hypothesis that certain characteristics of organisms were functionally or developmentally linked. Computer-aided morphometric techniques naturally complement the hypothesis suggested by Olson and Miller (1958) because potentially integrated, developmentally and functionally complicated structures such as vertebrate skulls are readily quantified with landmarks. Some advantages of using computer-aided morphometric techniques include: 1) applicability to photographs and quick data acquisition; 2) efficiency in terms of time, money, and effort (McPherron & Dibble, 1999); 3) its

suitability for quantitatively describing, and comparing any similarities and differences in shape; and 4) methodological repeatability (Webster & Sheets, 2010).

In the present study, three computer-aided morphometric techniques were used to discriminate individuals through the inter- and intra-specific differences of stomiiform fish morphology. The results from the CAP analyses were highly variable across taxa, with some species being perfectly identified, and some always being incorrectly identified depending on the computer-aided morphometric technique. LCA had the highest overall predictive success rate within this study and always successfully predicted *Photostomias guernei* individuals (100%). The success in predicting *Photostomias guernei* individuals may be attributed to the larger distances between landmarks and their higher caliper values, which were responsible for the most dissimilarity between body shapes. Webster and Sheets (2010) described the two limitations of LCA as the shape variation between landmarks not being detected (i.e., if not enough landmarks were selected to adequately represent the morphology of individuals), and its susceptibility to human error created during the manual imaging and digitization processes. While this study employed only five landmarks, potentially leading to missing body shape variations, it was still the most successful technique. The addition of further landmarks (e.g., the posterior end of the dorsal and anal fins) could be employed in the future and may help improve predictive rates as the position and length of these fins are often used to differentiate between individuals within certain genera (e.g., *Chauliodus* and *Photostomias*).

Outline analysis had the second-best predictive power, which was an unexpected finding. A 100% prediction success rate was only achieved for *Sternoptyx pseudobscura* individuals using outline analysis. An explanation for the successful prediction of Sternoptychidae species may be attributed to the body shapes of these individuals. Due to their easily identifiable shapes less harmonics may have been needed to distinguish their body shapes between other species. Overall, finer resolution in body shape differences could explain outline analysis' lack of success with other species predictions, since the noise in the data may have led to more overlap in outline values. Potential contributors to the addition of noise could have been due to the preservation process or the method of storage causing curling and arching of body shapes (Sotola et al., 2019). Previous studies have found that standard body lengths decreased after formalin fixation and ethanol preservation (Shields & Carlson, 1996; Greszkiewicz & Fey, 2018), while others an

increase in the weight of specimens from certain formalin solutions (Shields & Carlson, 1996), and temporary compression of specimens within jars (i.e., the jar "effect"; Valentin et al., 2008; Larochelle et al., 2016; Sotola et al., 2019). It is well known that body shape is altered during the preservation of biological specimens, however, there have been few detailed studies on the extent to which morphological changes occur during the preservation process. Sotola et al. (2019) used LCA to examine the effects of formalin and ethanol preservation on the body shape of 10 freshwater species over 90 days. They found that the body shape of fishes continued to change even after the entire preservation process was completed. Although the measurement error from preservation techniques is usually regarded as a relatively small component of variance in the data, steps were taken to attempt to minimize any influence within this study, while not directly measuring for it. These steps included: 1) smoothing of outlines; 2) standardizing data acquisition and image selection procedures; 3) one person collecting and analyzing data; and 4) a camera mounted for constant focal length and specimen placements. Nonetheless, minor changes in outline shape from preservation techniques could have led to important changes in body shape altering important results. Additionally, outline analysis methods have also been critiqued because their individual outlines are not biologically homologous (Zelditch et al., 1995). This criticism is only important in cases where a one-to-one comparison between individual variables and biological homology (i.e., shared features) is required. However, in the case of this study, because of the comparisons between overall shape, the fish outlines themselves are biologically homologous (Webster and Sheets, 2010).

The lowest predictive power was observed in SIMs. SIMs always successfully predicted *Argyropelecus aculeatus* individuals (100%). The success in predicting *Argyropelecus aculeatus* individuals may be attributed to their larger Haralick circularity values, which was one of the three SIMs contributing the most to dissimilarity between body shapes. While caliper size and centroid size contributed the most to dissimilarity between body shapes they were the most difficult SIMs to distinguish between, where individuals with these higher values (*Chauliodus sloani* and *Sigmops elongatus*) had weaker groupings. One limitation of SIMs that may have made this method less effective was its sensitivity to noisy and askew shapes. For instance, the compactness equation uses the perimeter and area of a region, where lower values correspond to

circular shape (Rosin, 2005), but is inherently sensitive to artifacts introduced by digitization, and can incorrectly assign non-circular values to noisy circles (Rosin, 2005).

Within deep-sea fish ecology, a study conducted by Caillon et al. (2018) used outline analysis to describe the morphological diversity of marine fishes. Elliptical Fourier analysis revealed three body shape variations when depth increases (Caillon et al., 2018). The most important component of body shape variation was the elongation of the body; the second was the development of the pelvic fin; and the third was the shape of the dorsal and caudal fins (Caillon et al., 2018). LCA and outline analyses from this study revealed somewhat contradictory results to that of Caillon et al. (2018), where the greatest contributors to variation with this study's sample set were the caudal and pelvic fins. However, the SIMs highlighted caliper size (i.e., the longest distance between two points; *Table 2*) and Haralick circularity (i.e., how circular a fish is; *Table 2*) as two important components of variation in body shapes. These two SIMs can be compared to elongation further supported by Caillon et al.'s (2018) findings.

Part 4: Considerations for Future Work

Several considerations should be made when reviewing the validity of the results from this study for future work. An original aim was to analyze the entire morphology of stomiiform fishes within the sample set. However, a high percentage of the collected specimens from the ONSAP and DEEPEND programs had damaged fins that could not be accurately incorporated into the LCA or outline analysis, resulting in only the body shape of the stomiiform fishes being assessed. To fully capture any variability present with the morphology of individuals the specimen conditions needed to remain consistent (i.e., no missing fins or curvature of the body). Additionally, the results of this study may have been affected by the number of individuals per species and were only representative of the sample set analyzed rather than representing the taxon as a whole.

Only using body shape for individuals may have biased some results of this study. Different aspects of fish body morphology are separately analyzed to understand how the whole organism functions (Bonhomme et al., 2014). Individual aspects of the body reveal insights into an organism's functioning, such as body shape. The shape of a fish's body may reveal potential habitats that the individual lives in and certain aspects of their locomotion. However, the fins of

fishes can reveal additional characteristics of locomotion and stabilization. Additionally, this study only examined the 2-dimensional shape of fishes and could not consider body depth, which may contribute to the patterns shown through the traits assessed. Previous research on the morphology of stomiiform fishes is extensive and readily available (Sutton, 2003; Sutton et al., 2020b). The largest consideration for future research on the entire morphology of stomiiform fishes would be the quality of specimens, specifically focused on the success of imaging. As per Sotola et al.'s (2019) suggestion, photographing fresh specimens could be very useful for future studies using computer-aided morphometric techniques. Herler et al. (2007) suggested that using a flatbed scanner on live and/or recently captured specimens allowed for better manipulation of individuals to fully capture the shape, coloring, and positioning of all morphological features. Herler et al. (2007) discussed the advantages of a flatbed scanner which included: 1) a simple setup, 2) negligible material costs, 3) simple treatment of specimens, and 4) a decrease in human error within the imaging process. Flatbed scanners may be a viable option in the future for automatically capturing a specimen's shape and not having to worry about damage done by preservation techniques.

Only external morphological features were analyzed here, rather than both external and internal features. While only three functional traits of stomiiform fishes were assessed during this study, more functional traits should be analyzed to assess if they are good predictors of individuals identity or are drivers of the form of individuals. Future studies should focus on functional traits, such as diet, as well as other morphological traits such as eye size and type or presence of swim bladders, to name a few. Diet and feeding modes may dictate where a fish resides within the water column, its behaviors/interactions with other organisms, gape size, and nutrient requirements. Studies have shown a link between the body shape and resource use of fish species (Kassam et al., 2003; Maldonado et al., 2009). The diet and locomotive strategies of deep-sea fishes have also been extensively described for certain species, but far more remain undescribed (Collins et al., 1999; Carmo et al., 2015; Priede, 2017). Additionally, swim bladder morphology could be assessed due to its role in rising or sinking within the water column, which may be related to the DVM types that an individual exhibits (Fänge, 1983). For example, Marshall (1960) surveyed deep-sea fish swim bladders and discussed different patterns found within the mesopelagic and bathypelagic zones. Within the mesopelagic zone, most species of

myctophids (lanternfishes) and Sternoptychidae (hatchetfishes) have swim bladders, however some species have reduced or lipid-filled swim bladders. Within the bathypelagic zone, stomiids, ceratioid anglerfishes, and deep-living Gonostomatidae lacked a gas-filled swim bladder (Marshall, 1960). Additionally, certain demersal species (i.e., Macrourids, Brotulids, and Halosaurs) have fully functional swim bladders, but they are mostly absent in others. Bone (1973) classified myctophid species into four groups according to their buoyancy characteristics and discovered that the species that made the longest DVM migrations lacked a swim bladder. Fänge (1983) suggested that the swim bladder hinders more than aids fishes in vertical movements. However, these morphological studies have only been conducted on a small number of species. The assessment of diet and swim bladder types were beyond the scope of the present study due to the wide range of swim bladder prevalence and types within similar species. Further investigations assessing ecological traits of individuals may reveal new patterns connecting the form and functions of stomiiform fishes.

One large obstacle when using computer-aided morphometric techniques is removing the size of individuals as a factor from analysis. Many techniques employ methods to assist in the removal of obstacles (i.e., size) including Procrustes superimpositions, scaling, and rotating of the individuals. However, in the case of fishes, size may be an important determinant of traits in and of itself and warrants further consideration in future work. Body size will always differ in some ways due to biological variables such as individual growth rates or ontogeny, and through measurement errors (e.g., photos rotated or centered differently no matter how carefully the images were photographed; Klingenberg, 2011; Savriama et al., 2018). Future research questions should focus on the concept of size and its potential implications for effecting shape and function of individuals.

Before computer-aided morphometric techniques become standard tools for describing the variability of fish body shape, more research on measurement error should be conducted. Savriama et al. (2018) accounted for two measures of error within landmark configuration analysis and they included measurement and digitizing errors. Measurement errors focused on images of individuals (i.e., differences in pictures of the same specimen). The digitizing errors focused on the technique being used (i.e., differences in landmarks of the same picture of a specimen). Savriama et al. (2018) employed a Procrustes ANOVA through MorphoJ to assess

whether the error from measurements and digitization was statistically significant and had an impact on the variability of flower petals. The Procrustes ANOVA revealed that the variation among the flower petals was greater than the measurement error due to imaging and digitization. When comparing imaging and digitization error, imaging error was more significant than digitization error (Savriama et al., 2018). These results suggested that the biological variation at the population level was so large that it exceeded any sources of error. Additionally, extra care should be taken during the imaging process for any computer-aided morphometric techniques. Future research using computer-aided morphometric techniques should incorporate replicate imaging and digitizing of specimens for among-specimen shape comparisons to calculate within-specimen measurement error (Webster & Sheets, 2010; Savriama et al., 2018).

Conclusion:

The results of this study showed combining computer-aided morphometric techniques with taxonomic and traditional assessments can open a wide range of new potential applications to further understand deep-sea fish morphologies and how they relate to their functioning within the deep sea. The results of this study indicate that the body shape of stomiiform fishes alone does not correlate closely with their described DVM patterns or daytime depth distributions, suggesting that behavioral factors may override strict morphological constraints in deep-pelagic ecosystems. The morphotypes described by Sutton (2003) corresponded with the body shape of stomiiform fishes analyzed in this study. Additionally, landmark configuration analysis appeared to offer a useful and reliable method that may assist researchers in the prediction of individuals and traits through their morphologies. This project only used five landmarks and several damaged specimens, yet was still able to predict body shapes down to meaningful taxonomic levels and functional traits. The addition of landmarks and other morphologies in future research may make landmark configuration analysis a common tool for assisting taxonomists in identification of specimens.

References:

Afonso, P., McGinty, N., Graça, G., Fontes, J., Inácio, M., Totland, A., & Menezes, G. (2014). Vertical migrations of a deep-sea fish and its prey. PLoS ONE, 9(5), 97884-97884. doi:10.1371/journal.pone.0097884.

Angel, M., & Pugh, P. (2000). Quantification of diel vertical migration by micronektonic taxa in the northeast Atlantic. Hydrobiologia, 440, 161-179. doi:10.1023/A:1004115010030.

Badcock, J., & Merrett, N. (1976). Midwater fishes in the eastern North Atlantic. Vertical distribution and associated biology in 30°N, 23°W, with developmental notes on certain myctophids. Progress in Oceanography, 7(1), 3-58. doi: https://doi.org/10.1016/0079-6611(76)90003-3.

Blanchard, J., Dulvy, N., Jennings, S., Ellis, J., Pinnegar, J., Tidd, A., & Kell, L. (2005). Do climate and fishing influence size-based indicators of Celtic Sea fish community structure? ICES Journal of Marine Science, 62, 405-411. doi:10.1016/j.icesjms.2005.01.006.

Bone, Q. (1973). A note on the buoyancy of some lantern-fishes. (Myctophoidei). Journal of the Marine Biological Association. U.K., 53, 619-633.

Bonhomme, V., Picq, S., Gaucherel, C., & Claude, J. (2014). Momocs: outline analysis using R. Journal of Statistical Software, 56(13). doi:10.18637/jss.v056.i13.

Bookstein, F. L. (1991). Morphometric tools for landmark data: Geometry and Biology. Cambridge University Press. doi: 10.1017/CBO9780511573064.

Bookstein, F. L., B., Chernoff, R. L., Elder, J. M., Humphries, Jr., Smith, G. R., & Strauss, R. E. (1985). Morphometrics in evolutionary biology. Special Publication 15, Academy of Natural Sciences, Philadelphia.

Borazjani, I., & Sotiropoulos, F. (2009). Numerical investigation of the hydrodynamics of anguilliform swimming in the transitional and inertial flow regimes. Journal of Experimental Biology, 212, 576–592. doi:10.1242/jeb.025007.

Brierley, A. S. (2014). Diel vertical migration. Current Biology, 24(22), 1074-1076. doi:10.1016/j.cub.2014.08.054.

Buesseler, K. O., Lamborg, C. H., Boyd, P. W., Lam, P. J., Trull, T. W., Bidigare, R. R., Bishop, J. K., Casciotti, K. L., Dehairs, F., Elskens, M., Honda, M., Karl, D. M., Siegel, D. A., Silver, M. W., Steinberg, D. K., Valdes, J., Van Mooy, B., & Wilson, S. (2007). Revisiting carbon flux through the ocean's twilight zone. Science (New York, N.Y.), 316(5824), 567–570. doi: https://doi.org/10.1126/science.1137959.

Caillon, F., Bonhomme, V., Möllmann, C., & Frelat, R. (2018). A morphometric dive into fish diversity. Ecosphere, 9(5). doi:10.1002/ecs2.2220.

Carmo, V., Sutton, T., Menezes, G., Falkenhaug, T., & Bergsta, O. A. (2015). Feeding ecology of the Stomiiformes (Pices) of the northern Mid-Atlantic Ridge. 1. The Sternoptychidae and Phosichthyidae. Progress in Oceanography, 130, 172-187. doi: 10.1016/j.pocean.2014.11.003.

Childress, J. J. (1995). Are there physiological and biochemical adaptations of metabolism in deep-sea animals? Trends in Ecology and Evolution, 10(1), 30–36. doi: https://doi.org/10.1016/S0169-5347(00)88957-0.

Clarke, T. A. (1973). Some aspects of the ecology of lanternfishes (Myctophidae) in the Pacific Ocean near Hawaii. Fishery Bulletin. US, 71, 401-434.

Clarke, K. R., & Gorley, R. N. (2015). PRIMER v7: User manual/tutorial. PRIMER-E, Ltd., Plymouth, United Kingdom.

Claude, J. (2008). Morphometrics with R. Springer, New York, New York, USA. doi:10.1007/978-0-387-77789-4.

Claverie, T., & Wainwright, P. C. (2014). A morphospace for reef fishes: elongation is the dominant axis of body shape evolution. PLoS One. 9(11):e112732. doi: 10.1371/journal.pone.0112732.

Collins, M. A., Bailey, D. M., Ruxton, G. D., & Priede, I. G. (2005). Trends in body size across an environmental gradient: A differential response in scavenging and non-scavenging demersal deep-sea fish. Proceedings of the Royal Society B: Biological Sciences, 272(1576), 2051-2057. doi:10.1098/rspb.2005.3189.

Collins, M. A., Priede, I. G., & Bagley, P. M. (1999). In situ comparison of activity of two deep-sea scavenging fish occupying different depths zones. Proceedings of the Royal Society, Series B, 266, 2011-2016.

Cook, A. B., Bernard, A. M., Boswell, K. M., Bracken-Grissom, H., D'Elia, M., deRada, S., Easson, C. G., English, D., Eytan, R. I., Frank, T., Hu, C., Johnston, M. W., Judkins, H., Lembke, C., Lopez, J. V., Milligan, R. J., Moore, J. A., Penta, B., Pruzinsky, N. M., Quinlan, J. A., Richards, T. M., Romero, I. C., Shivji, M. S., Vecchione, M., Weber, M. D., Wells, R. J. D., & Sutton, T. T. (2020). A multidisciplinary approach to investigate deep-pelagic ecosystem dynamics in the Gulf of Mexico following Deepwater Horizon. Frontiers in Marine Science, 7(548880). doi:10.3389/fmars.2020.548880.

Dhingra, R. D., Barnes, J. W., Brown, R. H., Burrata, B. J., Sotin, C., & Nicholson, P. D. (2019). Observational evidence for summer rainfall at Titan's north pole. Geophysical Research Letter, 46, 1205-1212. doi: 10.1029/2018GL080943.

Drazen, J. C., & Sutton, T. T. (2017). Dining in the deep: the feeding ecology of deep-sea fishes. The Annual Review of Marine Science, 9, 337-66. doi: 1146/annrev-marine-010816-060543.

Dypvik, E., Klevjer, T. A., & Kaartvedt, S. (2012). Inverse vertical migration and feeding in glacier lanternfish (*Benthosema glaciale*). Marine Biology, 159(2), 443–453. doi: 10.1007/s00227-011-1822-4.

Eduardo, L. N., Bertrand, A., Mincarone, M. M., Santos, L. V., Frédou, T., Assunção, R. V., Silva, A., Ménard, F., Schwamborn, R., Le Loc'h, F., & Lucena-Frédou, F. (2020). Hatchetfishes (Stomiiformes: Sternoptychidae) biodiversity, trophic ecology, vertical niche partitioning and functional roles in the western tropical Atlantic. Progress in Oceanography, 187(102389). doi: https://doi.org/10.1016/j.pocean.2020.102389.

Elmer, K. R., Kusche, H., Lehtonen, T. K., & Meyer, A. (2010). Local variation and parallel evolution: Morphological and genetic diversity across a species complex of neotropical crater lake cichlid fishes. Philosophical Transactions of The Royal Society B Biological Sciences, 365(1547), 1763-1782. doi:10.1098/rstb.2009.0271.

Fänge, R. (1983). Gas exchange in fish swim bladder. In: Reviews of Physiology, Biochemistry and Pharmacology. Reviews of Physiology, Biochemistry and Pharmacology, Springer, Berlin, Heidelberg, 97. doi: https://doi.org/10.1007/BFb0035347.

Farré, M., Tuset, V. M., Maynou, F., Recasens, L., & Lombarte, A. (2016a). Selection of landmarks and semilandmarks in fishes for geometric morphometric analyses in ecological studies: a comparative from analytical methods. Scientia Marina, 80(2). doi:10.3989/scimar.04280.15A.

Farré, M., Tuset, V. M., Cartes, J. E., Massutí, E., & Lombarte, A. (2016b). Depth-related trends in morphological and functional diversity of demersal fish assemblages in the western Mediterranean Sea. Progress in Oceanography, 147, 22-37. doi: https://doi.org/10.1016/j.pocean.2016.07.006.

Fink, W. L. (1985). Phylogenetic interrelationships of the stomiid fishes (Teleostei: Stomiiformes). Miscellaneous Publications Museum of Zoology. University of Michigan, 171, 1–127.

Fricke, R., Eschmeye, W. N., & Van der Laan, R. (eds) 2022. Eschmeyer's Catalog of Fishes: Genera, Species, References.

Friedman, S. T., Price, S. A., Corn, K. A., Larouche, O., Martinez, C. M., & Wainwright, P. C. (2020). Body shape diversification along the benthic-pelagic axis in marine fishes. Royal Society Publishing Proceedings B, 287. doi: 10.1098/rspb.2020.1053.

Freer, J. J., & Hobbs, L. (2020). DVM: The World's biggest game of hide-and-seek. Frontiers for Young Minds, 8(44). doi: 10.3389/frym.2020.00044.

Gower, J. C. (1975). Generalized procrustes analysis. Psychometrika, 40(1), 33-51. doi:10.1007/BF02291478.

Gjøsæter, J., & Kawaguchi, K. (1980). A review of the world resources of mesopelagic fish, 193, 1-151, FAO Fisheries Technical Paper, Food, and Agriculture Organization of the United Nations, Rome.

Greszkiewicz, M., & Fey, D. P. (2018). Effect of preservation in formalin and alcohol on the growth rate estimate of larval northern pike. North American Journal of Fisheries Management, 38(3):601–5. doi: 10.1002/NAFM.10059.

Haralick, R. M. (1974). A measure for circularity of digital figures. IEEE Transactions on Systems, Man, and Cybernetics, 4, 394-396. doi: 10.1109/TSMC.1974.5408463.

Hays, G. (2003). A review of the adaptive significance and ecosystem consequences of zooplankton diel vertical migration. Hydrobiologia, 503(1), 163-170. doi:10.1023/B:HYDR.0000008476.23617.b0.

Herler, J., Lipej, L., & Makovec, T. (2007). A simple technique for digital imaging of live and preserved small fish specimens. Cybium: International Journal of Ichthyology, 31(1), 39-44.

Hubbs, C. L., & Lagler, K. F. (1964). Fishes of the Great Lakes region. University of Michigan Press, Ann Arbor.

Humphries, J. M., & Cashner, R. C. (1994). *Notropis suttkusi*, a New Cyprinid from the Ouachita Uplands of Oklahoma and Arkansas, with comments on the status of ozarkian populations of *N. rubellus*. Copeia, 1, 82-90. doi:10.2307/1446673.

Ingels, J., Clarke, M. R., Vecchione, M., Perez, J., Levin, L. A., Priede, I., Sutton, T. T., Rowdon, A. A., Smith, C., Yasuhara, M., Sweetman, A., Soltwedel, T., Santos, R., Narayanaswamy, B., Ruhl, H., Zettler, L. A., Jones, D., Gates, A., Snelgrove, P., & Gaever, S. (2016). Open Ocean Deep Sea. In first global marine assessment. Oceans and Law of the Sea, United Nations.

Judkins, H., Vecchione, M., Cook, A., & Sutton, T. T. (2016). Diversity of midwater cephalopods in the northern Gulf of Mexico: comparison of two collecting methods. Marine Biodiversity, 47(3), 647-657. doi:10.1007/s12526-016-0597-8.

Kassam, D. D., Adams, D. C., Hori, M., & Yamaoka, K. (2003). Morphometric analysis on ecomorphologically equivalent cichlid species from Lakes Malawi and Tangannyika. Journal of Zoology, London, 260(2), 153-157. doi: 10.1017/S0952836903003571.

Kiørboe, T., Visser, A., & Andersen, K. H. (2018). A trait-based approach to ocean ecology. ICES Journal of Marine Science, 75(6), 1849-1863. doi:10.1093/icesjms/fsy090.

Kipanyula, M. J., & Maina, K. W. (2016). Morphological and adaptational changes associated with fish migration from fresh to marine water bodies. International Journal of Fishiers and Aquatic Studies, 4(4), 125-129.

Klevjer, T. A., Irigoien, X., Røstad, A., Fraile-Nuez, E., Benítez-Barrios, V. M., & Kaartvedt, S. (2016). Large scale patterns in vertical distribution and behavior of mesopelagic scattering layers. Scientific Reports, 6(1), doi: 10.1038/srep19873.

Klingenberg, C. P. (2011). MorphoJ: an integrated software package for geometric morphometrics. Molecular Ecology Resources, 11, 353-357. doi: 10.1111/j.1755-0990.2010.02924.x.

Kremer, C., Williams, A., Finiguerra, M., Fong, A., Kellerman, A., Paver, S., Tolar, B., & Toscano, B. (2016). Realizing the potential of trait-based aquatic ecology: New tools and collaborative approaches. Limnology and Oceanography, 62. doi:10.1002/lno.10392.

Kuhl, F. P., & Giardina, C. R. (1982). Elliptic Fourier features of a closed contour. Computer Graphics and Image Processing, 18(3), 236–258. doi:https://doi.org/10.1016/0146-664X(82)90034-X.

Langerhans, R. B., & Resnick, D. N. (2010). Ecology and evolution of swimming performance in fishes: predicting evolution with biomechanics. In Fish Locomotion: an eco-ethological perspective (Domenici, P. & Kapoor, B. J., eds). Enfield, NH: Science Press. 200–248.

Larouche, O., Hodge, J. R., Alencar, L. R., Camper, V. B., Adams, D. S., Zapfe, K., Friedman, S. T., Wainwright, P.C., Price, S. A. (2020). Do key innovations unlock diversification? A case-study on the morphological and ecological impact of pharyngognathy in acanthomorph fishes. Current Zoology 66(5): 575-588.

Larochelle, C. R., Pickens, F. A. T., Burns, M. D., & Sidlauskas, B. L. (2016). Long-term isopropanol storage does not alter fish morphometrics. Copeia, 2, 411–420. doi: 10.1643/CG-15-303.

Lawing, A. M., & Polly, P. D. (2010). Geometric morphometrics: recent applications to the study of evolution and development. Journal of Zoology, 280, 1-7.

Levin, L. A., Bett, B. J., Gates, A. R., Heimbach, P., Howe, B. M., Janssen, F., McCurdy, A., Ruhl, H. A., Snelgrove, P., Stocks, K., Bailey, D., Baumann-Pickering, S., Beaverson, C., Benfield, M. C., Booth, D. J., Carreiro-Silva, M., Colaço, A., Elbé, M.C., Fowler, A. M., Gjerde, K. M., Jones, D. O. B., Katsumata, K., Kelley, D., Le Bris, N., Leonardi, A. P., Lejzerowicz, F., Macreadie, P. I., McLean, D., Meitz, F., Morato, T., Netburn, A., Pawlowski, J., Smith, C. R., Sun, S., Uchida, H., Vardaro, M. F., Venkatesan, R., & Weller, R. A. (2019). Global observing needs in the deep ocean. Frontiers in Marine Science, 6(241). doi:10.3389/fmars.2019.00241.

Loy, A., Boglione, C., Gagliardi, F., Ferrucci, L., & Cataudella, S. (2001). Geometric morphometrics and internal anatomy in sea bass shape analysis (*Dicentrarchus labrax L.*, Moronidae). Aquaculture, 186, 33-44.

Loy, A., Busilacchi, S., Costa, C., Ferlin, L., & Cataudella, S. (2000). Comparing geometric morphometrics and outline fitting methods to monitor fish shape variability of *Diplodus puntazzo* (Teleostea: Sparidae). Aquacultural Engineering, 21(4), 271-283. doi: 10.1016/S0144-8609(99)00035-7.

MacLeod, N. (2002). Geometric morphometrics and geological shape-classification systems. Earth and Science Reviews, 59, 27-47.

Maldonado, E., Hubert, N., Sagnes, P. & De Mérona, B. (2009). Morphology–diet relationships in four killifishes (Teleostei, Cyprinodontidae, Orestias) from Lake Titicaca. Journal of Fish Biology, 74, 502– 520.

Marcy, A. E., Fruciano, C., Phillips, M. J., Mardon, K., & Weisbecker, V. (2018). Low resolution scans can provide a sufficiently accurate, cost- and time- effective alternative to high resolution scans for 3D shape analyses. PeerJ, 6. doi:10.7717/peerj.5032.

Marks, A. D., Kerstetter, D. W., Wyanski, D. M., & Sutton, T. T. (2020). Reproductive ecology of dragonfishes (Stomiiformes: Stomiidae) in the Gulf of Mexico. Frontiers in Marine Science, 7(101). doi:10.3389/fmars.2020.00101.

Marshall, N. B. (1960). Swimbladder structure of deep-sea fishes in relation to their systematics and biology. Discovery Reports, 31, 1-22.

Martini, S., Larras, F., Boyé, A., Faure, E., Aberle, N., Archambault, P., Bacouillard, L., Beisner, B. E., Bittner, L., Castella, E., Danger, M., Gauthier, O., Karp-Boss, L., Lombard, F., Maps, F., Stemmann, L., Thiébaut, E., Usseglio-Polatera, P., Vogt, M., Laviale, M., & Ayata, S.-D. (2021). Functional trait-based approaches as a common framework for aquatic ecologists. Limnology and Oceanography, 66(3), 965-994. doi: https://doi.org/10.1002/lno.11655.

Mason, N., Mouillot, D., Lee, W., & Wilson, J. (2005). Functional richness, functional evenness, and functional divergence: the primary components of functional diversity. Oikos, 111(1), 112-118. doi:10.1111/j.0030-1299.2005.13886.x.

McGill, B., Enquist, B., Weiher, E., & Westoby, M. (2006). Rebuilding community ecology from functional traits. Trends in Ecology & Evolution, 21, 178-185. doi:10.1016/j.tree.2006.02.002.

McPherron, S. P., & Dibble, H. L. (1999). Stone tool analysis using digitized images: Examples from the lower and middle Paleolithic. Lithic Technology, 24(1), 38-52. doi: 10.1080/01977261.1999.11720944.

Mindel, B. L., Neat, F. C., Trueman, C. N., Webb, T. J., & Blanchard, J. L. (2016). Functional, size and taxonomic diversity of fish along a depth gradient in the deep sea. PeerJ, 4, 2387-2387. doi:10.7717/peerj.238.

Miya, M., & Nemoto, T. (1986). Life history and vertical distribution of the mesopelagic fish *Cyclothone alba* (family Gonostomatidae) in Sagami Bay, Central Japan. Deep Sea Research Part A. Oceanographic Research Papers, 33(8), 1053-1068. doi: https://doi.org/10.1016/0198-0149(86)90030-0.

Miya, M., & Nemoto, T. (1987). Reproduction, growth, and vertical distribution of the meso- and bathypelagic fish *Cyclothone atraria* (Pisces: Gonostomatidae) in Sagami Bay, Central Japan. Deep Sea Research Part A. Oceanographic Research Papers, 34(9), 1565-1577. doi: https://doi.org/10.1016/0198-0149(87)90109-9.

Mojekwu, T., & Anumudu, C. I. (2015). Advanced techniques for morphometric analysis in fish. Journal of Aquaculture Research and Development, 6, 1-6. doi:10.4172/2155-9546.1000354.

Moser, H. G. (1981). Morphological and functional aspects of marine fish larvae. In: Lasker, R. (Ed.), Marine Fish Larvae. Morphology, Ecology and Relation to Fisheries. University of Washington Press, Seattle, 89-131.

Mouillot, D., Graham, N. A. J., Villéger, S., Mason, N. W. H., & Bellwood, D. R. (2013). A functional approach reveals community responses to disturbances. Trends in Ecology & Evolution, 28(3), 167-177. doi: https://doi.org/10.1016/j.tree.2012.10.004.

Motta, P. J. & Kotrschal, K. M. (1992). Correlative, experimental and comparative evolutionary approaches in ecomorphology. Netherlands Journal of Zoology, 42, 400– 415.

Navarro, A., Lee-Montero, I., Santana, D., Henríquez, P., Ferrer, M. A., Morales, A., Soula, M., Badilla, R., Negrín-Báez, D., Zamorano, & Afonso, J. M. (2016). IMAFISH_ML: a fully-automated image analysis software for assessing fish morphometric traits on gilthead seabream (*Sparus aurata L.*), meagre (*Argyrosomus regius*), and red porgy (*Pagrus pagrus*). Computers and Electronics in Agriculture, 121, 66-73. doi: https://doi.org/10.1016/j.compag.2015.11.015.

Neat, F. C., & Campbell, N. (2013). Proliferation of elongate fishes in the deep sea. Journal of Fish Biology, 83(6), 1576-1591. doi: https://doi.org/10.1111/jfb.12266.

Olson, E. C., & Miller, R. L. (1958). Morphological integration. Chicago: University of Chicago Press.

Pauly, D. (2010). Gasping fish and panting squids: oxygen, temperature and the growth of water-breathing animals. Excellence in Ecology 22 Oldendorf/Luhe, Germany: International Ecology Institute.

Pearre, S., Jr. (2003). Eat and run? The hunger/satiation hypothesis in vertical migration: history, evidence and consequences. Biological Reviews, 78(1), 1-79. doi:10.1017/s146479310200595x.

Piet, G. J., & Jennings, S. (2005). Response of potential fish community indicators to fishing. ICES Journal of Marine Science, 62(2), 214-225. doi:10.1016/j.icesjms.2004.09.007.

Polly, P. D. (2008). Developmental dynamics and G-matrices: can morphometric spaces be used to model phenotypic evolution? Evolution Biology, 35, 1-20. doi: 10.1007/s11692-008-9020-0.

Priede, I. G. (2017). Deep-Sea Fishes: Biology, Diversity, Ecology and Fisheries. United Kingdom: Cambridge University Press. doi: 10.1017/9781316018330.

Priede, I. G., & Tytler, P. (2006). Heart rate as a measure of metabolic rate in teleost fishes; *Salmo gairdneri*, *Salmo trutta* and *Gadus morhua*. Journal of Fish Biology, 10, 231 - 242. doi: 10.1111/j.1095-8649.1977.tb05128.x.

Prosanta, C. (2006). Evolution and diversification of a sexually dimorphic luminescent system in ponyfishes (Teleostei: Leiognathidae), including diagnoses for two new genera. Cladistics, 20 (6), 501-517.

Quintana, X. D., Arim, M., Badosa, A., Blanco, J. M., Boix, D., Brucet, S., Compte, J., Egozcue, J. J., de Eyto, E., Gaedke, U., Gascón, S., de Solá, L. G., Irvine, K., Jeppesen, E., Lauridsen, T. L., López-Flores, R., Mehner, T., Romo, S., & Søndergaard, M. (2015). Predation and competition effects on the size diversity of aquatic communities. Aquatic Sciences, 77(1), 45-57. doi:10.1007/s00027-014-0368-1.

Radinović, M., & Kajtez, I. (2021). Outlining the knapping techniques: Assessment of the shape and regularity of prismatic blades using elliptic Fourier analysis. Journal of Archaeological Science: Reports. doi: 10.1016/j.jasrep.2021.103079.

Robison, B. H. (2009). Conservation of deep pelagic biodiversity. Conservation Biology 23(4), 847-858.

Rohlf, F. J. (1996). Morphometric spaces, shape components, and the effects of linear transformations. In L. F Marcus, M. Corti, A. Loy, G. Naylor, D. E. Slice, eds. Advances in morphometrics. NATO ASI Series A: Life Sciences, 284.

Rohlf, F. J. (2015). The Tps series of software. Hystrix, 26, 1-4. doi: 10.4404/hystrix-26.1-11264.

Rohlf, F. J., & Slice D. (1990). Extensions of the Procrustes method for the optimal superimposition of landmarks. Systematic Biology, 39: 40–59.

R Core Team. (2020). R: A language and environment for statistical computing. R Foundation for Statistical Computing. Vienna, Austria.

R Development Core Team. (2013). A language and environment for statistical computing. Vienna: R Foundation for Statistical Computing.

Richtsmeier, J. T., Burke DeLeon, V., & Lele, S. R. (2002). The promise of geometric morphometrics. American Journal of Physical Anthropology, 119(35), 63–91. doi:10.1002/ajpa.10174.

Richtsmeier, J. T., Cheverud, J. M., & Lele, S. (1992). Advances in anthropological morphometrics. Annual Review of Anthropology, 21(1), 283–305. doi:10.1146/annurev.an.21.100192.001435.

Riddell, B. E., Leggett, W. C., & Saunders, R. L. (1981). Evidence of adaptive polygenic variation between two populations of Atlantic Salmon (*Salmo salar*) native to tributaries of the S. W. Miramichi River, N.B. Canadian Journal of Fisheries and Aquatic Sciences, 38, 321-333.

Romero-Romero, S., Choy, C. A., Hannides, C. C. S., Popp, B. N., & Drazen, J. C. (2019). Differences in the trophic ecology of micronekton driven by diel vertical migration. Limnology and Oceanography, 64(4), 1473-1483. doi:10.1002/lno.11128.

Rooker, J. R., Simms, J. R., Wells, R. J. D., Holt, S. A., Holt, G. J., Graves, J. E., & Furey, N. B. (2012). Distribution and habitat associations of billfish and swordfish larvae across mesoscale features in the Gulf of Mexico. PLoS One, 7(4). doi: 10.1371/journal.pone.0034180.

Roper, C. F., & Sweeney, M. J. (1981). Techniques for fixation and preservation of cephalopods. Memoirs of the Museum of Victoria, 44, 28-47.

Rosin, P. (2005). Computing global shape measures. Computer Science. 10.1142/9789812775320_0010.

Savriama, Y. (2018). A Step-by-Step Guide for Geometric Morphometrics of Floral Symmetry. Frontiers in Plant Science, 9(1433). doi: 10.3389/fpls.2018.01433.

Seibel, B. A., Thuesen, E. V., & Childress, J. J. (2000). Light-limitation on predator-prey interactions: consequences for metabolism and locomotion of deep-sea cephalopods. Biological Bulletin, 198(2), 284–298. doi:10.2307/1542531.

Sébert, P., Scaion, D., & Belhomme, M. (2009). High hydrostatic pressure improves the swimming efficiency of European migrating silver eel. Respiration Physiology and Neurobiology, 165(1), 112–114. doi:10.1016/j.resp.2008.09.011.

Shields, P. A., & Carlson, S. R. (1996). Effects of Formalin and Alcohol Preservation on Lengths and Widths of Juvenile Sockeye Salmon. Alaska Fishery Research Bulletin, 3(2), 81-93.

Slice, D. E. (2007). Geometric morphometrics. Annual Review of Anthropology, 36, 261-281.

Smith, C., De Leo, F., Bernardino, A., Sweetman, A., & Martinez Arbizu, P. (2008). Abyssal

food limitation, ecosystem structure and climate change. Trends in ecology & evolution. 23. 518-28. 10.1016/j.tree.2008.05.002.

Somerfield, P. J., Clarke, K. R., & Gorley, R. N. (2021a). Analysis of similarities (ANOSIM) for 2-way layouts using a generalised ANOSIM statistic, with comparative notes on Permutational Multivariate Analysis of Variance (PERMANOVA). Austral Ecology, 46 (6), 911-926.

Somerfield, P. J., Clarke, K. R., & Gorley, R. N. (2021b). A generalised analysis of similarities (ANOSIM) statistic for designs with ordered factors. Austral Ecology, 46(6), 901-910.

Sotola, V. A., Craig, C. A., Pfaff, P. J., Maikoetter, J. D., & Martin, N. H. (2019). Effects of preservation on fish morphology over time: Implications for morphological studies. PLOS One, 14(3), e0213915. doi: 10.1371/journal.pone.0213915.

Staby, A., Røstad, A., & Kaartvedt, S., (2011). Long-term acoustical observation of the mesopelagic fish *Maurolicus muelleri* reveal novel and varied vertical migration patterns. Marine Ecological Progress Series, 441(1), 241–255. doi: 10.3354/meps09363.

Staby, A., & Salvanes, A. G. (2018). Mesopelagic fish. Encyclopedia of Ocean Sciences, Elsevier Incorporated. doi: 10.1016/B978-012-409548-9.11212-6.

Stich, H. B., & Lampert, W. (1981). Predator evasion as an explanation of diurnal vertical migration by zooplankton. Nature, 293, 396–398. doi:10.1038/ 293396a0.

Strock, C. (2021). Batch cropping images in ImageJ/Fiji. Zenodo. doi: 10.5281/zenodo.5559119.

Sutton, T. T. (2003). Stomiiformes: Dragonfishes and Relatives. In M. Hutchins (Ed.), Grzimek's Animal Life Encyclopedia, Gale, 2nd ed., 4, 421-430.

Sutton, T. T., Frank, T., Judkins, H., & Romero, I. C. (2020a). As gulf oil extraction goes deeper, who is at risk? Community structure, distribution, and connectivity of the deep-pelagic fauna. In S. A. Murawski, C. H. Ainsworth, S. Gilbert, D. J. Hollander, C. B. Paris, M. Schlüter, & D. L. Wetzel (Eds.), Scenarios and responses to future deep oil spills: fighting the next war, 403–418. Cham: Springer International Publishing. doi: 10.1007/978-3-030-12963-7_24.

Sutton, T. T., & Hopkins, T. L. (1996). Trophic ecology of the stomiid (Pisces: Stomiidae) fish assemblage of the eastern Gulf of Mexico: strategies, selectivity, and impact of a top mesopelagic predator group. Marine Biology, 127, 179-192. doi:10.1007/BF00942102.

Sutton, T. T., Hulley, P.A., Wienerroither, R., Zaera-Perez, D., & Paxton, J. R. (2020b). Identification guide to the mesopelagic fishes of the central and southeast Atlantic Ocean. FAO Species Identification Guide for Fishery Purposes. Rome, FAO. doi: 10.4060/cb0365en.

Sutton, T. T., & Milligan, R. (2018). Deep-Sea Ecology. Encyclopedia of Ecology, 35.

The GIMP Development Team. (2020). GIMP. Retrieved from https://www.gimp.org.

Thurber, A., Sweetman, A., Narayanaswamy, B., Jones, D., Ingels, J., & Hansman, R. (2014). Ecosystem function and services provided by the deep sea. Biogeosciences, 11, 3941–3963. doi:10.5194/bg-11-3941-2014.

Tilman, D. (2001). Functional diversity. In: Levin, S. A. (ed.), Encyclopedia of biodiversity. Academic Press, 3, 109-120. doi: https://doi.org/10.1006/rwbd.1999.0154.

Turan, C., Oral, M., Öztürk, B., & Düzgüneş, E. (2006). Morphometric and meristic variation between stocks of bluefish (*Pomatomus saltatrix*) in the Black, Marmara, Aegean, and northeastern Mediterranean Seas. Fisheries Research, 79(1), 139-147. doi: 10.1016/j.fishres.2006.01.015.

Tytell, E. D., Borazjani, I., Sotiropoulos, F., Baker, T. V., Anderson, E. J., & Lauder, G. V. (2010). Disentangling the functional roles of morphology and motion in the swimming of fish. Integrative and Comparative Biology, 50(6), 1140-1154. doi:10.1093/icb/icq057.

van Ginneken, V., Antonissen, E., Müller, U. K., Booms, R., Eding, E., Verreth, J., & van den Thillart, G. (2005). Eel migration to the Sargasso: remarkably high swimming efficiency and low energy costs. Journal of Experimental Biology, 208(7), 1329–1335. doi:10.1242/jeb.01524.

Valentin, A. E., Penin, X., Chanut, J. P., Sévigny, J. M., & Rohlf, F. J. (2008). Arching effect on fish body shape in geometric morphometric studies. Journal of Fish Biology, 73, 623–638. doi: 10.1111/j.1095-8649.2008.01961.x.

Vervust, B., & Van Damme, R. (2009). Marking lizards by heat branding. Herpetological Review, 40(2), 173-174.

Videler, J. J. (1993). Fish Swimming. London: Chapman and Hall.

Violle, C., Navas, M.-L., Vile, D., Kazakou, E., Fortunel, C., Hummel, I., & Garnier, E. (2007). Let the concept of trait be functional! Oikos, 116(5), 882-892. doi:https://doi.org/10.1111/j.0030-1299.2007.15559.x.

Violle, C., Reich, P. B., Pacala, S. W., Enquist, B. J., & Kattge, J. (2014). The emergence and promise of functional biogeography. Proceedings of the National Academy of Sciences, 111(38), 13690. doi:10.1073/pnas.1415442111.

Wainwright, P. C. (1991). Ecomorphology: experimental functional anatomy for ecological problems. American Zoologist, 31(4), 680-693. doi:10.1093/icb/31.4.680.

Wainwright, P. C., & Richard, B. A., (1995). Predicting patterns of prey use from morphology of

fishes. Environmental Biology of Fishes, 44(1), 97-113.

Wang, X., Zhang, J., Zhao, X., Chen, Z., Ying, Y., Li, Z., Xu, D., Liu, Z., & Zhou, M. (2019). Vertical distribution and diel migration of mesopelagic fishes on the northern slope of the South China sea. Deep Sea Research Part II: Topical Studies in Oceanography, 167, 128-141. doi: 10.1016/j.dsr2.2019.05.009.

Webb, P. W. (1984). Form and function in fish swimming. Scientific American, 251, 58– 68.

Webster, M., & Sheets, D. H. (2010). A practical introduction to landmark-based geometric morphometrics. The Paleontological Society Papers, 16, 163-188. doi: 10.1017/S1089332600001868.

Wei, T., & Simko, V. (2017). R package "corrplot": Visualization of a correlation matrix. https://github.com/taiyun/corrplot.

Zaret, T. M., & Suffern, J. S. (1976). Vertical migration in zooplankton as a predator avoidance mechanism. Limnology Oceanography, 21, 804–813. https://doi.org/10.4319/lo.1976.21.6.0804.

Zelditch, M. L., Fink, W. L., & Swiderski, D. L. (1995). Morphometrics, homology and phylogenetics: quantified characters as synapomorphies. Systems Biology, 44, 179-189.